MINISTERUL EDUCAȚIEI
**Universitatea Națională de Știință și Tehnologie**
**POLITEHNICA București**
Școala Doctorală de Inginerie Mecanică și Mecatronică

# DOCTORAL THESIS

## SUMMARY

# Optimizing the operation of the condenser of the cryogenic hydrogen distillation installation and testing of its energy performance on an installation equipped with a Gifford-McMahon cryocooler

**PhD supervisor**: Prof. Dr. Eng. Viorel BĂDESCU

**Thesis committee**: Prof. Dr. Eng. Radu CHIRIAC
Prof. Dr. Eng. Valentin APOSTOL
CS1 Dr. Eng. Sebastian BRAD
Prof. Dr. Eng. Florin IORDACHE

**Author**: Brill Cătălin

**Bucharest**

**2024**

# CONTENTS

**Keywords**: condenser, cryorefrigerator, cryogenic distillation, isotopic separation, exergy, film condensation, thermal conduction

# 1. INTRODUCTION

Given the global shift of the world economy towards the use of hydrogen as a basic energy source, it implies that cryogenic distillation is becoming essential as a hydrogen separation and purification technology [22]. Reaching and maintaining the cryogenic temperatures of 20 K at which the isotopic separation of hydrogen takes place is, however, a more expensive and difficult process than achieving positive boiling temperatures. That is why special liquefaction cycles are used in installations equipped with high quality thermal insulation. On the other hand, at cryogenic temperatures, hydrogen and its isotopes develop spin isomerism, i.e. the ortho and para forms, which cause the evaporation of a part of the liquid, the reaction being exothermic. All these technical and operational peculiarities, recorded from the technological experience, lead to an increased instability of the isotopic separation plants due to the unstable conditions of the process. Therefore, an important requirement for the cryogenic cycle is that the minimum temperature achieved has high stability when oscillations of the nominal operating parameters of the distillation plant occur. Therefore, together with the diameter of the column and the capacity of the bolier, the shape and size of the condenser are the very important parameters in the efficient operation of the distillation column requiring experimentation with different technical solutions. As a result of the research carried out in this field, the "Experimental Pilot for the Separation of Tritium and Deuterium" (PESTD) facility was designed by transforming laboratory technology into industrial-grade technology, equivalent to a CANDU detritium unit [1]. For this installation, additional experimental stands were developed for testing column components: cryostat, heat exchangers, condenser or bolier.

Continuing this direction of development, we have designed and tested a new model of conical shaped condenser made of OFHC copper, the part that is dissimilar to the stainless steel body of the column. The conical shape allows to avoid film condensation of the cryogenic liquid and favors the realization of condensation in much more efficient droplets.

The tests are carried out separately from the distillation column, on a small-scale cryogenic stand equipped with a hydrogen liquefaction unit: the Gifford McMahon 4k cryocooler with two cooling stages. For a easy handling, the condenser is fixed, in a demountable assembly system, to the upper part of a hydrogen tank, protected by a radiation screen inside a vacuum chamber with a diameter of 370 mm and a height of 733 mm. The proposed method is to continuously liquefy hydrogen using condensers of different masses and geometric configurations to compare heat transfer mode.

## 1.1 THE ROLE OF THE CONDENSER IN AN ISOTOPIC AND CRYOGENIC DISTILLATION PLANT

In this paper we have carried out research on methods to improve the performance of cryogenic distillation plants in the following directions:

- stabilizing liquid levels in the condenser of the liquefaction plant by minimizing oscillations in operation and

- increasing the efficiency of the liquefaction process by increasing the liquid flow rate at the level of the cold surface of the condenser of the liquefaction plant.

During the work, the concept of a new generation of high conductivity condensers is presented, by developing the initial model of flat surface condensser in geometric configurations resulting from its processing with extended heat exchange surfaces (pins or fins) and channels, which allow heat dissipation and condensation mode in the form of droplets. The current scientific paper argues the proposed constructive choice by minimizing the condensation conditions in film form as well as by improving the heat transfer mode resulting from the implementation of this innovation. Condenser conductivity testing requires different conditions than the testing concept used to characterize commercial liquefaction catalysts [13], such as a wider temperature range and testing over a longer period to reach steady state.

The method proposed in the thesis, of testing the components separately from the distillation column has a wide use [14], was chosen for easy handling and avoiding the risks of handling large quantities of liquid hydrogen over a long test duration [7]. Taking these into account, the paper presents an experimental, small-scale hydrogen liquefyor made for determining the heat transfer coefficient of these new types of condensers. On this experimental stand, the specific conditions of heat transfer processes [15] in cryogenic distillation columns are recreated. The proposed method is based on the determination of the heat transfer coefficient when condensing hydrogen gas on the surface of the condenser [16] cooled in the second stage of the GM cryocooler to a temperature of 20K. The condenser is assembled on a liquid tank inside a vacuum chamber. The liquid formed is collected at the base of the tank in the form of condensate, its temperature level being controlled by means of electric heat sources. Regarding the increase in heat transfer, the option for the condenser material is OFHC copper [14]. The aim is to minimize liquid level oscillations by minimizing the conditions for condensate film formation and facilitating droplet flow, the test unit allowing the use of condensers of different shapes to determine the optimal geometry in this regard.

## 1.2 OBJECTIVES OF THE DOCTORAL THESIS

The main objectives of this work are:

a) To study the possibility of replacing the current tubular condenser of the isotopic and cryogenic hydrogen distillation plant with a new type of condenser, in order to improve the refrigeration performance of the isotopic and cryogenic separation process, with a similar or lower energy consumption and minimal impact on the environment;

b) Development of a model for the calculation of the minimization of entropy production that can be used for the calculation of condensers within isotopic and cryogenic separation facilities;

by achieving the following specific objectives:

a.1) Increasing the exergetic efficiency of the isotopic and cryogenic hydrogen distillation plant by geometric and functional optimization of the new condenser model of the isotopic and cryogenic separation plant;

b.1) Realization of a calculation program to minimize the production of entropy for the geometric optimization of the condensers of the cryogenic distillation plants of hydrogen isotopes within the widest possible range of materials, values of Reynolds and Prandtl invariances, thickness of the baseplate, dimensions and distances between pins.

## 1.3 STRUCTURE OF THE DOCTORAL THESIS

The thesis is structured in the form of 9 chapters. In the first chapter, an introduction is made to the field of isotopic gas distillation and the connection with the cryogenic field. The role of the condenser in a cryogenic isotopic distillation plant and the ways of stabilizing refrigeration processes are brought to attention. Depending on the arguments brought in this chapter, the objectives of the doctoral thesis and the structure of the doctoral thesis are presented.

Chapter 2 presents a bibliographic study of the literature, regarding the current state of performance of cryogenic isotopic distillation technologies, especially methods and technologies for stabilizing technological processes.

Chapter 3 presents the characteristics and evaluation of the energy and exergetic performance of the current $H_2$-$D_2$ cryogenic distillation plant for testing PEST components,

assembled within the Cryogenics Laboratory of the ICSI Research Institute from Râmnicu Vâlcea. Exergetic losses are evaluated by the irreversibility of the processes for the component equipment of the installation but also the ways to reduce them. One of the improvement solutions identified is to change the condenser with another that is conceptually different in terms of construction, respectively made of copper material and conical in shape. This new type of condenser is initially tested on the current operational $H_2$-$D_2$ isotope and cryogenic separation facility. At the end of the chapter, the exergetic efficiencies of the operation of this installation are compared for the two use cases of the condenser, tubular and conical type. The determination of a superior exergetic efficiency for the conical condenser, as well as the presentation of the technical dysfunctions of the present tubular condenser bring arguments in support of the continuation during the thesis of the study of the technical implications of the use of the new type of condenser in the cryogenic hydrogen separation plants.

Chapter 4 presents the experimental stand, made separately within the ICSI Cryogenics Laboratory, and dedicated to testing the new type of copper condenser, in different constructive versions. In this chapter, all the main elements of this test stand are technically and functionally described, namely the cryostat assembly and the cold source, the liquefaction chamber and the condenser. The experimental stand has small scale dimensions, compared to the current $H_2$-$D_2$ cryogenic distillation plant, it is equipped with a Gifford McMahon type cooling head. The experimental conditions, created specifically for the study in the present paper, led to rapid and eloquent tests. The new type of optimized condenser tested on the plant cooled with the Gifford McMahon cryocooler will be mounted and subsequently tested on the isotopic separation column of the current $H_2$-$D_2$ cryogenic distillation plant, to confirm the results obtained.

Chapter 5 describes the theoretical sizing calculation model of the new condenser model as an integral part of the specially assembled cryogenic hydrogen liquefaction experimental stand. The external and internal thermal loads of the cryogenic system, the heat transfer coefficients and the thermal losses in the system are determined. At the end of the chapter, a dimensional design of the installation's condenser is carried out.

Chapter 6 describes the theoretical model for optimizing the new condenser model, designed for isotopic and cryogenic distillation of hydrogen, by taking into account exergetic losses. The method of minimizing the production of entropy is used in this regard. In this chapter, a brief presentation of the theory of entropy minimization is presented and the optimized model of the gaseous hydrogen heat exchanger (condenser) is determined. The model is limited to low-temperature cooling (cryogenic cooling) of hydrogen gas from about 300K to 20K. The design of this heat exchanger as energy efficient as possible was achieved

by adapting previous models regarding minimizing the production of entropy. Thus, the condenser of the hydrogen liquefaction plant is assimilated with a heat exchanger with pins and heat dissipation channels. In this heat exchanger, two major sources of entropy production are taken into account: heat transfer through the walls of the heat exchanger and pressure drop. In addition, the influence of both the shape and dimensions of the heat exchanger (condenser) and the operating conditions is taken into account in the model. The combined effect of thermal resistance and pressure drop is used in the calculations, which must be evaluated by simultaneous interaction with the condenser. The conservation equations for mass and energy combined with the entropy balance are applied. Analytical and empirical correlations are used for heat transfer. Also, this chapter presents optimal cooling strategies for hydrogen condensers, i.e. the identification of the optimal temperature profile of the cooling medium resulting from the production in a minimum entropy system. Finally, it is demonstrated that all relevant design parameters for the condensator, including geometric parameters, the material used, properties and flow conditions, can be simultaneously optimized.

Chapter 7 provides a comparative analysis of the operation of several condenser models. Different CAD models of condensers for computational calculation simulation in the field of CFD fluid dynamics were thus made, using the Ansys Fluent 2022 R2 program. Thus, the energy performance for two basic configurations, conical and rectangular, of the condenser and their versions with pins and fins are compared and studied. The physical and mathematical models of the condensers were built for this purpose and their operation in the installation was numerically simulated. The results obtained were analyzed in order to confirm the performance of the optimized condenser model from the previous chapter and to validate it against other models.

Chapter 8 analyzes from a functional point of view, in the experimental installation, the new optimized condenser model compared to other constructive versions. In this regard, experimental tests were carried out for the rectangular and conical models and their extended geometry versions (finned and pin), the same ones that were numerically simulated in the previous chapter. The optimized physical model of the condenser was fabricated and its functional behavior was evaluated under different conditions of pressure, flow and temperature, but also in comparison with the other condenser models.

In the last chapter, a summary of the main findings of this study is made, the personal and original contributions are highlighted, as well as the future research perspectives in this field.

# 2. HYDROGEN LIQUEFACTION AND ISOTOPIC SEPARATION TECHNOLOGIES

## 2.2.2 Working principle of cryogenic hydrogen distillation plants

In industrial plants for isotopic distillation of hydrogen at cryogenic temperature 20K, both deuterium is separated for the production of heavy water, used as a moderator and as a thermal agent in nuclear-electric drafts, and tritium, which is usually produced artificially.

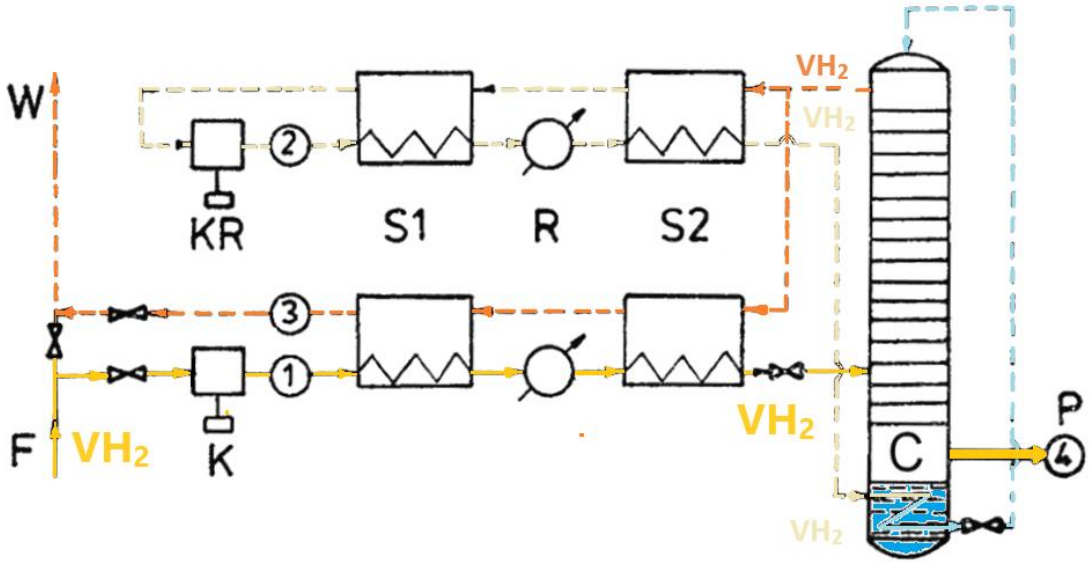


*Figure 2.2.2.2 General scheme of isotopic separation plants by cryogenic distillation of hydrogen [22]*
*C - distillation column; 1 - route F hydrogen refueling;*
*2 - the reflow route; 3- route W output of the resulting slight fraction;*
*4 - route elimination of the heavy fraction obtained; R - cooler;*
*S1 - primary debt collector; S2 - secondary recuperator; K - feed compressor; KR – recirculation compressor*

The most widely used non-polluting industrial method of separating deuterium and tritium from heavy water is isotopic hydrogen distillation combined with water-hydrogen isotopic exchange. The operating principle scheme of the hydrogen distillation plant (fig. 2.2.2.2 ) [22] comprises two main circuits: the distillation column reflow and the liquid hydrogen supply of the plant. Within the distillation plant, the process of separation of hydrogen and deuterium H2-D2 (isotopic separation) takes place at cryogenic temperatures. The role of the condenser and the boiler is to achieve an operating cycle so that the product that is extracted through the upper part of the column is in the form of saturated vapors and the product eliminated in the lower part is saturated liquid or saturated vapors (fig. 2.2.2.2).

The composition of the mixture subjected to separation and the low temperature level at which it is carried out, particularize this specific field of distillation [3] as follows: distillation at a temperature lower than 120K (-153 0C) is called cryogenic distillation [3]. However, the lower the operating temperature, the higher the specific energy consumption in a cryogenic plant [22] and the application of the solutions adopted must be analysed for continuous improvement.

The cryogenic distillation process is carried out by mass and heat exchange between the upstream and downstream streams under conditions considered adiabatic. The temperature is raised by heating in the boiler inside which the vaporization of the mass returned from the column by falling, in the form of liquid, takes place. Part of the vapor produced by the boiler (vaporizer) is used in the process by rising between the separating plates and heating them, and part is extracted from the process and used as a product. At the top of the column, part of the vapor of the gas mass is condensed and directed by free fall through the separation plates, thus ensuring the necessary cooling. The rest of the liquid is called reflow, characterized by the ratio between the mass flow of the reflow and that of the extracted vapors, also called the reflow ratio. Distillation columns are therefore technological installations within which the conditions for creating the best possible contact between the liquid being processed and the vapor are achieved [118][119]. The indicator of the separation process is the phase separation factor which represents the ratio of the volatilities of the components in a mixture [119]:

$$\alpha = K_i / K_j \qquad (2.2.2.1)$$

where: k i, j = fraction of the separated phase

A separation process is all the more efficient the greater the phase separation factor than the unity:

$$\alpha \geq 1 \qquad (2.2.2.2)$$

The space allocated to the mass exchange in a distillation column (separation) that represents the quality of having an ideal balance of phases is called *the theoretical plate*. The theoretical plate is an ideal unit (of measurement) whose height is called the equivalent height of the theoretical plate HETP. The lower the equivalent height of the theoretical HETP plate for a given load, the more suitable the conditions for carrying out the mass process will be. The HETP is determined by design calculation, influencing in turn or the calculation of the height of the column:

$$H_{col} = n \cdot HETP \qquad (2.2.2.3)$$

so that the separation requirement is met [119].

### 2.2.2.1 METHODS AND STEPS NECESSARY FOR STABILIZING THE CRYOGENIC DISTILLATION PROCESS

From the point of view of the process itself, isotopic distillation of hydrogen at cryogenic temperatures does not differ from distillation at positive temperatures. The low temperature at which the process takes place, the special physico-chemical properties of hydrogen and its isotopes, however, have particularities regarding the technology, the equipment used and the working conditions. Thus, due to the process itself of phase separation by cryogenic distillation in the columns of the plant, complex phenomena occur that must be controlled in order to avoid them or to maintain the parameters in certain ranges of variation.

The operating efficiency of a cryogenic hydrogen distillation plant therefore depends on two main conditions:

- ensuring and maintaining the condensation temperature of hydrogen in the condenser of the distillation column as well as
- the use of liquid-vapor contact elements of the column that have high efficiency in the separation of hydrogen isotopes

Therefore, a very important role in the optimal development of the distillation process is played by the element of contact between the phases, namely through:

- increasing the contact interface between the liquid and the vapor circulating in the counter-current and
- ensuring a homogenization as intense as possible [22].

Also, the operating mode of the column is another factor on which the distillation process depends in optimal conditions, since all the factors that directly determine the operation of the plant are influenced by the vapor flow (in the column). The vapor flow rate, which is produced by the column bolier, in turn directly depends on the size of the column diameter. Consequently, if the vapor flow decreases, the amount of liquid that remains in the voids of the filling decreases, causing the phenomenon of *dripping*, otherwise when the flow of vapor increases, the liquid no longer reaches the bolier of the column, thus producing the phenomenon of *flooding* [119].

Consequently, the sizing of the 3 main subassemblies of the distillation plant regarding the diameter (body) of the column, the cryogenic power of the condenser and the capacity (shape) of the bolier are very important factors in the operation within the designed parameters of the plant. Since special working conditions must be created and maintained at these low temperatures, the first condition is that the equipment must be designed in such a way as to

ensure this operation within the nominal parameters of the installation. For this, mathematical models are usually used to design, optimize and simulate the functioning of cryogenic cycles.

In this regard, there is a wide variety of technological solutions of cryogenic hydrogen distillation plants, at both laboratory and industrial levels. On a laboratory scale, isotopic distillation at temperatures of 20 K is primarily used for the production of deuterium and tritium for the purpose of scientific research and for the production of protium (light hydrogen) which is of high isotopic purity, used for scientific experiments of proton capture of muons. In this regard, within the research institute INC-DTCI-ICSI Rm.Vâlcea, the technology of separation of deuterium and tritium from deuterated and tritiated waters has been patented on a laboratory scale, by means of the combined method: catalyzed isotopic exchange and cryogenic distillation. The purpose of the research was and is to design a heavy water detritiation plant for the CANDU type reactors at Cernavoda NPP units 1 and 2.

Given that these applied technological solutions present large oscillations [22] in the operation of liquefaction and distillation plants (unstable operation), practical solutions must be found to remedy the non-static operation. From practical use, it has been determined that for an immediate and effective effect, solutions must be identified in increasing the efficiency of cryogenic operating cycles, i.e. in intensifying heat transfer.

The non-static regimes that occur in operation due to the variation of the liquid level in the condenser of the distillation plant are explained precisely by this variation in the condenser temperature due to the reduced heat transfer. So the efficiency of the hydrogen liquefaction process at the condenser must be as high as possible to ensure the cold flow to the gas to be separated from the column.

It follows from these considerations that the liquefaction of a mixture in a cryogenic distillation column is the essential phenomenon for distillation, boiling and separation based on the different volatilities of the existing compounds.

The condenser of a hydrogen distillation column can be cooled by means of cryogenic cycles with helium or hydrogen refrigerant, in the temperature range 18K÷22K, corresponding to the pressure at which the distillation column operates, so that the total condensation of hydrogen and its isotopes is achieved in this area. Maintaining the constant temperature at the distillation column condenser can therefore be achieved, in the first phase, through an efficient operation of these cryogenic cycles related to the plant.

# 3. EVALUATION OF THE ENERGETIC AND EXERGETIC PERFORMANCE OF THE CURRENT CRYOGENIC DISTILLATION PLANT $H_2$-$D_2$

## 3.2 DESCRIPTION OF $H_2$-$D_2$ ISOTOPE SEPARATION PLANT WITH CRYOGENIC DISTILLATION COLUMN

As shown, the purpose of using distillation columns in industry is to facilitate the best possible contact between the processed liquid and the vapor. Therefore, the need to maximize the contact surface between the phases, respectively to improve the liquid-vapor balance as well as the operating mode, are determining factors of the quality of the separation process in a cryogenic distillation column.

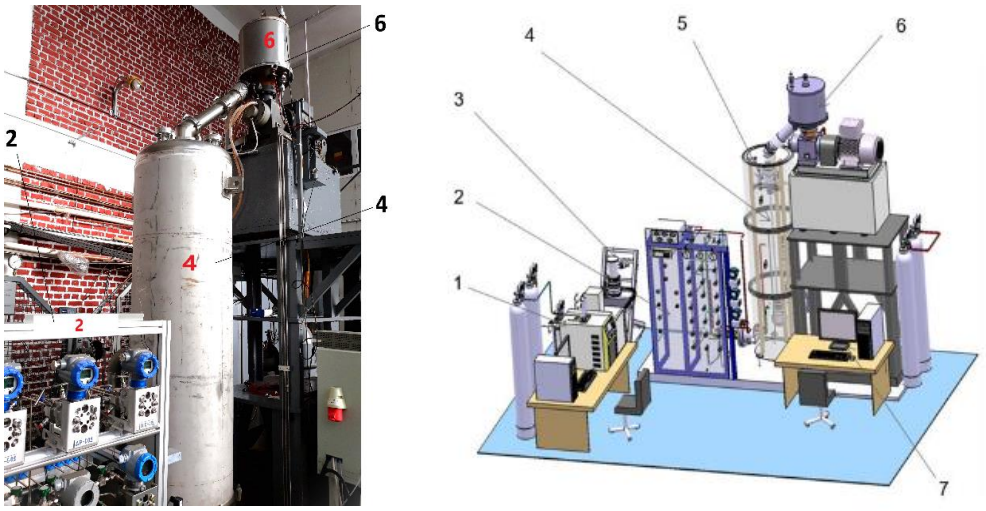


*(a)* *(b)*

*Figura 3.2.1 a) Image and b) 3D-CAD drawing of cryogenic separation plant $H_2$-$D_2$$H_2$-$D_2$ [8]*
*1. Agilent SCION 456-GC gas chromatograph equipped with an HPID detector 2. Panel with control and control elements 3. Varian-Agilent vacuum system TPS mobile 304 FS; 4. Cryostat 5. Distillation column 6. Hydrogen liquefier type PPH 7. SCADA data acquisition system*

The development of liquid-vapor phase contact elements of distillation columns (ordered or disordered fills) is a common practice in the chemical industry (e.g. Sulzer and Koch-Glitsch) with applications in extremely wide fields [118]. The testing of the functional parameters of these fillers is determined by using water and air as technological fluids. The problem is that none of the orderly fillers developed so far are specifically dedicated to the cryogenic distillation of hydrogen isotopes [119].

That is why commercial columns and fillers have been tested for cryogenic distillation of hydrogen isotopes through the development of their own experimental facilities [119].

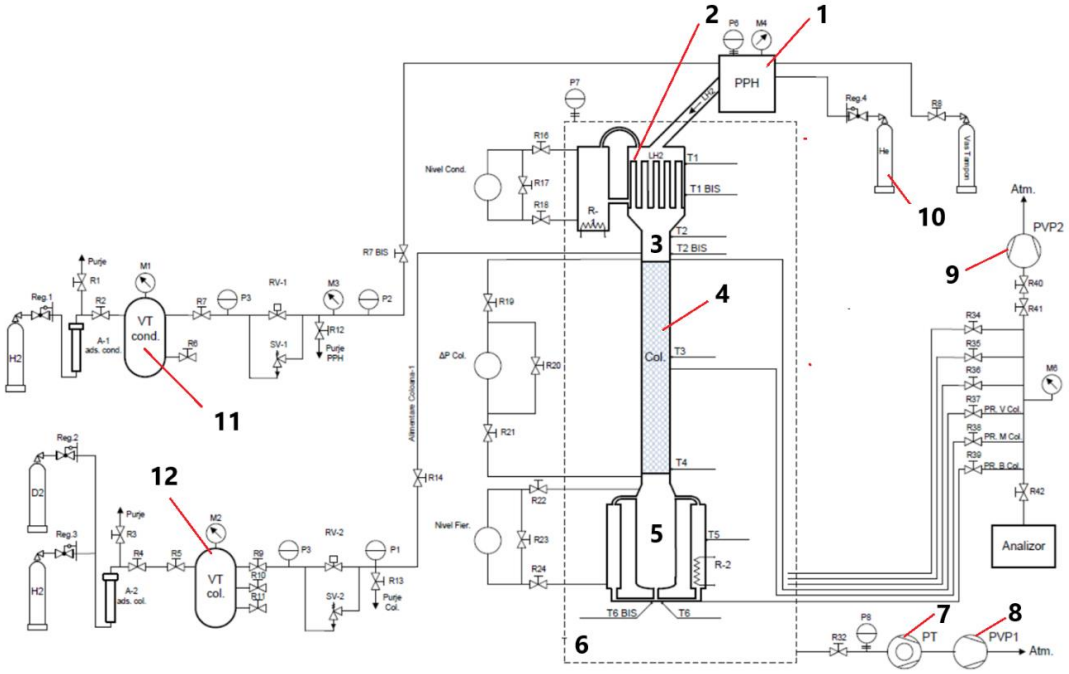


*Figura 3.2.2 Scheme of the experimental operational Cryogenic Distillation Plant [108]*
*1. Hydrogen liquefier 2. Multi-tube condenser 3. Distillation column 4. Filling the distillation column 5. Bolier 6. Vacuum chamber (cryostat) 7,8,9 Vacuum pumps. 10. Gas tank (He), 11. Gas tank (H2) 12. Gas tank (H2+HD); PPH – hydrogen cryogenerator, VT - buffer vessel, VA - feed vessel, VP - sample vessel, PVP - preliminary vacuum pump, PTM - turbomolecular pump, BA - mixing cylinder, BH- hydrogen cylinder, HX - heat exchanger, C - compressor, BN - nitrogen cylinder, CD - cryogenic distillation column, IE - electric heater, GC- gas chromatograph, A – adsorber, MB - metal bellow pump, EQ - balancer, R - manual valve, RV - valve, RM - micrometric valve, RL - lamination valve, SS - safety valve, S – disc, Δp - differential pressure, TI - temperature indication, TIR - temperature measurement with indication and recording, PI - pressure indication, PIR - pressure measurement with indication and registration, PIRA - pressure measurement with indication, registration and alarm, F - flow regulator, FIRC - flow measurement with indication, registration and control*

In this direction, within ICSI, experiments are periodically carried out to separate hydrogen isotopes by cryogenic distillation [8] for:

- testing the performance of separation of hydrogen isotopes on new types of filler[8].
- collection and processing of measurement data for cryogenic distillation process optimization,
- development/creation of efficient methods and appropriate equipment for tritium extraction [107]
- testing and determination of material properties at cryogenic temperatures [8].

In order to support the experimental activities of the PESTD plant, necessary for the execution of the design of the of hydrogen isotopes cryogenic distillation, for the tritium separation plants, the operational facility was developed within the ICSI Cryogenics Laboratory: "*Experimental cryogenic separation stand $H_2$-$D_2$*" (fig. 3.2.1) in which tests are carried out on the operation and then the implementation on the PESTD base plant [7], [8]. The designed cryogenic distillation column has an inner diameter of 12 mm and is equipped on a height of 260 mm with unordered filling made of stainless steel metal spirals with a diameter and height of 2mm. With this experimental installation (fig. 3.2.4) the following are tested [121]:

- Heli-Pack B5 and B7 fillers combined with hydrophilic plates with special geometry;
- More efficient technical solutions for cryostats, heat exchangers, condensers and boilers. The results of the tests carried out so far can be found in [8] and [107].

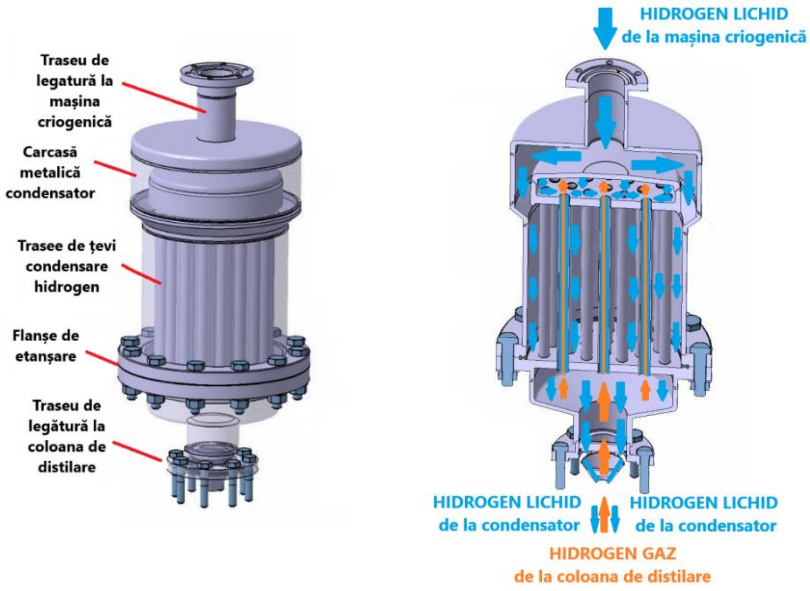


(a) ( b)

*Figura 3.2.3 Multitubular condenser used in ICSI's current cryogenic distillation plants a) image b) cross-section*

The current condenser used in the cryogenic distillation plant in the cryogenics laboratory (fig 3.2.3) is of the multitubular type. It consists of a system of pipes welded on a heat exchange plate with the liquid coming from the cryogenic machine. The gases go up from the column through the condenser pipes and at the top there is an enclosure where condensation takes place. The heat exchange is carried out through the walls of the pipes and the liquid flows through the pipes and falls on the conical surface of the inlet in the distillation column (fig 3.2.3), thus being collected and directed inside the distillation column.

## 3.4 CONDUCTING TESTS WITH THE NEW TYPE OF CONDENSER MOUNTED ON THE CRYOGENIC DISTILLATION PLANT

Previous experiments have shown [108] that a tidy fill separation performance has been reached, although several filler versions have been used. As we have shown, there is a solution of decreasing the diameter of the column and the diameter of the boiler. However, without a source of high cold capacity, the reflow necessary for vaporization cannot be ensured. To transfer this cooling capacity, a condenser is needed that can transfer the cold flow to the gas in the column with the highest possible efficiency [108].

a) b)

*Figure 3.4.1 Mounting options: a) removable ( flanges with screws ) b) non-removable ( flange welding ) for the new condenser for testing on the cryogenic distillation column*

That is why an experimental condenser model was designed and made for a cryogenic distillation column used for high concentrations of tritium. The new distillation column condenser model consists of a heat exchanger made of a conical shaped piece of OFHC copper, welded dissimilarly to the stainless steel body (316L or 304L) of the cryogenic liquid tank. The new shape avoids film condensation of the liquid and favors condensation in droplets, especially advantageous for distillation columns with small diameters. Since welding is a non-dismountable assembly, in order to perform multiple tests under the same technical conditions and thus verify a wider range of cryogenic power of such a condenser, an initial test model consisting of a demountable assembly system has also been developed (fig. 3.4.1).

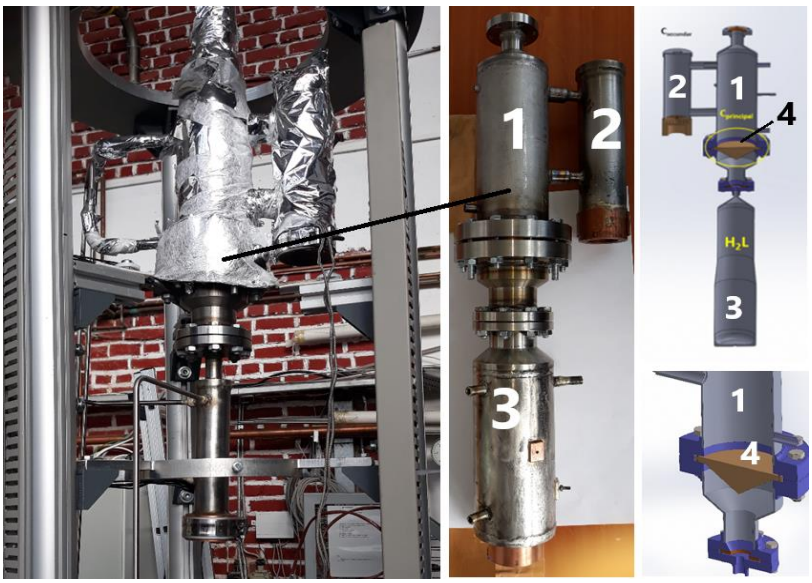


(a) ( b)

*Figure 3.4.2 a) Pictures and b) 3D section of the installation used for the preliminary testing of the new condenser for the screw and liquid hydrogen tank demountable version 1. Conical copper condenser assembly 2. Condenser level adjustment vessel 3.$LH_2$ liquid hydrogen tank 4.Conical copper condenser part*

The initial tests were carried out by replacing the column with a liquid tank in order to rigorously evaluate the amount of liquefied condensate (fig.3.4.2).

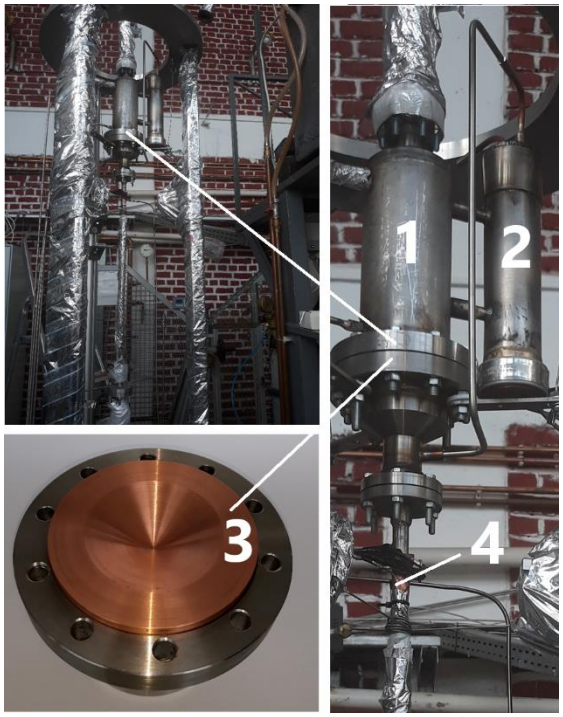


Figura 3.4.3 *Image of the installation used for testing the new condenser in the version of removable mounting with screws and cryogenic distillation column $H_2$ - $D_2$ 1. Conical copper condenser assembly 2. Condenser level adjustment vessel 3. Copper conical part condenser 4. Distillation column $H_2$ - $D_2$*

In the experiments, the heat transfer to the distillation column was successively evaluated for two different copper forms (fig. 3.4.1). In the subsequent tests, carried out for easy handling, on a specially made stand, the copper forms will have their roughness changed and then the thermal surface will be increased, by making fins or pins in the lower area of contact with the fluid.

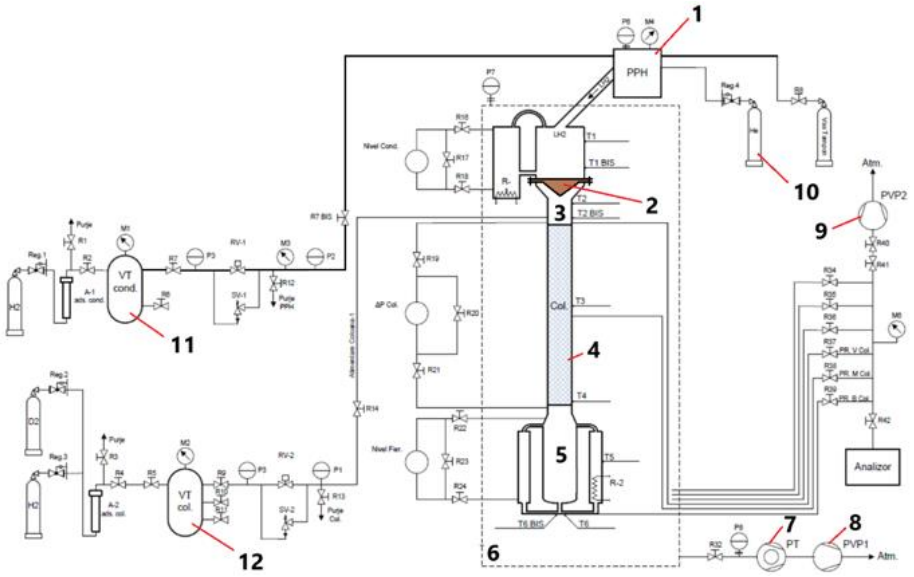


*Figura 3.4.5 Scheme of the plant used for testing the new condenser in the version of removable mounting with screws and cryogenic distillation column mixture H2-D2[108]*
*1. Hydrogen liquefier 2. Multi-tube condenser 3. Distillation column 4. Filling the distillation column 5. Boiler 6. Vacuum chamber (cryostat) 7,8,9 Vacuum pumps. 10. Gas tank (He), 11. Gas tank (H2) 12. Gas tank (H2 and HD); PPH – hydrogen cryogenerator, VT-buffer vessel, VA-feed vessel, VP-sample vessel, PVP- preliminary vacuum pump, PTM-turbomolecular pump, BA- mixing cylinder, BH - hydrogen cylinder, HX -heat exchanger, C- compressor, BN- nitrogen cylinder, CD-cryogenic distillation column, IE-electric heater, GC-gas chromatograph, A – absorber, MB – metal bellow pump, EQ- balancer, R- manual valve, RV - valve, RM - micrometric valve, RL - lamination valve, SS - safety valve, SD - disc, Δp - differential pressure, TI - temperature indication, TIR - temperature measurement with indication and recording, PI - pressure indication, PIR - pressure measurement, indication and recording, PIRA - pressure measurement with indication, recording, alarm, F - flow regulator, FIRC - flow measurement, indication, recording and control*

Experiments by mounting the condenser on the distillation column with the filling were carried out with the operation of the plant at total reflow, without extracting the products (fig.3.4.5). The condensation/vaporization power can be regulated by means of an electric resistance, mounted at its base [108]. Thus, the behavior and energy performance within the distillation plant of the new condenser were evaluated, determining for this purpose the separation performance ( HETP ) of some fillers developed by ICSI, with a diameter of 50 mm, type B5 and combined with hydrophilic plates with special geometry [3] [108].

As a result of the experiments, a stable temperature regime was obtained (fig. 3.4.7), at constant pressure, along the distillation column, with temperature differences in the range of 0.5÷0.9 K between the upper and lower part of the column. In the case of operation of the installation at different pressures, the range of temperature variation along the column was 1÷17 K.

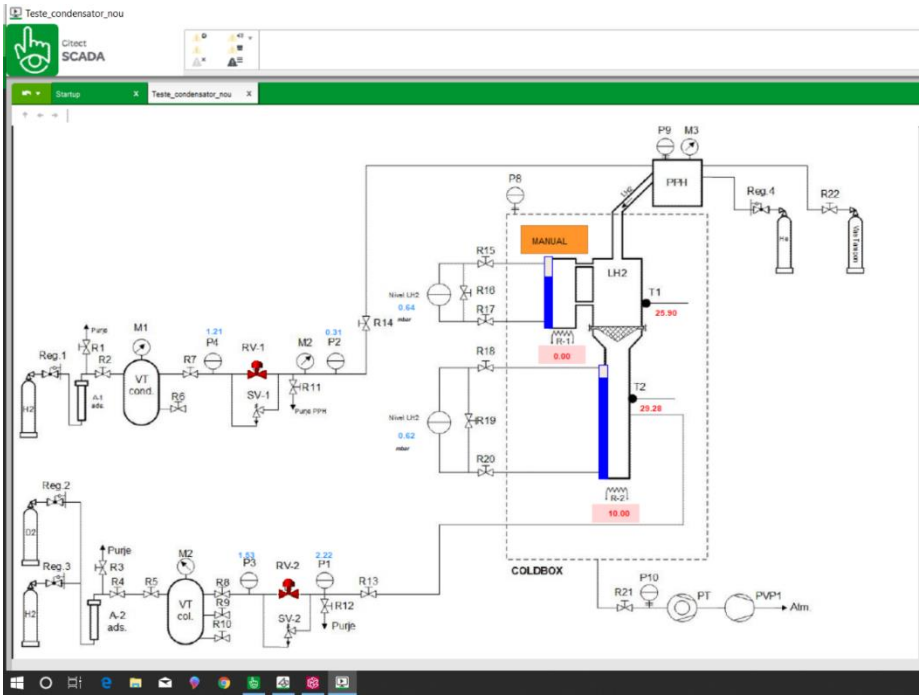


*Figura 3.4.7 Temperature level obtained during the test experiment of the new condenser on the $H_2$-$D_2$ mixture cryogenic distillation column*

Experimental tests were performed for different regimes of $H_2$-$D_2$ mixtures, from pressure 0.05 MPa per column with a pressure drop of maximum 0.2-0.4 mbar/m. Through these experimental tests, the appearance of the effect of ortho-para conversion of hydrogen was also pursued. The efficiency of deuterium separation in the filler developed by ICSI falls within the scope of results in this field [8].

## 3.5.4.2 EXERGETIC METHOD FOR EVALUATING THE EFFECTIVENESS OF PROCESSES

In order to highlight the irreversibility that occurred in the system and the possibility of improving them in order to improve the thermodynamic performance, the exergy of the distillation plant in operation equipped with the current multitubular condenser was determined.

The exergetic evaluation method used involves comparing the mechanical working capacity of the working fluid (or heat) at the entrance to the system (in the work equipment) with the loss of this capacity influenced by the ireversibility of the processes in the system.

In the method, the mechanical work production capacity is evaluated in relation to the external environment, as in the entropic method, but it is no longer related to the entire system, which ultimately leads to the simplification of calculations. The method associates exergetic flows to each component of the system, which is in progress, as follows: a resource exergy flow (fuel) $\dot{E}x^{Cb}$, a flow of exergy produced $\dot{E}x^{P}$ and a dissipated exergy flow (irreversibility) $\dot{E}x^{D}(I)$ (fig. *3.5.4.2.1* ).

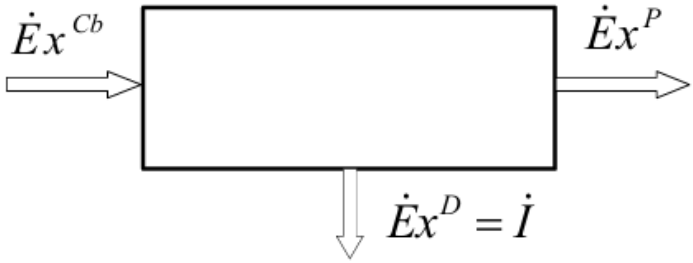


*Figure 3.5.4.2.1 Associated exergetic flows of system components*

Two qualitative factors are calculated, separately for each component:

- the exergetic efficiency which represents the ratio between the useful effect and the exergetic consumption for its realization (*fig. 3.5.4.2.1*):

$$\eta_{EX} = \frac{\dot{E}x^{P}}{\dot{E}x^{Cb_I}} \qquad (3.5.4.2.1)$$

- dissipation factor:

$$\zeta = \frac{\dot{E}x^{D}}{\dot{E}x^{Cb_I}} \qquad (3.5.4.2.2)$$

## 3.5.4.3.1 Exergetic calculation of Stirling PPH cryogenerator with partial heat regeneration

The specificity of the inverted Stirling cycle is the storage and release of heat in isochorous processes, which causes a greater amount of heat to be transferred for the same cooling power. The effect of these operating particularities leads to an increase in operating losses and implicitly to the inefficiency of real processes [27]. The purpose of the exergetic calculation is to determine the irreversible losses corresponding to the actual cycle operation of the machine and to identify the components to which the degree of irreversibility of the

operation must be reduced (fig. 3.5.4.3.1.1). The exergetic balance equations were applied for an open system for each heat exchanger as well as for the refrigeration cycle as a whole (fig. 3.5.4.3.1.1):

$$dEx_l + dEx_{reg} + dEx_h = 0 \qquad (3.5.4.3.1.4)$$

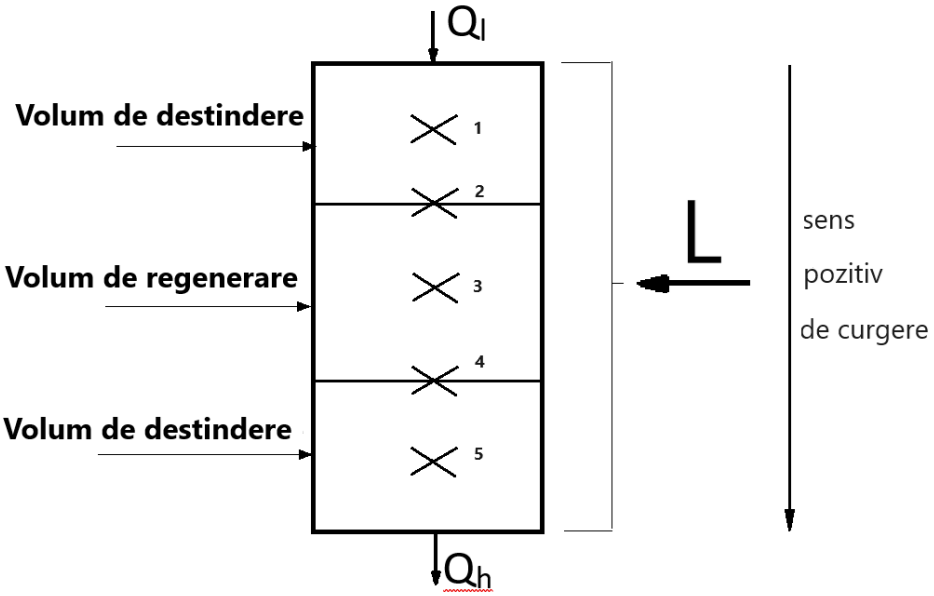


*Figura 3.5.4.3.1.1 Method of arranging gas volumes inside cryogenic machine*

Also, taking into account the technological experience, it was taken into account that the greatest destruction of exergy exists in the area of the regenerator, the calculations being made for the *refrigeration cycle with partial heat regeneration*.

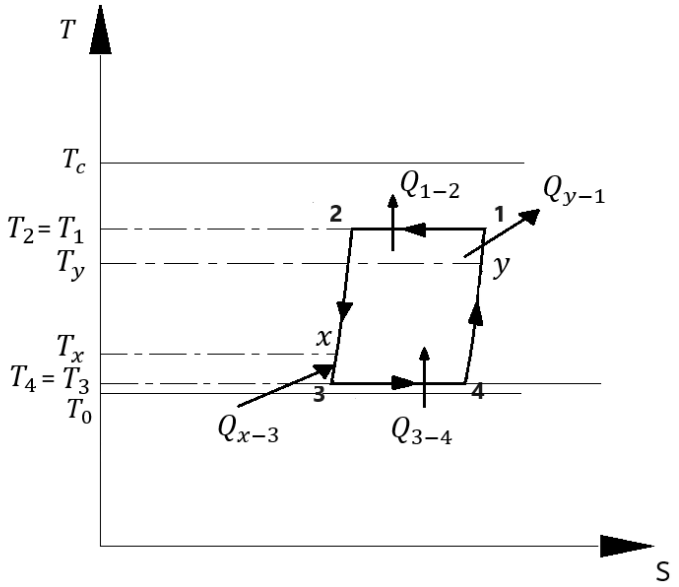


*Figure 3.5.4.3.1.2 Representation of the irreversibly inverted Stirling cycle in the T-s diagram*

Considering that at an incomplete regeneration of the gas ( $\eta_{reg} < 1$ ) the temperature of the gas leaving the regenerator at point 3 will be higher [27] than in the ideal case ( $\eta_{reg} = 1$ ), due to partial regeneration the surplus heat at the hot source will increase with the non-regenerated quantity.

The exergetic efficiency of the inverted Stirling cycle in one step [27] with partial (incomplete) regeneration for the actual working parameters was calculated as the actual regenerated heat flux in relation to the theoretically available energy (*fig. 3.5.4.3.1.2*) as follows:

$$\eta_{ir_{reg(X)}} = \frac{\left|\dot{Q}^{ir}_{3-4}\right|}{L} = \frac{|Q_{3-4}| - |Q_{x-3}|}{L} = \frac{|Q_{3-4}| - \Delta Q}{L} = \frac{|Q_{3-4}|}{L}\left[1 - \frac{\Delta Q_{\eta_{reg}}}{\left|\dot{Q}_{x-3}\right|}\right] =$$

$$= \eta_{reg} \cdot \left[1 - \left(\frac{X}{\gamma - 1} \cdot \frac{R(T_1 - T_3)}{\mu_{He} \cdot T_3(s_4 - s_3)}\right)\right] = 0.36 \cdot (1 - 0.1) = 0.32 \quad (3.5.4.3.1.11)$$

in care:

$$\dot{Q}_{3-4} = \upsilon \cdot m_{He} \cdot T_3 \cdot (s_4 - s_3) \quad (3.5.4.3.1.12)$$

$$C_v = \frac{R}{\gamma - 1} \quad (3.5.4.3.1.13))$$

$$\gamma = \frac{C_p}{C_v} = 1.7 \quad (3.5.4.3.1.14)$$

$$\dot{Q}_{x-3} = X \cdot \dot{Q}_{2-3} = X \cdot \dot{Q}_{1-4} = \Delta Q \quad (3.5.4.3.1.6)$$

unde :

$\dot{Q}_{x-3}$ = represents the flow of unregenerated heat

$\Delta Q$ = represents the thermal losses caused by this inefficiency of the regenerator

$\dot{Q}_{3-4}$ = represents the absorbed heat flux, in [W]

$C_p$ si $C_v$ = represents the specific heats of the gas, in [J/mol K], at the working temperature and pressure (in the regeneration phase)

R (= 8314) = represents the universal gas constant [ J/mol K]

$\upsilon = \frac{\mu_{He}}{\rho_{He}}$ - represents the kinematic viscosity of helium gas in [J/kg s]

$\rho_{He}$ = represents the density of helium gas, in [$m^3$/kg]

$m_{He} = 4$ - represents the molar mass of helium gas, in [ kg/ kmol ]

$\eta_{reg} = 0.97$ - regenerator efficiency (conform date tehnice după 1000 h) [109]

X = represents the fraction of unregenerated heat according to the equation:

$X = 1 - \eta_{reg} = 1 - 0.97 = 0.1$ (10% Losses due to non-regeneration) *(3.5.4.3.1.15)*

$T_1 = 293K$ - represents the inlet temperature of the helium working gas into the machine

$T_4 = 77K$ - represents the output temperature of the helium working gas

$s_1$ si $s_2$ [J/kg K] = specific process entropies (*according to Table 3.5.3.1*)

$\eta_{reg}$ = 0.36 - regenerator efficiency under ideal (theoretical) conditions

The initial working parameters in points 2 and 4 in the T-S diagram of the inverted Stirling refrigeration cycle correspond to the data determined from the operation of the hydrogen cryogenerator. For the determination of all the parameters related to the known temperatures, [NIST] [73] is used, and for the pressures in points 1 and 3, the equation of state of perfect gas and the equations of isothermal and isochore transformations are used. The wear of the regenerator was considered to be 10 %, resulting in a regeneration efficiency $\eta_{reg}$ = 97%. *(ec 3.5.4.3.1.15).* The exergetic efficiency of the inverted Stirling cycle in a stage with partial regeneration resulted under these conditions (ec 3.5.4.3.1.11)) as:

$$\eta_{ir_{reg(X)}} = 0.32 \qquad (3.5.4.3.1.16)$$

lower than the calculated efficiency of the ideal cycle:

$$\eta_{proces} = 0.36 \qquad (3.5.4.3.1.17)$$

### 3.5.4.4.4 Exergetic calculation of cryogenic hydrogen distillation column under adiabatic conditions

In the temperature-entropy diagram (fig. 3.5.4.4.4.1) the amount of exergy can be highlighted as the area of the inverted Carnot Cycle (refrigeration cycle) necessary to cover an exchange of thermal exergy at the given temperature in relation to the ambient conditions.

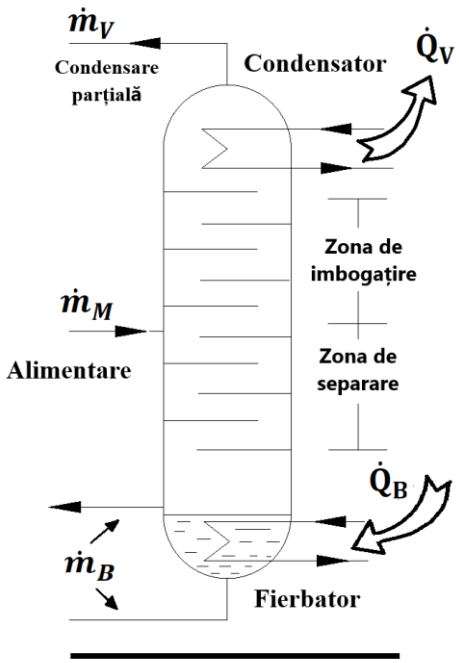


*Figure 3.5.4.4.3.1 Principle scheme of the distillation column*

The process temperature is considered stable at 0.1 Mpa. Under adiabatic conditions ($\dot{Q}_{IZ} = 0$) and neglecting changes in kinetic and potential energy, the mixture of hydrogen and deuterium $H_2$-$D_2$ is considered to be separated into the two dry hydrogen and deuterium products by saturated vapours (*Fig. 3.5.4.4.3.1*) so that the sum of the enthalpies of the products is practically equal to the enthalpy of the resulting mixture:

$$\dot{Q}_B = \dot{Q}_V \qquad (3.5.4.4.3.4)$$

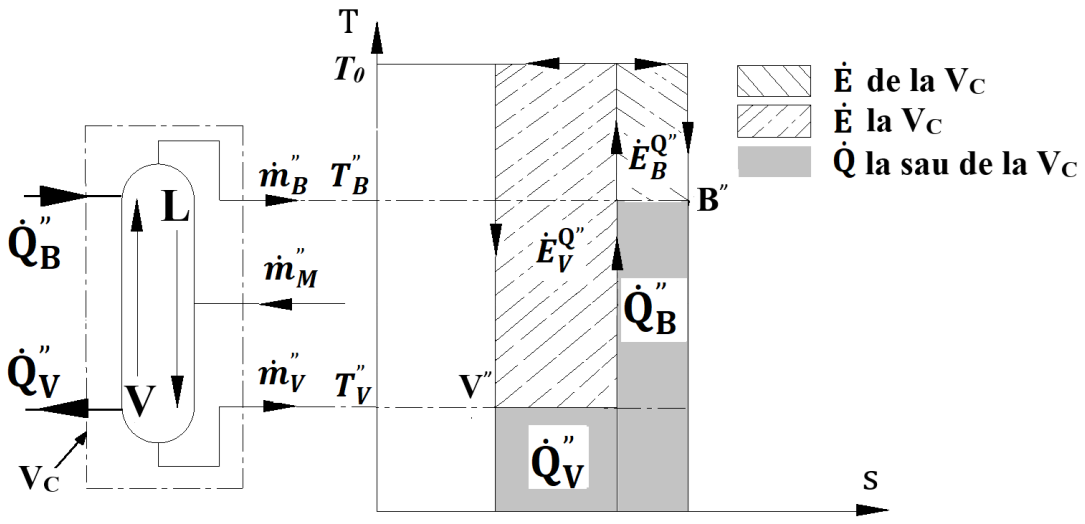


*Figure 3.5.4.4.4.1 T-s diagram heat transfers and exergy highlighted for adiabatic cryogenic distillation column and $V_C$ control volume*

Irreversibilities strictly for the distillation processes in the column can be evaluated from the exergetic balance as follows:

$$I = \Delta Ex^{Q}_{NET} - \Delta Ex_{MIN} \qquad (3.5.4.4.4.1)$$

in which:

- Subscriptions represent:

B = lower area of the column (boiler),

V = upper area of the column (condenser)

M = mixing area of the column

$$\Delta Ex_{MIN} = Ex_V + Ex_B - Ex_A = 755 \text{ [kJ /kmol]} \qquad (3.5.4.4.4.2)$$

= represents the minimum amount of exergy (determined from the concentration-exergy diagram)

$$\Delta Ex^{Q}_{NET} = \dot{E}x^{Q}_{V} + \dot{E}x^{Q}_{B} = Q_C \cdot \tau_C + Q_F \cdot \tau_F = Q_C \frac{T_C - T_0}{T_C} + Q_F \frac{T_F - T_0}{T_F} \qquad (3.5.4.4.4.3)$$

$$= -741.66 \left[\frac{20.32 - 293.15}{20.32} + \frac{23.12 - 293.15}{23.12}\right] = 741.66(13.42531 - 11.678602) = 1295.46 \left[\frac{kJ}{kmol}\right]$$

It follows that:

$$I = 1295 - 755 = \mathbf{540}\ [\mathbf{kJ\ /kmol}] \qquad (3.5.4.4.4.3')$$

where:

$\dot{Q}_B = \dot{Q}_V = 741.66$ [kJ /kmol] *(3.5.4.4.3.5)*

= represents the value determined from the enthalpy-concentration diagram at the appropriate temperatures for this state:

$T_F = 23.12\ K$ = corresponding temperature enthalpy boiler *(3.5.4.4.3.6)*

$T_C = 20.3\ K$ = corresponding temperature enthalpy condenser *(3.5.4.4.3.7)*

$T_0 = 293.15\ K$ = ambient temperature *(3.5.4.4.3.8)*

$\dot{Q}_B$ = represents the heat transfer to the column (from the boiler)

$\dot{Q}_V$ = represents the heat transfer from the column (from the condenser)

$Ex_V + Ex_B - Ex_A$ = represents the difference between the exergy of the products and the exergy of the mixture

$\dot{Ex}_V^Q + \dot{Ex}_B^Q$ = represents the net exergy input into the distillation column at which:

- cryogenic source operating after an inverted Carnot cycle (refrigerated)
- exergy in condenser $\dot{Ex}_V^Q$ is greater than exergy in a boiler $\dot{Ex}_V^Q$ (for columns operating at a temperature higher than the ambient temperature, this ratio of exergies is reversed - normal Carnot cycle)

Considering the necessary exergy $\Delta Ex_{NET}^Q$ and respectively, according to (eq. 3.5.4.4.4.2), the output exergy $\Delta\, Ex_{MIN}$, the exergetic efficiency of the column results as:

$$\psi' = \frac{\Delta\, Ex_{MIN}}{\Delta Ex_{NET}^Q} = \frac{755}{1295} = \mathbf{0.58} \qquad (3.5.4.4.4.4)$$

This efficiency value is considered the maximum possible for the existing parameters of the installation. For the distillation column that works with a limited number of plates and has reflow, with the reflow ratio of about 20% it is calculated:

$$\dot{Q}_B = -\dot{Q}_V = 755 \cdot 1.21 = 890\ [\text{kJ /kmol}] \qquad (3.5.4.4.4.5)$$

- thermal input exergy:

$$\Delta Ex_{NET}^Q = 890\ (13.42531 - 11.678602) = \mathbf{1554.56}\left[\frac{\mathbf{kJ}}{\mathbf{kmol}}\right] \qquad (3.5.4.4.4.6)$$

- irreversibility that increases with:

$$I = 1555 - 755 = 800\ [\text{kJ /kmol}] \qquad (3.5.4.4.4.7)$$

The exergetic efficiency of the reflow column becomes:

$$\psi' = \frac{\Delta\, Ex_{MIN}}{\Delta Ex_{NET}^Q} = \frac{755}{1555} = \mathbf{0.48} \qquad (3.5.4.4.4.8)$$

### 3.5.4.4.5 Exergetic calculation of cryogenic hydrogen distillation column under non-adiabatic conditions

The idealization represented by the existence of non-adiabatic conditions (external heat input) can be approached in a practical distillation column by providing intermediate condensers and boilers and in which the inlet flows into the mixing region must be preheated. By assuming a large number of steps, the VMB curve, representing the heat transfer process, becomes flattened ( fig. 3.5.4.4.5.1) with respect to the stepped curve (fig. 3.5.4.4.4.1), from adiabatic operation.

The representation in the T-s diagram of the heat and exergy transfers under non-adiabatic conditions *( fig. 3.5.4.4.5.1* ) shows that, compared to the adiabatic columns (diagram *fig. 3.5.4.4.4.1*), for the same heat transfer rates $Q_V$ and $Q_B$, the increase (addition) of thermal exergy $\dot{E}x_V^Q$, $\dot{E}x_B^Q$ is higher for the non-adiabatic columns. This situation is explained by the fact that the operation of non-adiabatic reversible columns operates with net minimum exergy inputs which, according to (*ec.3.5.4.4.3.3*), must be equal (for I=0) to the minimum separation exergy: $Ex_V + Ex_B - Ex_A$

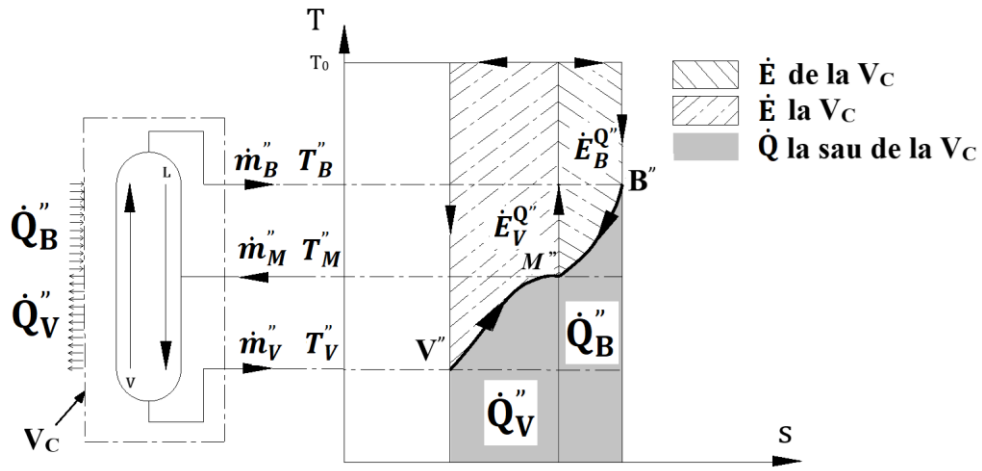


*Figure 3.5.4.4.5.1 T-s diagram heat transfers and exergy highlighted for ideal cryogenic distillation columns, non-adiabatic, for $V_C$ control volume*

### 3.5.4.4.6 Irreversibility in condenser and boiler

In real operation, the heat transfers from the condenser and boiler are made at a temperature difference that results from repeated tests, respectively 3K, the heating agent must

have a higher temperature and the cooling medium a lower temperature. Thus, the *actual* temperatures required will be:

$$T_{condensator} = T_v = (20.32 + 3)\text{K} = 23.32\ \text{K} \qquad (3.5.4.4.6.1)$$

and

$$T_{fierbator} = T_B = (23.12 + 3)\text{K} = 26.12\ \text{K} \qquad (3.5.4.4.6.2)$$

The calculation of irreversibility arising due to a finite temperature difference (3 K) is:

a) For the boiler: $I_B^{\Delta T} = Q_B\ T_0 \left[\frac{1}{T_B} - \frac{1}{T_B^x}\right]$ *(3.5.4.4.6.3)*

$$= 890\ x\ 293.15 \left[\frac{1}{23.12} - \frac{1}{26.12}\right] = 1295.8\ [kJ/\ Kmol]$$

b) For the condenser: $I_V^{\Delta T} = Q_V\ T_0 \left[\frac{1}{T_V} - \frac{1}{T_V^x}\right]$ *(3.5.4.4.6.4)*

$$= 890\ x\ 293.15 \left[\frac{1}{20.32} - \frac{1}{23.32}\right] = 1651.31\ [kJ/\ Kmol]$$

The total increase in irreversibility will be:

$$I^{\Delta T} = 1296 + 1651 = \mathbf{2947}[\boldsymbol{kJ/\ Kmol}\ ] \qquad (3.5.4.4.6.5)$$

Leading to increased net thermal exergy entered into the column as well *(eq. 3.5.4.4.4.6)* :

$$\Delta Ex_{NET}^{Q} = 2946 + 1555 = 4502\ [kJ/\ Kmol] \qquad (3.5.4.4.6.6)$$

With an exergetic efficiency (4,111) of the distillation column:

$$\psi' = \frac{\Delta\ Ex_{MIN}}{\Delta Ex_{NET}^{Q}} = \frac{755}{4502} = 0.16 \qquad (3.5.4.4.6.7)$$

### 3.5.4.4.7 Methods to minimize irreversibility and increase the operating efficiency of the condenser of the cryogenic distillation plant

The operation under ideal (non-adiabatic) conditions of the distillation column (T-s diagram, fig. 3.5.4.4.5.1) involves increasing the thermal exergy. Thus, for the same heat transfer rates as in adiabatic operation, the area of the Carnot Cycle of thermal exergetic exchange is increased in non-adiabatic operation. In (fig. 3.5.4.4.5.1) the exergetic curve in the T-s diagram appears flattened, but in reality it is in steps. A method of flattening this curve (and stabilizing the distillation process) can be achieved by increasing the number of distillation stages (plates), an ideal condition and difficult to achieve due to the need for the very large number of such stages. A practical method is to introduce intermediate boilers and condensers into the system.

The distillation column condenser (fig. 3.2.3 ) uses liquid hydrogen produced by the Philips PPH-A20 refrigerant as a coolant. The temperature regulation inside the distillation column is achieved by regulating the liquid level in the condenser, with level indication and a safety valve (a higher level of liquid hydrogen in the condenser means a higher cryogenic power inside the

distillation column). A major problem of the cryogenic distillation installation is the operation in stationary conditions and the stabilization of the working parameters due to this liquid flow from the condenser, which is variable.

The current condenser used in the cryogenic distillation installation in the cryogenics laboratory (fig. 3.2.3) is a multi-tube heat exchanger. It consists of a system of pipes welded on a heat exchange plate with the liquid from the cryogenic machine. The gases rise from the column through the condenser pipes and at the top there is an enclosure where condensation takes place. The heat exchange is carried out through the walls of the pipes and the flow of the liquid back into the distillation column encounters difficulties due to its restriction by the gas that rises producing the clogging of the pipe. Thus, the operation of a number of pipes is canceled, producing blockages (clogging), areas of thermal accumulation and finally a decrease in thermal exergy. Also, the liquid that has left the pipes falls undirected on a cone-shaped surface where, due to the temperature of the walls, a second vaporization occurs, which leads to thermal losses. So, one cause of the occurrence of these instabilities in operation is the condensation method, more precisely the level of liquid in the condenser that does not stabilize and consequently the supply of variable liquid flow. A second cause of instability in operation is the way of transferring the liquid to the column, which also leaks on the walls of the column, leading to defective internal or external heat exchange through the walls (with the environment), which leads to an increase in the irreversibility of the process and a decrease in exergy.

In this context, as a result of the tests carried out with the current condenser on distillation columns at different pressures (fig. 3.4.3) it was found that the average temperature difference between the top of the column and the base of the column decreased. This fact leads to an intensification of the longitudinal thermal conduction along the column as follows: the substantially different temperatures of the ends of the column and the temperature gradients in the column structure increase the heat transfer through local thermal conduction, which is certainly an irreversible phenomenon and which leads to a decrease in useful energy and to the destruction of thermal exergy. Therefore, the decrease of the exergy (inlet) input into the distillation columns (eq. 3.5.4.4.6.6) can only be achieved by improving the distillation efficiency achievable by increasing the efficiency of the boiling and condensing process.

In this paper we have continued the research in this direction with the following goals:

- stabilization of the liquid level in the condenser of the liquefaction installation by minimizing oscillations in operation

- increasing the efficiency of the liquefaction process by increasing the liquid flow rate at the level of the cold surface of the condenser of the liquefaction plant

Taking into account all these technical difficulties regarding the operation of the distillation column, and starting from the experiments conducted by Alekseev [9], we have developed a conical condenser concept as a new constructive solution that minimizes the possibility of hazard in the condensation process leading to its stabilization. This condenser has a relatively simple thermal conduction flange construction (fig. 3.4.1 ) with a flat face on the side of the cryogenic machine and the other side machined in a conical shape or with pins or finned, to increase the heat transfer surface and oriented vertically to ensure the easy sliding of the condensed hydrogen droplets [10]. The sloping shape of the face in contact with the liquid thus creates two advantages:

(a) facilitating a flow predominantly in the center of the column, thus leading to minimal contact with the walls of the column, and

(b) The flow (leakage) on the inclined surface is made in the form of droplets and thus eliminates the disadvantage of film formation on the contact surface, which leads to thermal losses and minimal heat transfer.

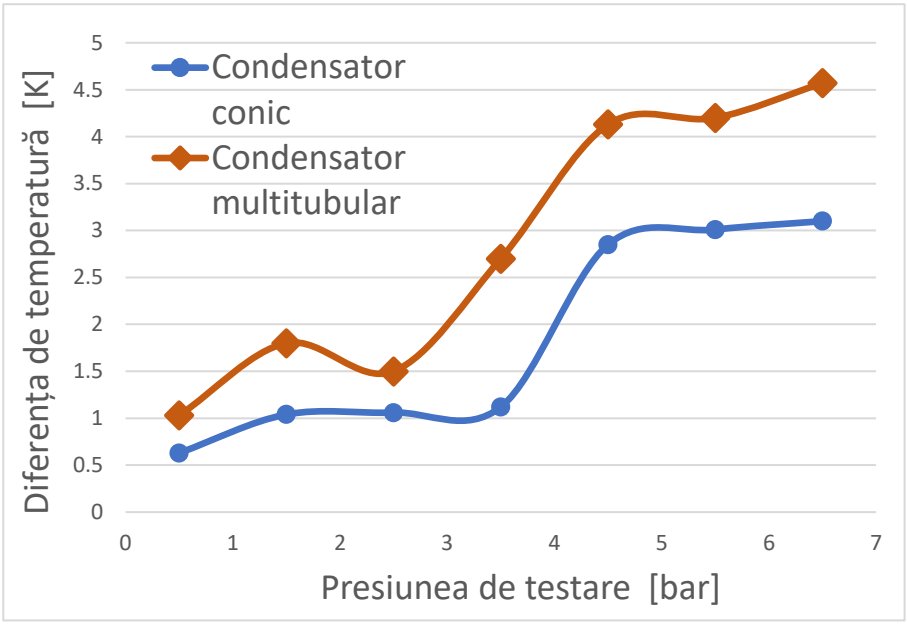


*Figure 3.5.4.4.7.1 Temperature differences between condenser and boiler obtained for the use of multitubular and conical condenser respectively*

In order to confirm the operation of the new type of condenser, a series of tests were carried out by mounting the conical type condenser on the cryogenic distillation column with a length of 1 m and a diameter of 12 mm ( fig. 3.4.3 ). As a result of the tests carried out, an average temperature difference of 1.8 K between the top of the column and the base of the column was

found, at constant pressure. In the case of using the new condenser model, the temperature difference between the top and the base of the column is reduced by an average of 1K ( fig. 3.5.4.4.7.1), compared to the current condenser. The overall exergetic efficiency of the distillation column, calculated with eq. 3.5.4.4.6.7, will increase with the use of the conical condenser to 18 % compared to 16 % with the tubular condenser.

However, in order to test the heat transfer coefficient for different constructive configurations of this new condenser (finned or pin) it is necessary to carry out multiple tests. A cryogenic distillation column with hydrogen as a working agent is massive, complicated to seal (hydrogen is extremely explosive) and does not justify the time and resources for its assembly and disassembly very often [7]. In this regard, the paper presents an experimental hydrogen liquefaction installation on which this new constructive form of condenser was tested in different versions of geometric configurations from the point of view of heat transfer mode.

# 4. TECHNICAL AND FUNCTIONAL DESCRIPTION OF THE EXPERIMENTAL STAND

## 4.2 CONDENSER TEST METHOD

The efficient operation of distillation columns is largely determined by the refrigeration efficiency of the condenser.

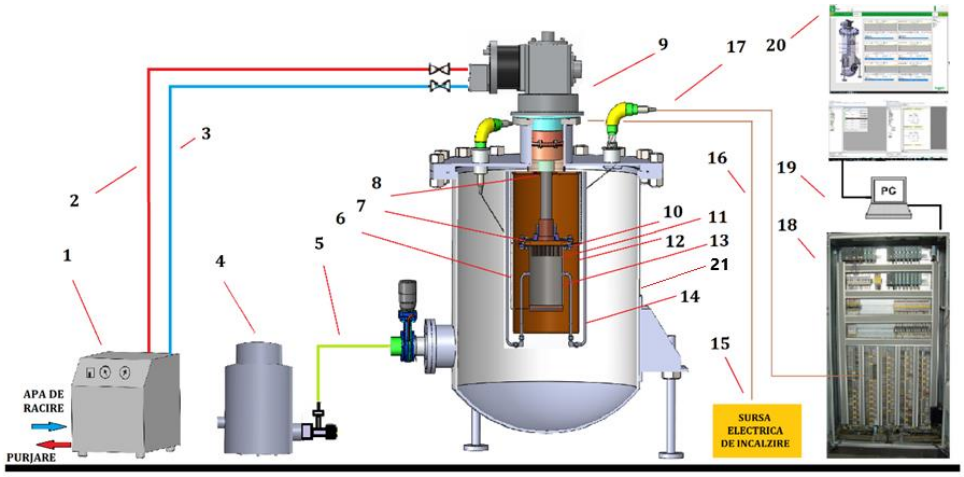


*Figure 4.2.1.1 Scheme of the cryogenic experimental stand for testing the hydrogen condenser*
*1) helium compressor 2) He return route 3) He tour route 4) vacuum pump 5) vacuum route 6) electric heating resistance 7) second cooling stage of GM cryocooler 8) first cooling stage of GM cryocooler 9) cold head of GM cryocooler 10) cold temperature sensor $T_r$ 11) CuOFHC condenser12) thermal radiation protection screen 13) liquefaction chamber 14) gas route 15) electric heating source 16) electrical heating cable route 17) electrical signal cable route to PLC panel 18) PLC panel 19) process calculator SCADA program Vijeo Citect Schneider Electric 20) process data visualization 21) cryostat*

However, the method of testing the various components separately from the distillation column is widely used [14] precisely to allow the verification of a wider range of temperatures and, in the long term, to reach the equilibrium state. So, the new experimental condenser will be tested on a separate stand from the distillation column to which it is dedicated. That is why the condenser must be tested at various operating regimes specific to the separation of different compositions of mixtures. Such a type of testing is necessary in the process of selecting the most efficient shape and size of the most efficient condenser possible from several options.

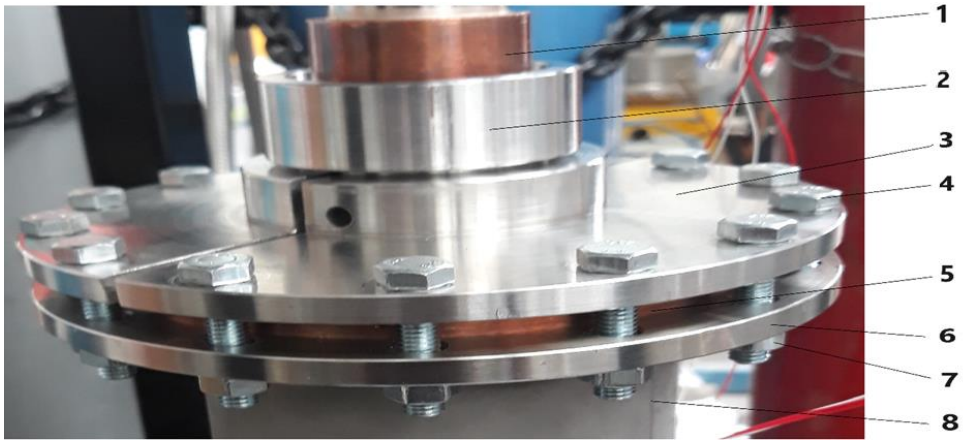


*Figura 4.2.1.2 Screw tightening condenser assembly on liquefaction chamber flange*
*1. cooling stage; 2. mounting nut; 3. upper flange condenser;4. mounting screw; 5. condenser; 6. bottom flange; 7. mounting nut; 8. liquefaction chamber*

The condenser (11) is cooled to a minimum stable temperature of 20 K (fig. 4.2.1.1) inside a test chamber (13) (liquid hydrogen tank) located in a vacuum chamber (10e-6 mbar), namely the cryostat (21). The cryostat chamber is vacuumed by means of the PT (4) turbomolecular pump with vacuum level indication. The GM cryocooler, located in the upper part of the cryostat (21), achieves the minimum liquefaction temperature by means of the coldhead (9) with two cooling stages (7) and (8) respectively. It works with the helium gas that is conveyed and supplied by an F-50 compressor (1) via the helium tour (3) and return (2) routes.

The temperature control reached is achieved by inducing an external temperature produced by an electrical resistance (6) attached to the test chamber (13) ( figure 4.2.1.1). The control of the heating power at the cooling stages is carried out by means of a cryogenic temperature controller monitored and controlled by the PLC module (18). The measurement data are processed by a process computer with Schneider Electric Vijeo Citect SCADA program (19) and visualized (20).

The condensation of hydrogen vapor is achieved, within the experimental cryogenic facility, by means of a thermal conduction-cooled configuration, which consists of a mechanical coupling (fig. 4.2.1.2) between the base of the condenser and the 2nd cooling stage of the

cryocooler. In order to ensure easy handling, the condenser part is mounted on the cold head in the cryogenic test stand by means of a removable screw assembly (fig. 4.2.1.2).

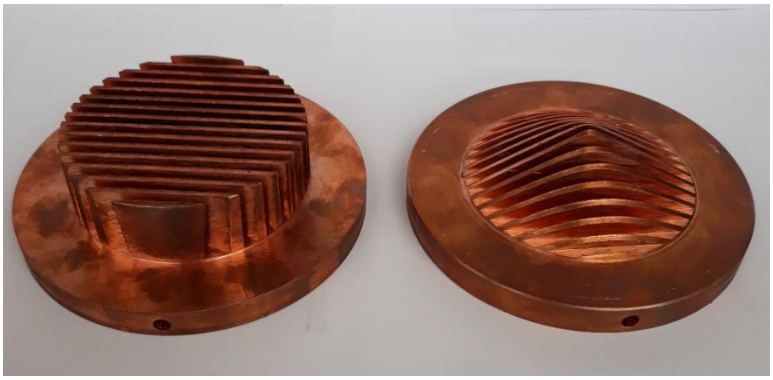

(a) ( b)

*Figura 4.2.1.3 Picture of geometric configuration of hydrogen condensers with fins a) rectangular and b) conical*

The ultimate goal of condenser design is to configure the type of condenser that is close to an ideal heat transfer in case of low average temperatures, i.e. to reduce its thermal resistance as much as possible [40]. Thus, a design solution for increasing the amount of hydrogen vapor condensate on the condenser is the extension of the heat transfer surface of the condenser, the experimental models of the OFHC copper condenser being provided with different configurations of fins and pins for the unobstructed flow of the liquid (fig. 4.2.1.3 and fig. 4.2.1.6).

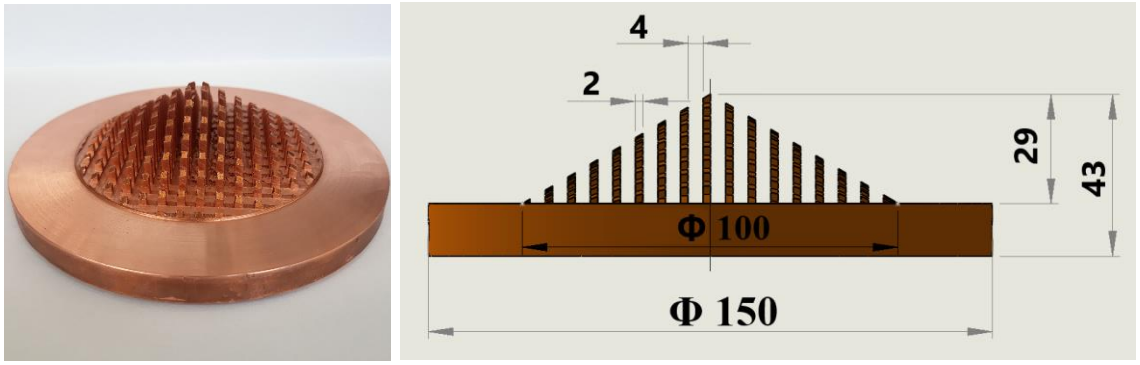


(a) ( b)

*Figure 4.2.1.6 a) Picture b) Dimensional scheme for the geometric configuration of the conical pin condenser tested on the experimental stand*

The vertical orientation of the fins and pins ensures that the droplets of condensed hydrogen slide down easily. The problem with drip condensation is not to achieve it, but rather to sustain it for long periods of time. Thus, in constant operation, the heat transfer between surfaces depends on the sum of the thermal resistances in the direction of the heat flow, and a

high thermal resistance remaining in the system will dominate the heat transfer process [50], even if other smaller resistances have been cancelled (reduced).

### 4.2.2 Experimental method for determining the heat transfer coefficient of the condenser of the hydrogen liquefaction plant

The testing process of hydrogen condensers consists of creating conditions similar to the columns of hydrogen isotope distillation in terms of working parameters, temperature and pressure, and experimenting with conditions for increasing the cooling efficiency of different constructive types of hydrogen condensers.

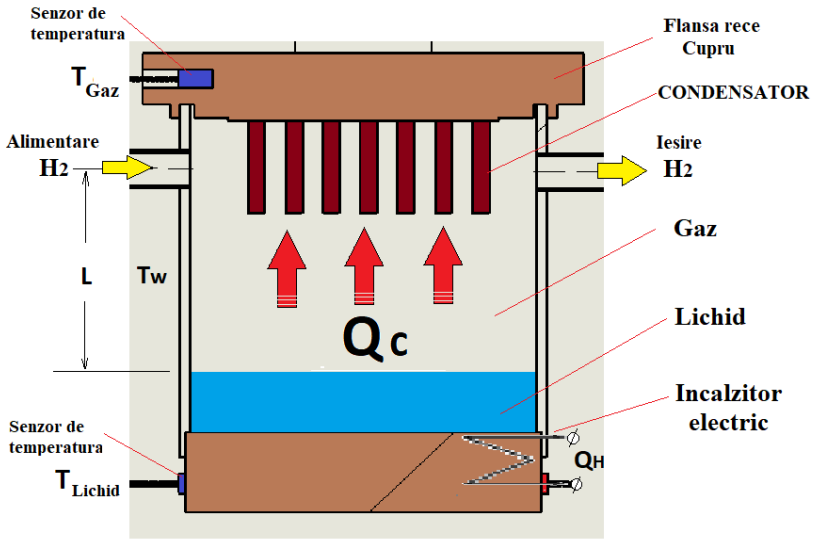


*Figure 4.2.2.1 Experimental method for determining the heat transfer coefficient of the hydrogen condenser for different thermal capacities*

Inside the test chamber, the heat transfer is mostly achieved by thermal conduction, through the condenser surface, from the flange of the second cooling stage of the cryorefrigerator. There is also a convective heat transfer between the gases and the surface of the condensate film. The thermal efficiency of the condenser depends on the value of the total heat transfer coefficient at the contact surface of the ondenser in W/(m2K). When condensing gases on vertical surfaces, the condensation that occurs forms a film on the wall [47] which is continuous for a flat surface (fig. 4.2.2.3).

Due to the formation of this film, condensation resulting from condensation is the main resistance to heat transfer through condensation [50]. In this regard, we have developed a PI&D configuration and a method for testing the experimental condenser models as precise as possible (fig. 4.2.2.1).

Considering the stabilized process (stationary conditions) and a unidirectional heat flow, the amount of heat transferred between:

- the surface of the condenser and the boiling liquid is:

$$\dot{Q}_f = h_f \cdot A_f \cdot \Delta t_f \qquad (4.2.2.3)$$

si

- the surface of the condenser and the condensing vapor is:

$$\dot{Q}_c = h_c \cdot A_c \cdot \Delta t_c \qquad (4.2.2.4)$$

in which:

$h_f$ si $h_c$ = represents the average heat transfer coefficients $h_f$ and $h_c$ in [W/(m2K)] because, in reality, the thickness of the boiling and condensing film varies

$A_f$ si $A_c$ = represents the area of the heat transfer surfaces, depending on the geometry exposed to the gas flow, of the condenser to be tested, in [$m^2$]

The heat flux transferred depends mainly on: latent heat of condensation and condensate vapor flow rate.

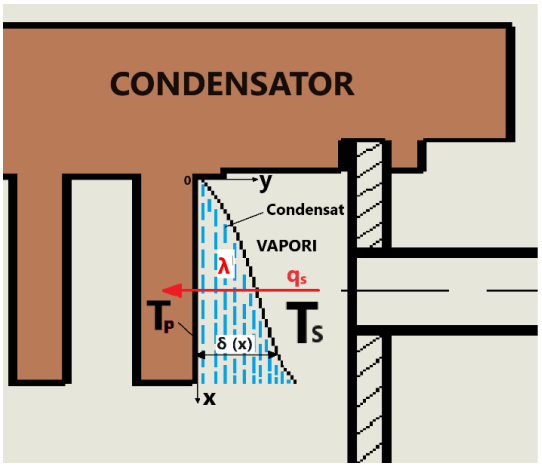


*Figure 4.2.2.3 Representation of film condensation of pure vapour on the vertical surface of the condenser*

The correspondence of real gases and the perfect gas is valid only for certain ranges of pressure, volume and temperature, or in other words, the behavior of real gases is not very correctly modeled by the equation of the perfect gas, which leads to important errors [47]. Taking into account these considerations, for the current real (experimental) case, the density of saturated vapors was calculated using the Redlich-Kwong equation of state [126]:

$$p = \frac{RT}{v-b} - \frac{a}{\sqrt{T}\, v(v+b)} \qquad (4.2.2.7)$$

where:

R = 8314 is the universal constant of gases in [ kJ/kmol K]

a si b = are constant values [126] specific to hydrogen in the normal state n-$H_2$:

$$a = 0.4275 \frac{R^2 T_k^{2.5}}{p_k} \quad (4.2.2.8)$$

$$b = 0.0867 \frac{RT_k}{p_k} \quad (4.2.2.9)$$

$P_k$, $T_k$, $v$ = parameters of the critical state of the gas, according to NIST [73]

The Redlich–Kwong equation has the advantage of using only two constants in computation to correctly estimate the behavior of real gases [126] at high pressures and temperatures higher than critical. The heat of vaporization is calculated by means of the Clapeyron-Clausius equation [47]:

$$\frac{dp_{vap}}{dT} = \frac{\Delta h_v}{T \Delta v_v} \quad (4.2.2.10)$$

According to Mittelhauser [126], on the saturation curve of hydrogen and its isotopes the pressure varies as a function of temperature after the relationship:

$$log p_{vap} = A + \frac{B}{T} + C \cdot logT + D \cdot \frac{p}{T^2} \quad (4.2.2.11)$$

Replacing *eq. (4.2.2.11) in eq. (4.2.2.10*) the equation of the enthalpy of vaporization is obtained:

$$h_{fg} = \Delta v_v \left[ \frac{C \cdot T^2 - B \cdot T - 2 \cdot D \cdot p}{\frac{T^2}{P} - D} \right] \quad (4.2.2.12)$$

where:

$\Delta v_v$ = represents the calculated difference between the specific volume of the gas in the vapor state and the specific volume of the liquid phase, in [$m^3$/kg]

p, T = parameters measured during the process

A, B, C, D = are specific constant values for hydrogen in the normal state n-$H_2$

The experimental method involves comparing the heat transfer coefficients at condensing $h_c$, obtained experimentally, to determine the performance of the different types of condensers tested.

## 4.4 CONDUCTING PRELIMINARY PERFORMANCE TESTS FOR DETERMINING THE COOLING CAPACITY OF GM RDK-415D CRYOCOOLER IN THE CONDNESER TEST FIELD

From the refrigeration capacity diagram of the GM SRDK-415D cryocooler [49], the cooling capacity of the 2nd stage can be visualized up to 25 K. In order to achieve these special temperatures up to 35K, higher than those contained in its load diagram, the operating temperature range for the GM cryocooler mounted on the current cryogenic experimental stand

was determined by performing additional performance tests and in the Cryogenics Laboratory (fig. 4.4.1).

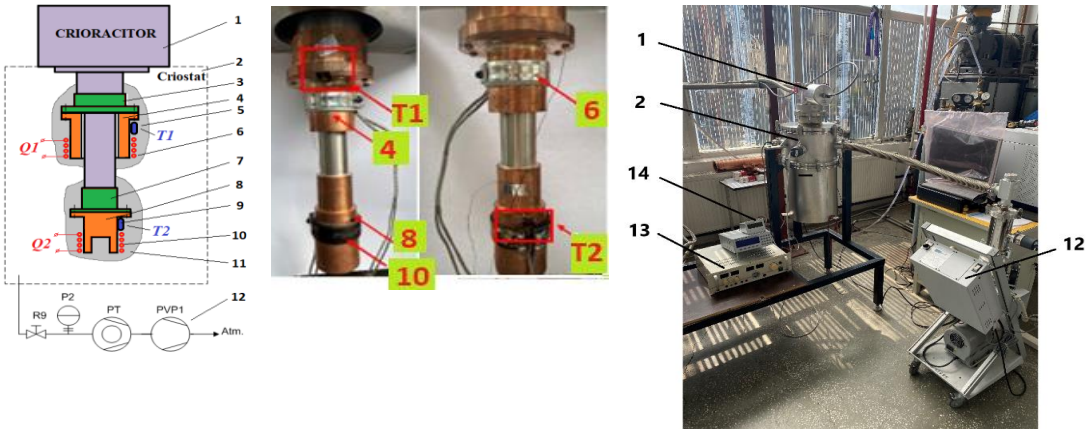


(a) ( b)

*Figure 4.4.1.a) Mounting scheme for the SRDK-415D cryocooler performance test*
*b) Pictures of the experimental configuration of the performance test*
*1. GM cryocooler cold head; 2. Cryostat 3. Cold head stage I; 4. Adapter stage I (intermediate copper parts for the heater); 5, 9. Temperature sensors; 6.10. Electric heaters 7. Cold head stage II; 8. stage II adapter (copper intermediate parts for the heater);11. Vacuum thermal insulation area 12. Vacuum pump system (turbomolecular vacuum pump);13.Temperature controller, model 54 Cryo-Con; 14. Vacuum level indicator for cryostat; $T_1$ - Temperature sensor on stage 1; T2- temperature sensor on stage II;*

Performance tests use the method of inducing varying thermal loads at the two cooling stages of the cryocooler until the planned temperatures are reached (fig.4.4.4).

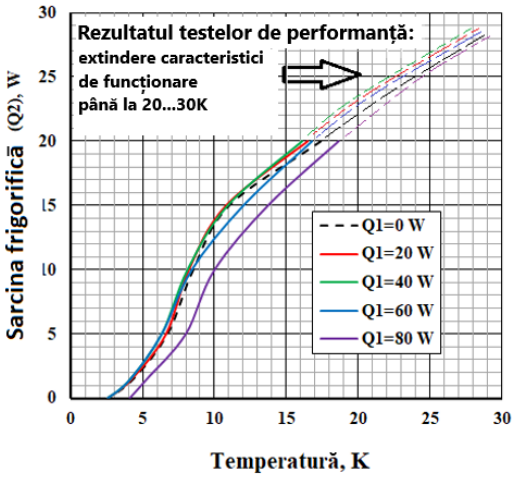


*Figure 4.4.4 Extended cooling capacity of the SHI GM RDK-415D cryocooler [49] and domain of experimental results.Q1 and Q2 represent the capacities for the 1st and 2nd cooling stages*, respectively

## 4.4.1 Alternative method of estimating the capacity and condensation rate of GM RDK-415D cryocooler

*Table 4.4.1.1 Calculation for the determination of the cooling capacity of the GM SRDK 415D cryocooler*

| | **Cooling capacity at 2nd stage** | **Cooling capacity at stage 1** | **Carnot's theoretical efficiency** | **Equivalent cooling capacity at stage 2** | **Equivalent cooling capacity at stage 1** |
|---|---|---|---|---|---|
| T[K] | $Q_{c\ (tr.2)}$ [W] | $Q_{c\ (tr.1)}$ [W] | η[%] | $Q_{echiv.\ (tr.\ 2)}$ [W] | $Q_{echiv.\ (tr.\ 1)}$ [W] |
| **4.2** | **1.5** | | 0.0142 | **55.6** | |
| *20* | 22 [a] | | 0.0714 | **162** | |
| 22.4 | 26 [b] | | 0.0807 | 169.5 | |
| **50** | | **35** | 0.2000 | | **92** |
| *96* | | 80 [b] | 0.4706 | | **89.4** |
| 103.4 [c] | | | 0.5259 | | |

*a) experimental data*
*b) data extrapolated from the cryocooler manufacturer's power diagram [49]*
*c) the average logarithmic temperature calculated according to eq. 4.4.1.8*

The results of the cryo-referer performance tests *(fig. 4.4.4)* show values close to the estimated results. Thus, at the temperature of 20K, the performance tests resulted in a cooling capacity (*fig. 4.4.4*) with a condensation rate of 0.0116 g/s (0.60 L/h) compared to the one estimated by this method *(table 4.4.1.2)* of 0.0165 g/s (0.83 L/h). Also, the thermal calculation performed after pre-dimensioning (*Chapter 5.5.3*) resulted in a condensation rate of 0.0124 g/s (0.61 L/h).

Table 4.4.1.2 Values obtained for the condensation rate of the GM SRDK 415D cryocooler

| **Calculation method** | **Condensation rate** | |
|---|---|---|
| | (g/s) | (L/h) |
| Alternative calculation method | 0.0165 | 0.83 |
| Thermal calculation method | 0.0124 | 0.61 |
| Experimental method | 0.0116 | 0.60 |

The estimation method explains within reasonable limits both the experimental and theoretical verification results, so it can be used as an alternative method for pre-dimensioning the liquefaction installation according to the condensation rate.

# 5. THEORETICAL MODEL OF THE CONDENSER

## 5.4 TOTAL LOAD OF CRYOGENIC INSTALLATION

The total thermal load of the cryogenic installation (*tab. 5.4.1*) is calculated by taking into account all thermal loads [57] (in the solid structure, electrical conductors, waste gas and external radiant walls of the cryostat), the heat transfer being carried out in three ways:

(a) thermal conduction (through solid structures, electrical conductors – the Joule effect),

(b) thermal radiation (through the space between the equipment and the radiant walls),

(c) convection (through liquids and waste gas)

*Table 5.4.1 Estimated cryostat heat load of the cryogenic installation*

| Component | Heat Load / Power [W] | Temperature [K] |
|---|---|---|
| Cryostat Walls Radiation at 300K | 5.22 | |
| Passage neck in the test room at 300K | 11.92 | |
| Measuring instrumentation | 0.6 | |
| Gas line in the sample chamber at 300K | 0.013 | |
| TOTAL ( Heat load at 20K ) | **17.71** | |
| GM cryocooler power achieved at 20K | 22 | ~20 |

Thus, the total heat balance of the cryostat is:

$$\dot{Q}_H = \dot{Q}_c + \dot{Q}_r + \dot{Q}_g + \dot{Q}_l = 11.92 + 5.18 + 0.013 + 0.6 \quad (5.4.1)$$

$$\dot{Q}_H = \mathbf{17.71\ W} \quad (5.4.1')$$

unde:

$\dot{Q}_H$ = the thermal load of the cryostat,in [W]

$\dot{Q}_c$ = heat flux due to thermal conduction of the supporting surfaces, in [W]

$\dot{Q}_r$ = heat flux due to thermal radiation, in [W]

$\dot{Q}_g$ = heat due to thermal conduction through waste gases, in [W] and

$\dot{Q}_l$ = the heat flux generated by the Joule effect, in [W]

In the calculation for the final result, the specifics of the cryogenic installation [42] were taken into account and the load reductions due to the improvement methods presented were not taken into account. There are two methods in this regard that have reduced the thermal load by approximately 3.61 W by:

a) achieving a high vacuum by reducing the gas pressure in the cryostat and implicitly significantly reducing the heat transfer through gas convection;
b) the introduction of radiation screens that halves the heat exchange from thermal radiation.

The thermal load of the major components of the thermal conduction-cooled cryostat of 17.71 W can be supported by the 22 W capacity at 20 K of the Gifford McMahon cryocooler used *(Table 4.5.1)* resulting from the additional tests carried out to determine the extended cooling capacity of the GM SHI GM RDK-415D cryocooler [49] *( fig. 4.4.4.)*.

### 5.5.3.1 Determination of the maximum evaporation rate of liquid hydrogen in the liquefaction chamber

Under the conditions of proper sealing and a high vacuum level (greater than $10^{-3}$ Pa), conductive transfer *(Table 5.4.1 )* through the cryostat neck is considered to be the main factor in the evaporation of liquid from the tank (*eq. 5.2.17*):

$$\dot{Q}_c = 11.92\ W \qquad (5.6.3.1.1)$$

The evaporation rate of hydrogen due to the thermal conduction load is:

$$\dot{m}_{ev.cond} = \frac{\dot{Q}_c}{\lambda_{lat_{H2}}} = \frac{11.92\ (\frac{J}{s})}{448.710\ (\frac{J}{g})} = \mathbf{0.026}\ \left[\frac{g}{s}\right] \qquad (5.6.3.1.2)$$

$$= 1.35\left[\frac{L}{h}\right] \qquad (5.6.3.1.4)$$

where:

$$\lambda_{lat_{H2}} = 448.71\ [\mathrm{J/g}] \qquad (5.6.3.1.6)$$

= is the latent heat of hydrogen vaporization [73], under operating conditions (*rel. 5.2.4*)

$$\rho_{H2} = 70.922\ [g/L] \qquad (5.6.3.1.7)$$

= represents the density of hydrogen at the average liquefaction temperature at $T_{Lm}$=20.307 K [73] under operating conditions (*rel. 5.2.4*)

## 5.6.3 Calculation of condenser height according to condensation rate on condenser head

In the first stage of the condenser sizing calculation of the hydrogen liquefaction plant, the dimensions of the flange diameter (base plate) ($D_c$) and the height of the condenser ($L_c$) are chosen from practical experience. The calculations presented in the previous chapters on the evaluation of the thermal load (*chapter 5.1)* and the determination of the thermal losses (*chapter 5.5)* and the evaporation and condensation rates (*chapter 5.5.3*) shall be performed.

After performing the calculations, it is determined:

(a) the capacity of the installation to sustain the thermal load under refrigeration efficiency conditions *(chapter 5.1 and chapter 5.5*)

(b) a theoretical average heat transfer coefficient of the vapors condensing at the condenser surface and forming the laminar film layer (*chapter 5.6*)

as follows.

At the end of the first design stage, the following is calculated:

(i). the heat flux of the condensing vapour at the surface of the condenser (film layer) according to the Newton relation *(eq. 5.6.2.2):*

$$\dot{Q} = h_{vert} \cdot A \cdot (T_{sat} - T_s) \qquad (5.6.3.1)$$

$$\dot{Q} = 4463.1 \cdot 0.0098 \cdot (20.368 - 20.245)$$

$$Q = \mathbf{5.38\ W} \qquad (5.6.3.2)$$

(ii). condensation rate on the condenser head:

$$\dot{m}_{th} = \frac{\dot{Q}}{h'_{fg}} = \frac{5.38}{449.524}$$

$$\dot{m} = \mathbf{0.012}\ \left[\frac{g}{s}\right] \qquad (5.6.3.3)$$

under the initially imposed dimensional conditions: the diameter of the base plate ($D_c$) and the height of the condenser ($L_c$) considered established by design.

where:

$A_c$ = represents the surface area of the condenser,in [$m^2$]

$$A_c = \pi \cdot D_c \cdot L_c = 3.14 \cdot 0.010 * 0.029 = 0.0098\ m^2 \qquad (5.6.3.4)$$

$D_c$ = 0.0108 m represents the diameter of the condenser base plate considered established as the distillation column design requirement, in [m] (*fig. 4.1.2.5.2 si 4.1.2.5.3)*

$L_c$ = 0.029 m represents the height of the condenser, in [m] (*fig. 4.2.1.6* )

$T_{sat}$ = 20.368 K represents saturation temperature $H_2$ to the pressure 0.1013Mpa (*cf.rel.5.2.4)*

$T_s$ = 20.245 K represents the average liquefaction temperature at the surface of the condneser (*cf.eq.5.2.4)*

$h'_{fg} =$ 449.524 $\left[\frac{J}{g}\right]$ represents the modified latent heat of vaporization $h_{fg}$, (*cf. eq. 5.6.2.12),* in [ kJ/kg]

In the second design step, a real condensation rate resulting from experiments carried out under the same pressure and temperature conditions is chosen *(cf.rel.5.2.4).*

From the experimental data, the condensation rate of $\dot{m}_{re} = 0.009$ g/s resulted and the heat transferred for the condensation of hydrogen gas is calculated as:

$$\dot{Q}_{re} = \dot{m}_{re} \cdot h'_{fg} = 0.009 \cdot 10^{-3} \cdot 449.524 \quad (5.6.3.5)$$

$$\dot{Q}_{re} = \mathbf{4.05\ W} \quad 5.6.3.6)$$

From the expression of the heat flux *(eq. 5.6.3.1)* the area of the surface necessary for the vapors to condense at the surface of the condenser (film layer) with an experimentally resulting condensation rate $\dot{m}_{re} = 0.009$ g/s is calculated:

$$A_{cond} = \frac{\dot{Q}_{re}}{h_{vert} \cdot (T_{sat} - T_S)} = \frac{4.05}{4463.1 \cdot (20.368 - 20.245)} \quad (5.6.3.7)$$

$$A_{cond} = \mathbf{0.0074\ m^2} \quad (5.6.3.8)$$

From which it follows,

for a design-determined diameter of the condenser base plate (*fig. 4.2.1.6* ):

$$D_c = 0.0108 \text{ m} \quad (5.6.3.9)$$

Effective condenser height $L_c$:

$$L_{cond} = \frac{A}{\pi \cdot D_{cond}} = \frac{0.0074}{3.14 \cdot 0.0108}$$

$$L_{cond} = \mathbf{21.8\ mm} \quad (5.6.3.10)$$

It is noted that for the calculated heat exchange level, the effective (actual) length of the condenser is shorter than initially designed. This fact can be explained in two ways:

a) There is a higher heat flow but the lower part and the peripheral part of the condenser have a role for pre-cooling the heat flow.
b) Theoretical calculation does not take into account all process data.

# 6. GEOMETRIC OPTIMIZATION OF THE CONDENSER BY MINIMIZING THE PRODUCTION OF ENTROPY

The increase in the refrigeration performance of the condenser is achieved in two ways: intensifying the heat transfer to the condenser surface (increasing the vapor condensation rate) in the first phase and then stabilizing the parameters on a level in order to ensure a constant condensate rate. The two ways of thermal efficiency of the process can be achieved through technical solutions [128]:

*a)* decreasing the thermal resistance of the thermal transfer surface
*b)* expansion of the heat transfer surface of the condenser
*c)* use of a very good thermally conductive material for the condenser at low temperatures (cryogenic).

Therefore, the application of the technical solutions from *letters b) and c)*, above, is conditioned by the resolution of the requirement from *letter a)*: *the decrease of the thermal resistance of the thermal transfer surface*.

Respecting this concept, the design of the condenser with an extended heat transfer surface in the form of fins or pins, which cools at the process temperature, does not guarantee its good thermal efficiency, even if a convection coefficient more than 10 times higher [50] is achieved due to the drip condensation process, i.e. the breaking of the continuous liquid film and the formation of only droplets of different diameters. It may be necessary to adjust the dimensional, material and functional parameters of this heat exchanger in order to obtain an optimized condenser option that will increase the refrigeration efficiency of the system as a whole (by taking into account *points b) and c) above*), because the problem of drip condensation is not to achieve it, but rather to sustain it for long periods of time [50]. Thus, in order to improve the performance of the condenser, in relation to the design criteria, several independent variables can be modified, such as the material properties (thermal conductivity), the properties of the working gas (viscosity, thermal conductivity density), the dimensions of the base flange as well as the dimensions and number of pins. However, the improvements made must be interlinked with each other in order to achieve an optimal effect. The pressure drop $\Delta P$ on the condenser during the heat exchange process represents the path that needs to be carefully investigated. This is due to the fact that, for a pressure drop that is too high, there is a possibility that the gas vapor will bypass the condensing surface or the thermal contact will be made with a lower volume of vapor (*fig. 6.2.1*).

The condensation of vapors on the surface of the condenser leads to the formation of a condensate film that covers the entire heat transfer area and accumulates over time. This phenomenon leads to a decrease in the heat transfer rate by increasing the thermal resistance of the condenser.

On the other hand, if only one parameter is optimized and the other design parameters are imposed, an optimized design solution can be identified, but one that is not robust and is not always efficient when other design parameters vary. Thus, in constant operation, the heat transfer between surfaces depends on the *sum of the thermal resistances in the direction of the heat flow*, and a large thermal resistance remaining in the system can cover all the others and dominate the heat transfer process [50]. In such cases, improving the level of a lower thermal resistance (such as that due to condensation or boiling) but not other types of thermal resistances in the system makes the improvement of the overall heat transfer coefficient

insignificant. The performance of a condensing heat exchanger depends [130] on *the total resistance of the condenser* and the *pressure drop* on the cooling head.

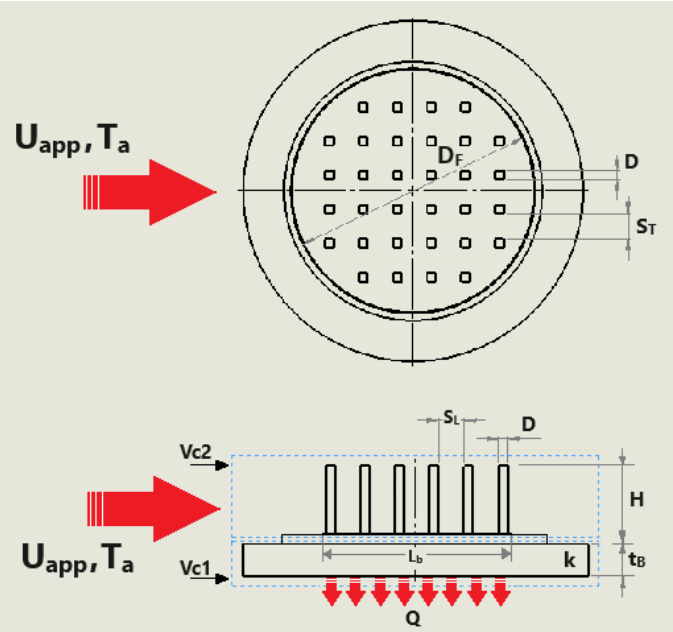


*Figure 6.2.1 Scheme of the in-line pin condenser in contact with the gas flow Q - the thermal load of the condenser; $U_A$ and $T_a$ - gas inlet speed and temperature $S_T$ and $S_L$ - transverse and longitudinal pitch of the pins, D and H - side of the square section and height of the pin, tb - width of the baseplate, $D_f$ - diameter of the flange supporting the baseplate, $V_{c1}$ and $V_{c2}$ - control volume calculation of pins and base plate for the energy balance*

The objective of this chapter is to identify the point at which the optimization of a minimum number of parameters leads to the simultaneous optimization of both of the above properties, in order to achieve the thermal performance of the condenser. Therefore, considering the accumulation of factors that influence the general heat transfer coefficient (geometric shape, heat transfer surface characteristics, material), it is necessary to exergetic optimization of the condenser by minimizing the production of entropy and maximizing the useful effect of the heat transfer process at the condenser level.

## 6.6 MPE MATHEMATICAL MODEL FOR PIN ARRAY CONDENSER GEOMETRY OPTIMIZATION

Unlike the exergetic method, the entropy production minimization (EPM) method, used in this chapter, consists [78] of combining thermodynamic principles and methods with those of heat transfer, fluid mechanics, and other transport processes.

In the cryogenic field of low-temperature cooling, methods of minimizing irreversibility [78] are often used as optimization and design processes, due to the high generation of entropy mainly as a result of this large temperature difference with respect to the ambient environment.

By applying the laws of conservation of mass and energy with the entropy equilibrium equation for a fluid flowing over a condenser (*fig. 6.6.1*), the expression of the rate of entropy generation [78] for a fluid flowing over a condenser (*fig. 6.6.1*) has the expression:

$$\dot{S}_{gen} = \left(\frac{Q^2}{T_a \cdot T_b}\right) R_{hs} + \frac{\dot{m} \cdot \Delta p}{\rho \cdot T_a} \qquad (6.6.1)$$

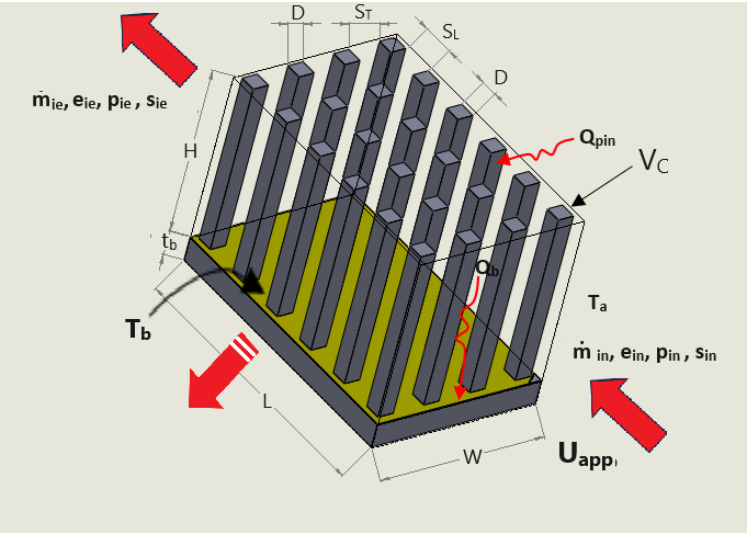


*Figure 6.6.1 Control volume for entropy generation rate calculation $\dot{S}_{gen}$ in the case of a rectangular pin array in contact with the gaseous hydrogen flow*

where: it is observed that the rate of entropy generation depends only on:

- condenser resistance and
- pressure drop on pins,

with simplifying conditions:

- established pin geometry,
- known heat load and
- certain constant thermophysical properties of the fluid

and where:

$R_{hs}$ = represents the total thermal resistance of the condenser, in [K/W] determined by the equation:

$$R_{hs} = R_m + R_{fins} \qquad (6.6.2)$$

$R_m$ = represents the strength of the material, in [K/W]

$\dot{m}$ = represents the unit mass flow of gas over the pin network,in [$m^3/s$]

$\Delta p$ = represents the total pressure drop on the surface of the condenser (hydraulic resistance), in [Pa]

$T_a$ = represents the ambient temperature,in [K]

$T_b$ = represents the temperature of the baseplate, in [K]

$R_{hs}$ = represents the total resistance of the pins and the baseplated exposed to heat transfer, in [K/W] and is calculated with *eq. ( 6.5.4)*

$\rho$ = represents the density of the fluid at medium temperature, in [$kg/m^3$]

The form *eq. (6.5.46)* can be simplified to obtain the final version of the dimensionless entropy generation rate as follows:

$$N_s = \frac{\dot{S}_{gen}}{Q^2 \cdot U_{app} / k \cdot \nu \cdot {T_a}^2} = \frac{C_8}{Re_D} + \frac{1}{2} C_{10} \cdot B \cdot \gamma \cdot Re_D^2 \quad (6.6.17)$$

where:

$C_8$, $C_9$ si $C_{10}$ = represent constants determined with the equations:

$$C_8 = \frac{T_a}{T_b}\left[\frac{\psi}{\sqrt{\epsilon_2 \cdot N \cdot S_L \cdot S_T}} + \frac{1}{C_9\left(\frac{k_f}{k}\right) Re_d^{1/2} Pr^{1/3}}\right] \quad (6.6.18)$$

$$C_{10} = N_T \frac{S_T^3}{(S_T - 1)^2}(f \cdot N_L + k_c + k_e) \quad (6.6.19)$$

where:

$C_9$ = is the constant determined with the equations:

$$C_9 = N\left[\pi \cdot C_1 \cdot \gamma \cdot \eta_{fin} + \frac{0.75}{\sqrt{N_L \cdot S_L}}\left(S_T \cdot S_L - \frac{\pi}{4}\right)\right] \quad (6.6.20)$$

$\psi$ = represents the determinate constant with the relationship:

$$\psi = \frac{\epsilon \cdot \tau}{\sqrt{\pi}} + \frac{1}{2} \cdot (1 - \varepsilon)^{\frac{1}{2}} \quad (6.6.21)$$

unde:

$\epsilon$ = represents the constant determined by the relationship:

$$\varepsilon = \frac{a}{b} \quad (6.6.22)$$

in which:

$$a = \sqrt{\frac{A_s}{\pi}} \quad (6.6.23)$$

$$b = \sqrt{\frac{A_b}{\pi}} \quad (6.6.24)$$

$A_s$ = Base plate section Area, in [$m^2$]

$A_b$ = the area of the base plate section excluding the base surface of the pins, in [$m^2$]

$\varepsilon_2$ = represents the fraction of the surface covered by the cold source on the baseplate

$C_1$ = represents the constant determined by *eq. ( 6.5.45)*

$S_L$ = the distance between pins in the longitudinal direction (longitudinal pitch),in [m]

$S_T$ = distance interpins in transverse direction (longitudinal pitch), in [m]

$\gamma$ = represents the dimensionless ratio according to *eq. 6.3.6*:

$$\gamma = \frac{H}{D} \tag{6.6.25}$$

D = represents the side of the pine,in [mm]

H = represents the height of the pine, in [m]

## 6.7 WORDING OF THE OPTIMIZATION PROBLEM

We consider the function f (xi,Pi) which represents the *rate of generation of entropy* and whose minimum must be determined taking into account the limitations:

- of equality: $g_j(x_i,P_i) = 0$ and ( 6.7.1)
- de inegalitate: $l_k(x_i,P_i) \geq 0$ ( 6.7.2)

The values of the following terms of the equation are established as constant values as follows:

- L = 0.108 m (baseplate length) ( 6.7.3)
- W = 0.108 m (baseplate width)
- l×w = 0.050 x 0.050 m (dimensions of the heat source)
- Q = 22 W ( thermal load)
- $T_a$ = 300 K ( ambient temperature)

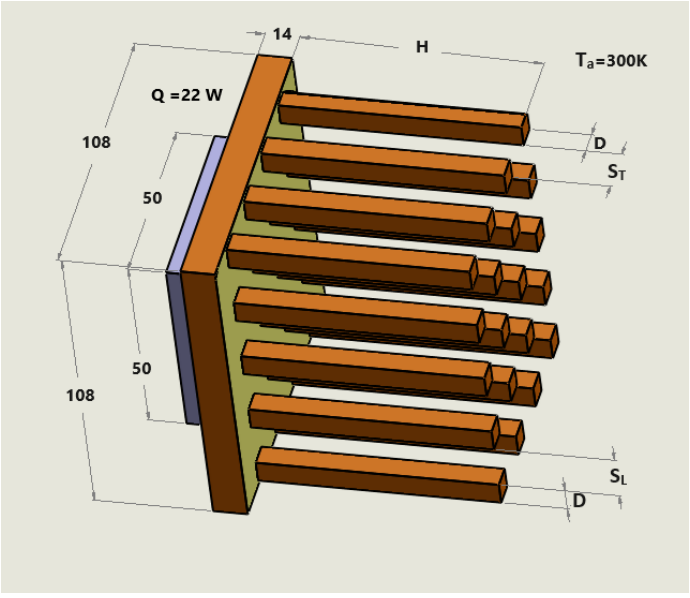


*Figure 6.7.1 Constant dimensions and optimized dimensions of the rectangular section pin array condenser*

Depending on these values, the other geometric (dimensional) or hydraulic variables of the condenser are optimized in this study as follows::

- side of the pine section ( D ) ( 6.7.4)
- pine height (H )
- pin density on the baseplate( N )
- local speed ( $U_{app}$ ) (resulting from the optimal geometric configuration)

The detailed general form of the optimization problem is as follows:

$$minim\ f(x_i, P_i) = \dot{S}_{gen}(x_i, P_i) \quad (6.7.5)$$

with the limitations of equality:

$$g_j(x_i, P_i) = o,\ j = 1,2 \dots, m \quad (6.7.6)$$

and the limitations of inequality:

$$l_j(x_i, P_i) \geq o,\ j = 1,2.., p \quad (6.7.7)$$

where:

$g_j$ si $l_j$ - are the constraints imposed by equality and inequality

$x_i$ - represents the vector of the design variables $(x_1, x_2, x_3, \dots, x_n)^T$ and what are:

$$x_i = [\ D, H, N, Uapp] \quad (6.7.8)$$

$P_i$ - represents the vector of the parameters ( $P_1, P_2, P_3, \dots, P_n$ )$^T$ . The parameter Pi is considered to be the thermal conductivity k [W/(m·K)] of the condenser material.

Equality limitations as equations of the model are given by:

$$C_8 = \frac{T_a}{T_b}\left[\frac{\psi}{\sqrt{\epsilon_2 \cdot N \cdot S_L \cdot S_T}} + \frac{1}{C_9\left(\frac{k_f}{k}\right)Re_d^{1/2}Pr^{1/3}}\right] \quad (6.7.9)$$

$$C_{10} = N_T \frac{S_T^3}{(S_T-1)^2}(f \cdot N_L + k_c + k_e) \quad (6.7.10)$$

$$C_9 = N\left[\pi \cdot C_1.\gamma \cdot \eta_{fin} + \frac{0.75}{\sqrt{N_L \cdot S_L}}\left(S_T \cdot S_L - \frac{\pi}{4}\right)\right] \quad (6.7.11)$$

and the limitations of inequality are defined as follows:

$$\eta_{fin} - 0.75 \geq 0 \quad (6.7.12)$$
$$Re_D - 1000 \leq 0$$
$$H - 0.03\ (m) \leq 0$$
$$0.5 \leq U_{app}\ (m/s) \leq 6$$
$$1 \leq D\ (mm) \leq 3$$
$$1.25 \leq S_L \leq 3$$
$$1.25 \leq S_T \leq 3$$
$$3 \leq \gamma \leq 8$$

unde:

$\eta_{fin}$ = represents the efficiency of a pine that is determined [74] with *eq. 6.5.38*

$Re_D$ = the dimensionless Reynolds criterion

$H$ = pine height,in [m]

D = represents the side of the pine, in [mm]

H = represents the height of the pine, in [m]

$U_{app}$ = reprezintă viteza locala in vecinătatea pinului, in [m/s]

$S_T$ = pitch between pins transverse in the direction of flow, in [m]

$S_L$ = pitch between pins longitudinally in the direction of flow, in [m]

$\gamma = \frac{H}{D}$ = represents the dimensionless ratio according to eq. 6.3.6

For the nonlinear equation, presented above, the objective function has been established as:

$$L(x_1 \dots., x_n, \lambda_1 \dots., \lambda_p, \sigma_1 \dots., \sigma_{p-m}) = f(x_i) + \sum_{j=1}^{m} \lambda_j g_j(x_i) + \sum_{k=m+1}^{p} \lambda_k [l_k(x_i) - \delta_k] \quad (6.7.13)$$

where:

$x_i$ = represents the vector of the variables $(x_1, x_2, x_3, \dots., x_n)^T$: $x_i$ =[ D, H, N, Uapp] *(cf. eq. 6.7.8)*

$g_j(x_i)$ = represents the vector of equality limitations *(cf. eq. 6.7.9÷6.7.11)*

$l_k(x_i)$ = represents the vector of inequality limitations *(cf. eq. 6.7.12)*

$\lambda_{j,k}$ = represent the Lagrange multipliers and

$l_k(x_i) - \delta_k$ = represents the expression of the constraints of inequality: $l_k(x_i) \geq \delta_k$ ( eq. 6.7.12) in the form : $l_k(x_i) - \delta_k \geq 0$ (introduction of the Karush-Kuhn-Tucker conditions for generalizing the Lagrange method )

Given the fact that there are also general constraints of inequality, the generalized form of the Lagrange method using the Karush-Kuhn-Tucker (KKT) conditions was used to define the above objective function, in order to identify the extremes of this function (subject to both types of constraints). The explanation is given by the fact that Lagrange multipliers only take into account equality constraints while KKT conditions allow for general inequality constraints.

## 6.8 OPTIMIZATION TECHNIQUE

The optimization problem *(eq. 6.7.13*) boils down to solving the following system of equations:

$$\frac{\partial L}{\partial x_i} = 0 \qquad i = 1, \dots, n \quad (6.8.1)$$

$$\frac{\partial L}{\partial \lambda_j} = 0 \qquad j = 1, \dots, m \quad (6.8.2)$$

$$\frac{\partial L}{\partial \sigma_k} = 0 \qquad k = 1, \dots, p - m \quad (6.8.3)$$

The above system of equations is solved by numerical methods, respectively the Newton Raphson multivariable method. This method was presented by Stoeker [89] and applied to the limited optimization of the entropy generation rate [130]. A procedure was performed in the mathematical software Mathcad 9 that solves the system of N nonlinear equations using the Newton-Raphson multivariable method. Given the Lagrange function L, a vector of the solution [x], an initial estimate [$x_0$] and a maximum number of Nmax of 218 iterations, the procedure applies the Newton-Raphson method systematically within the limit of the maximum number of iterations until the established convergence criteria are reached. The method is quite robust, provided that an adequate initial assumption is made.

## 6.9 THE OPTIMAL SOLUTION AND THE SENSITIVITY OF THE RESULTING SOLUTION

The next step is to check if $x^*$ is a minimum point and not a stationary point or even a maximum, because the Lagrange function can present a *saddle* point with respect to x, $\lambda^*$ and $\sigma^*$ at the optimal level. The necessary condition applied for $x*$ to be a local minimum of the problem, is that the *Hessian* matrix of L is positive, i.e.:

$$v^T \Delta^T [L(x^*, \lambda^*, \sigma^*)] v \geq 0 \quad (6.9.1)$$

The condition for the identified local minimum to be a global minimum is that all *eigenvalues* of the Hessian matrix are positive [89]. The Lagrange method is effective in the sense of analyzing the sensitivities of the parameters in problems where multiple constraints arise.
The sensitivity indication of the objective function L is as: $\partial L/\partial p0$, where the sensitivity of the location of the optimal is expressed as: $\partial xi/\partial p0$, where $p_0$ is the model parameter.
Value:

$$\partial L/\partial p_0 = 0 \quad (6.9.2)$$

indicates in most cases, that as the parameters change, the value of the objective function changes, but the value:

$$\partial xi/\partial p_0 = 0 \quad (6.9.3)$$

which proves that the location of the optimal *is not a function of the parameters.*

## 6.10 RESULTS AND CONCLUSIONS

The objective of the optimization is to identify the best condenser for the base plate that is 108 x 108 mm in size and has an optimal height in relation to the size of the pin side. The conditions at the external limit are established as the ambient temperature of 27°C and the cooling power cold source of 22 W. Different thermal conductivities of the materials aluminum, 237 W/m·K and copper (401 W/m·K) are considered for comparison.

The problem is analyzed as a multivariable optimization in which there are three design variables:

- Size D of the side of the pine in [mm],
- Height H of the pin, in [mm] and
- Local velocity of hydrogen gas (at pins) Uapp, in [m/s].

In the first phase of the optimization process, one of the design variables is kept constant, while the other two parameters vary in the range imposed by the limiting conditions.

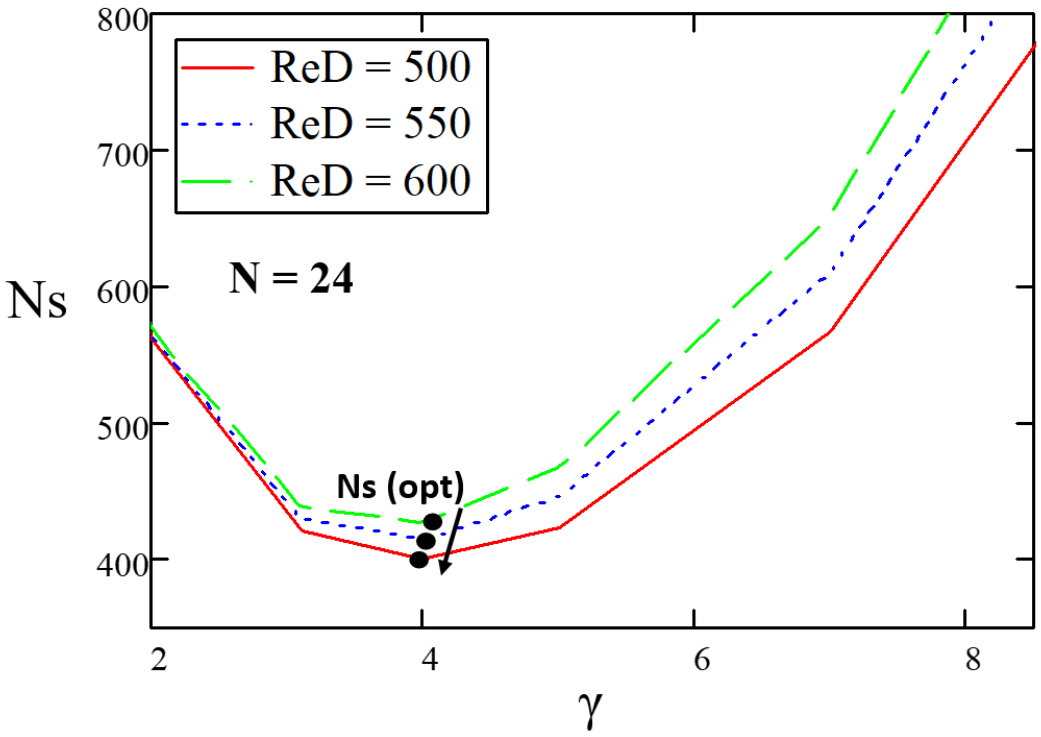


*Figure 6.10.1 Dimensionless rate of entropy generation as a function of geometric ratio γ and Reynolds number*

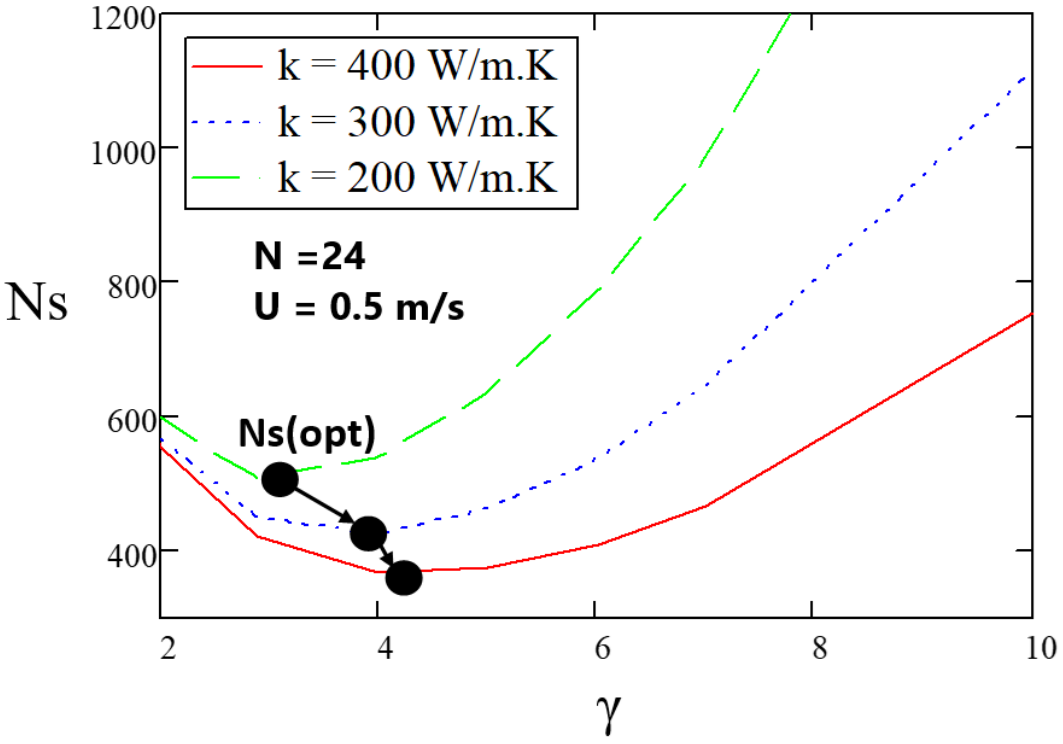


*Figure 6.10.2 Dimensionless rate of entropy generation as a function of geometric ratio γ and material thermal conductivity*

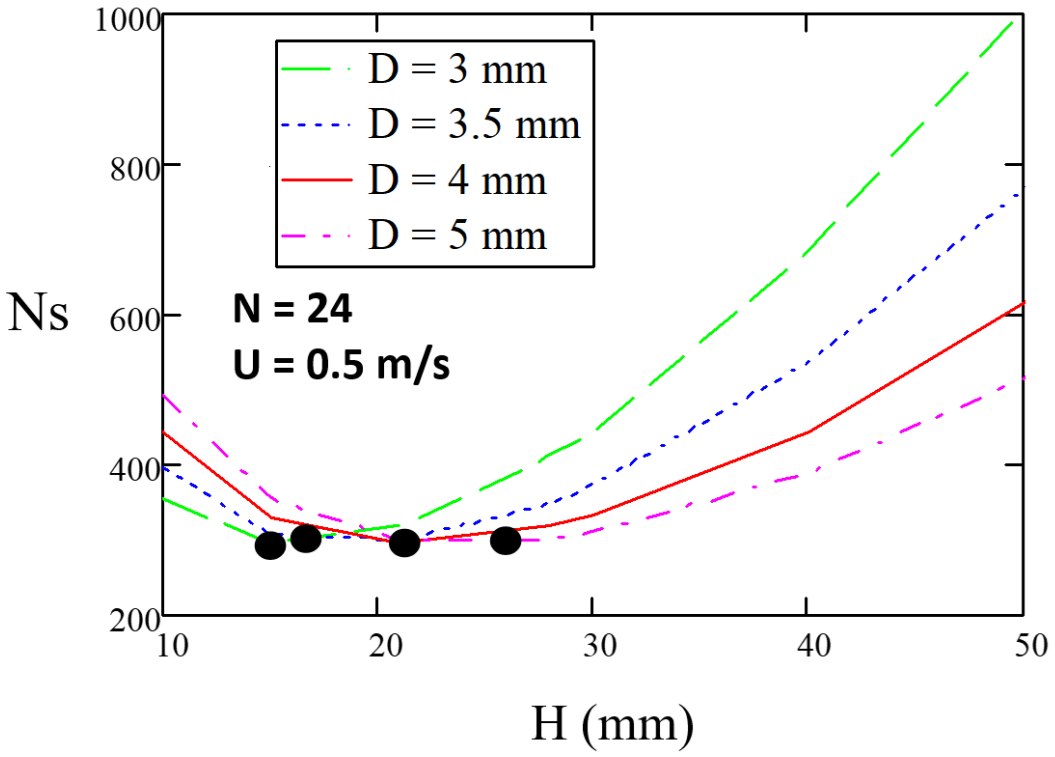


*Figure 6.10.3 Effect of pin height and diameter on dimensionless entropy generation rate*

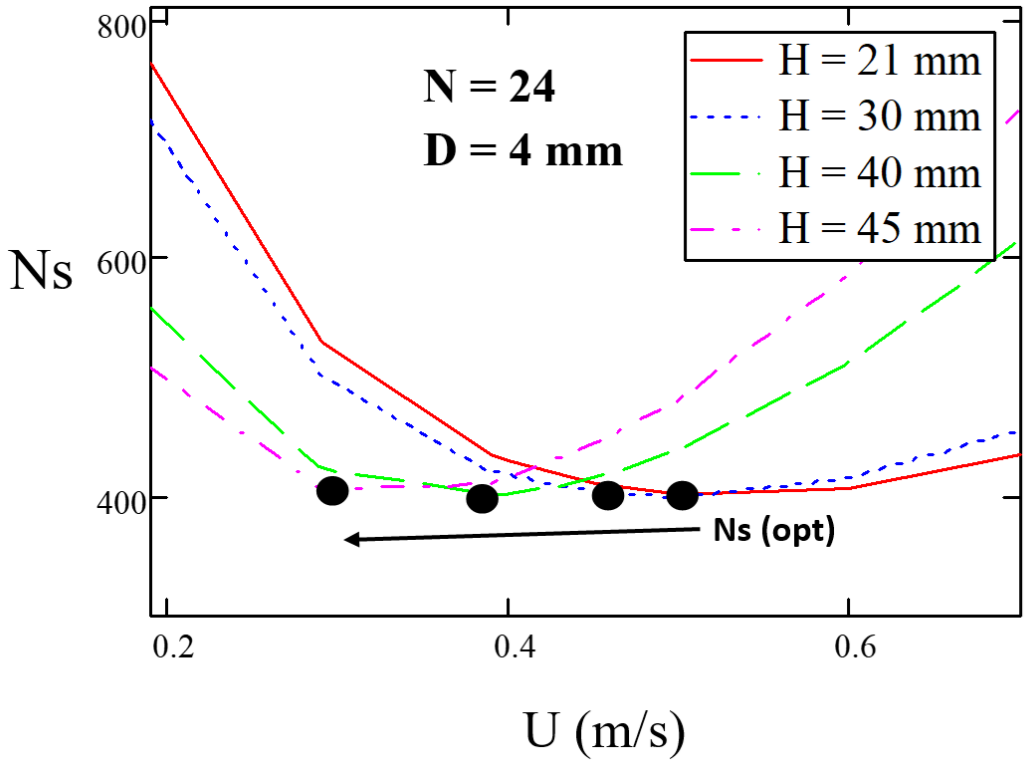


*Figure 6.10.4 Effect of local velocity and pin height on dimensionless entropy generation rate*

The following were thus determined:

- The geometric ratio of the pin γ= H/D (according to *ec. 6.3.6*) decreases with the increase of the Reynolds number (*fig.6.10.1*), leading to a decrease in the rate of entropy generation. This shows that at a set height, a wider pin is needed for a larger Reynolds number.
- As the thermal conductivity of the material increases, the geometric ratio of the pin γ increase (*fig.6.10.2*), which shows that, at the same given height, a thinner pin made of copper material will be required than one made of plastic or steel.
- The optimal height of the pine corresponds to an optimal diameter of the pine that generates a minimum entropy rate (*fig.6.10.3*), for the given conditions.
- The optimal speed around the pine decreases with increasing pine height, for a minimum entropy generation rate (*fig.6.10.4).*

The process is then resumed as a multivariate optimization with three design variables: pin side (D), local speed (Uapp) and pin height (H) (*Table 6.10.1*).

*Table 6.10.1 Results obtained for the optimization of three condenser parameters*

| **Thermal conductivity base material** | **Pin Configuration** | **Geometric variables** | | | **Performance criteria** | | |
|---|---|---|---|---|---|---|---|
| | | Pine side | Gas speed | Pine Height | Entropy generation rate | Thermal resistance | Pressure difference |
| k [W/(m K)] | N [$N_T$ x $N_L$] | D [mm] | $U_L$ [m/s] | H [mm] | $N_S$ x $10^{-2}$ | $R_{hs}$ [K / W] | Δp [Pa] |
| 237 | 6 x 4 | 4.0 | 3 | 21 | 5.07 | 4.02 | 11.13 |
| | 6 x 6 | 3.0 | 3 | 15 | 4.08 | 2.58 | 4.80 |
| 401 | 6 x 4 | 4.0 | 3 | 21 | 3.07 | 2.51 | 10.58 |
| | 6 x 6 | 3.0 | 3 | 16 | 3.54 | 2.57 | 4.70 |

From the centralization of the data it follows that for a higher thermal conductivity of the material, the thermal resistance Rhs and the entropy generation rate Ns are lower, in both cases of pin densities. It is also found that, for the same material, in both cases, there is a certain difference in pressure drop depending on the density of the pins.

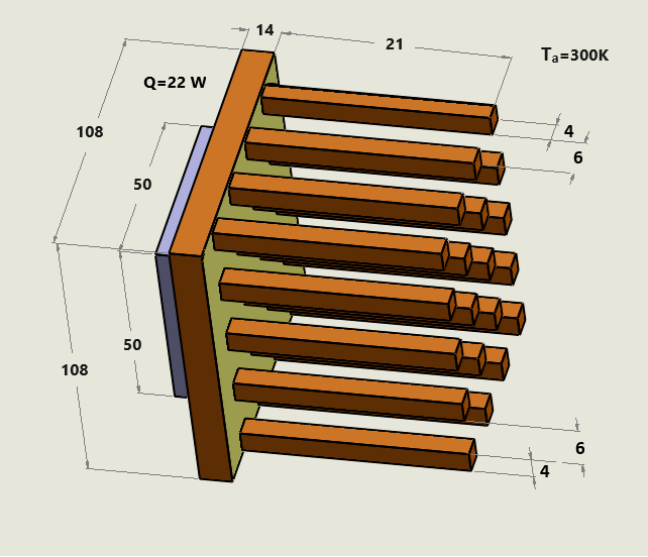


*Figure 6.10.5 Optimized final dimensions of the 24-pin rectangular and copper condenser*

The explanation lies in the fact that this type of finned heat exchangers are usually designed based on the determination of the thermal resistance to the flow between the thermal source and the cooling medium in the vicinity, being known the volume flow and in some cases the speed at the limit of the exchanger. It does not take into account the local pressure drop that occurs at contact with the gas flow and leads to a reduction in fluid flow and a decrease in the convection coefficient on heat transfer surfaces.

Therefore, the effects of fluid viscosity must be taken into account to fully determine the overall performance of the heat dissipation channels. Parametric studies can be used to obtain relationships between thermal performance and design parameters, but these methods do not guarantee that an optimal design will be achieved, only that a preferred configuration has been chosen from the configurations already tested. However, the rate of entropy generation associated with heat transfer (ec. 6.6.1) determines a convenient measure of the thermal performance of the heat exchanger (fig. 6.10.5). The optimised dimensions of the hydrogen condenser are shown in fig. 6.10.5.

# 7. NUMERICAL SIMULATION CONFIRMATION OF THE OPTIMIZED CONDENSER MODEL

Separate models *(fig. 7.2.1.2)* have been created for computational calculation simulation in the field of CFD fluid dynamics, using the Ansys Fluent 2022 R2 program, which uses the finite element (FE) method for numerical calculation.

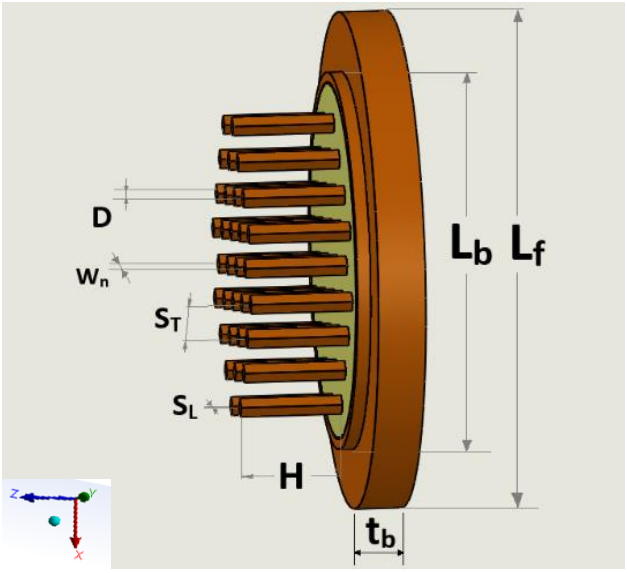


*Figure 7.2.1.1 Geometric parameters of the simulated condenser*

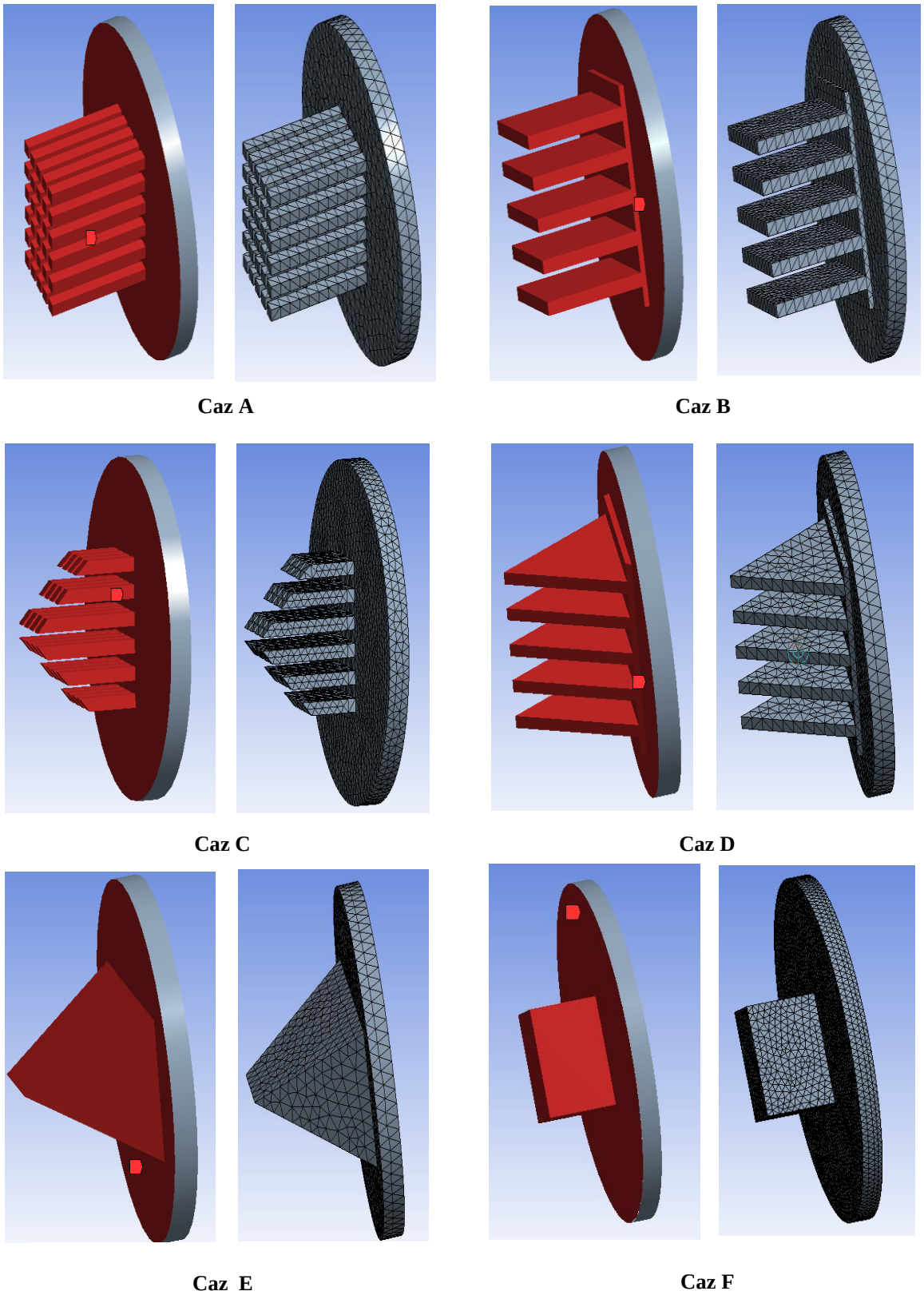


*Figure 7.2.1.2 Geometric and discretized structures of simulated condensers*

Four numerical simulations are performed for velocities of: 0, 0.5, 1, 1.5 (m/s). Based on the velocities, the Reynolds number, the mass flow, and then the average heat transfer coefficients for each simulation are calculated, and the results of the average heat transfer coefficients for the simulated condensers are compared with the theoretical and experimental ones. The simulated geometry and coordinate system are shown in fig. 7.2.1.3. Thus, the solution domain consists of the solid domain and the fluid domain.

The solid range consists of the enclosure of the liquefaction chamber (1) of dimensions ( H x D): 0.174 x 0.130 (mm) on whose upper wall the condenser (3) is fixed. The fluid domain consists of hydrogen gas introduced through an inlet connection (2) inside the chamber it fills and which is cooled and liquefied by the condenser. The geometric structure of the simulated condensers can be found graphically in (*fig. 7.2.1.2)*. The finned mesh and pins represent the same body as the baseplate. The non-condensed gaseous fraction is discharged through an outlet connection (6). The condenser is established to be cooled through the upper wall (5), considered isotherm, at a constant temperature of 20 K and atmospheric pressure (p = 0.013MPa). The lower wall (8) is also considered isothermal and the side walls (7) adiabatic at a constant temperature of 68 K.

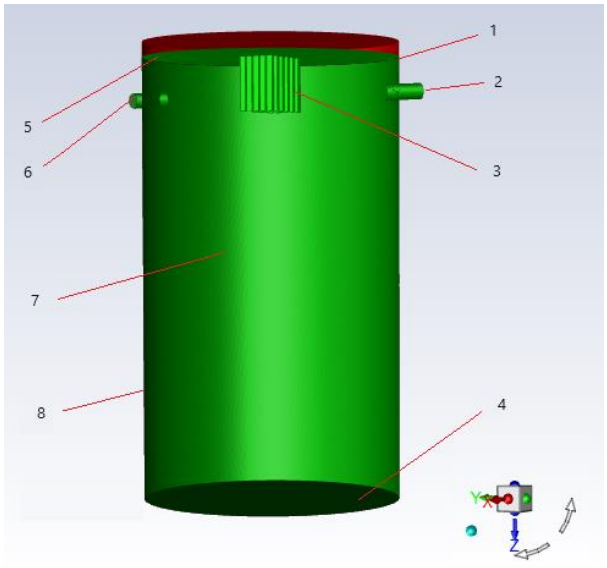


*Figure 7.2.1.3 Geometric structure of the solution domain*
*1. hydrogen liquefaction chamber 2. gas inlet connection 3. condenser 4. lower wall liquefaction chamber 5. upper wall liquefaction chamber 6. gas outlet connection 7. fluid domain 8. side wall liquefaction chamber*

### 7.3.1 Defining boundary tasks and conditions

In this analysis, a numerical simulation of the convective heat transfer (natural and forced) due to the flow over the extended surface of a base surface (finned shape, respectively, pins) was performed. Through each extension of the heat transfer surface (pine, fin) heat was extracted from its top (released by the flowing gas) at temperature $T_c$ and was transferred, by convection, to the refrigeration machine at temperature $T_r$.

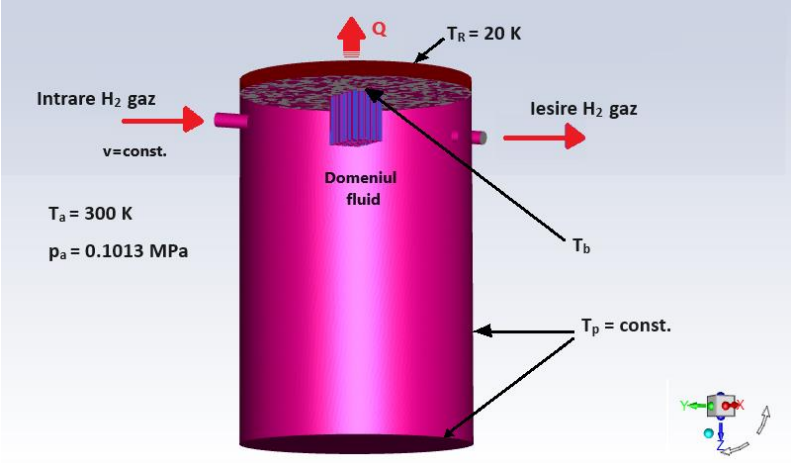


*Figure 7.3.1.1 Boundary conditions of the solution model*

The numerical analysis is performed in the following assumptions (*fig. 7.3.1.1*):

a) The flow is stationary, perfectly compressible and three-dimensional gas and has the values of: 0, 0.5, 1 and 1.5 [m/s], respectively, at constant pressure p = 0.1013 MPa;
b) The fluid is hydrogen gas and the solid material is copper;
c) The properties of the fluid (density ρ, specific heat at constant pressure $C_p$, thermal conductivity k and dynamic viscosity μ are temperature dependent;
d) The properties of the solid (density ρ, specific heat at constant pressure Cp and thermal conductivity k are dependent on temperature ( fig. 7.3.1.2 );
e) The difference in density of the fluid is considered the direction of gravity (Boussinesq approximation) on the OZ axis, with the value g = - 9.81 [m/s2];
f) Heat transfer is considered a stationary phenomenon;
g) The outside temperature is considered to be $T_{amb}$ = 300K and the outside pressure $p_{amb}$ = 0.1013 MPa;
h) The temperature of the cold source is considered constant: $T_R$=20K;
i) Transferul de căldură prin radiație este neglijabil, temperatura peretelui exterior este considerata constanta: $T_p$ = 68 K;
j) There is no liquid flow on the walls of the vessel (program command: *no slip* ).

## 7.3.2 Establishing the equations for solving the mathematical flow simulation model

The basic equations in the case of natural convection are the same as those of forced convection and supplemented with two other equations. The difference between the two modes of heat transfer lies in the fact that, in natural convection, the flow is driven by the difference in density of the fluid that occurred as a result of the change in temperature, on which the density is directly dependent.

For the case of a constant fluid flow in the laminar flow regime of a perfectly compressible gas, the form of the basic equations (continuity, conservation momentum and energy) used in this study and which the flowing fluid must comply with is as follows:

*I. Continuity equation*

The general form of the conservation of mass equation determined from the continuity equation in differential form that can be applied for constant or transient flow, compressible or incompressible flow of fluid is:

$$\frac{\partial \rho}{\partial t} + \nabla(\rho \vec{w}) = 0 \qquad (7.3.2.1)$$

*II. The equation of conservation of momentum*

The general form of the momentum conservation equation, also known as the Navier–Stokes equation, for a compressible fluid is:

$$\overline{w}_j \frac{\partial(\rho \overline{w}_i)}{\partial x_j} = -\frac{\partial \bar{p}_i}{\partial x_i} + \mu_{ef} \cdot (\nabla^2 \overline{w}_i) - (\rho - \rho_\alpha) \cdot g \qquad (7.3.2.3)$$

*III. Energy Conservation Equation*

The form, used in this numerical simulation for the equation of conservation of energy in the case of a compressible fluid flow, is:

$$\frac{\partial(\rho w_x T)}{\partial x} + \frac{\partial(\rho w_y T)}{\partial y} + \frac{\partial(\rho w_z T)}{\partial z} = \rho \left[ \left( \frac{\nu}{Pr} + \frac{\nu_t}{P_{turb}} \right) \left( \frac{\partial^2 T}{\partial x^2} + \frac{\partial^2 T}{\partial y^2} + \frac{\partial^2 T}{\partial z^2} \right) \right] \qquad (7.3.2.7)$$

*IV. Turbulent transport equation*

In addition to the basic equations presented above, the mathematical flow model was established, which was the basis of the computer numerical calculation, namely *the standard k-omega turbulence model SST, pressure-based*, with two equations that has the ability to take into account the two flows, laminar at the entrance to the enclosure and turbulent at the phase change of the fluid. This model is programmed to differentiate between the two flow regimes

and to differentially calculate the thermodynamic parameters. The kinetic energy in turbulent regime k and the specific dissipation rate ω are obtained from the following transport equation [115]:

$$\frac{\partial(\rho k)}{\partial t} + \frac{\partial(\rho k w_i)}{\partial x_i} = \frac{\partial}{\partial x_j}\left[\tau_k \frac{\partial k}{\partial x_j}\right] + G_k + Y_k + S_k \quad (7.3.2.8)$$

$$\frac{\partial(\rho \omega)}{\partial t} + \frac{\partial(\rho \omega w_i)}{\partial x_i} = \frac{\partial}{\partial x_j}\left[\tau_\omega \frac{\partial \omega}{\partial x_j}\right] + G_\omega + Y_\omega + S_\omega \quad (7.3.2.9)$$

*V. Nusselt number*

The initial determination of the actual heat transfer rate at the local level facilitates the calculation of the evaluation of the temperature of the fluid that for the entire volume which is quite difficult to achieve practically. Thus, the total Nusselt coefficient for the base of the condenser determined from the temperature difference between the baseplate $T_b$ (*fig. 7.2.1.1)* and the temperature of the cooling head of the GM cryocooler, $T_R$ is evaluated as follows:

$$Nu_{tot} = \frac{\int_o^L \left( \int_0^H \left(\frac{dT}{dx}\right)\Big|_{x=S_T+0.5\cdot D} dy - \int_{0.5\cdot D}^{S_T+0.5\cdot D} \left(\frac{dT}{dy}\right)\Big|_{y=0} dx \right) dz}{L\,(2H+S_L+D)(T_b-T_R)} \quad (7.3.2.11)$$

in which:

$S_L$ = distance interpins in longitudinal direction (longitudinal pitch), in [m]

$S_T$ = Interpini distance in the transverse direction (transverse pitch), in [m]

D = Size of pine side/square section fin, in [m]

H = height of the pin/fin, in [m]

L = finned surface length, in [m]

$T_p$ = liquefaction vessel temperature, in [K]

$T_b$ = temperature at the base of the pine/fin, in [K]

$T_R$ = GM cryocooler cooler head temperature, in [K]

## 7.4 SOLVING THE MATHEMATICAL MODEL. PERFORMING THE CALCULATION AND DETERMINING THE SOLUTIONS OF THE MATHEMATICAL MODEL

Although the *continuity residue* does not converge completely (*fig. 7.4.2*), the fact that the slope of the curve is leveled near the accepted criterion chosen by 1 x e-3, and the other residuals (velocity-x, velocity-y, velocity-z, energy, k, omega) are well below the permissible convergence tolerance, it can be considered that the solution actually converges (the errors are negligible).

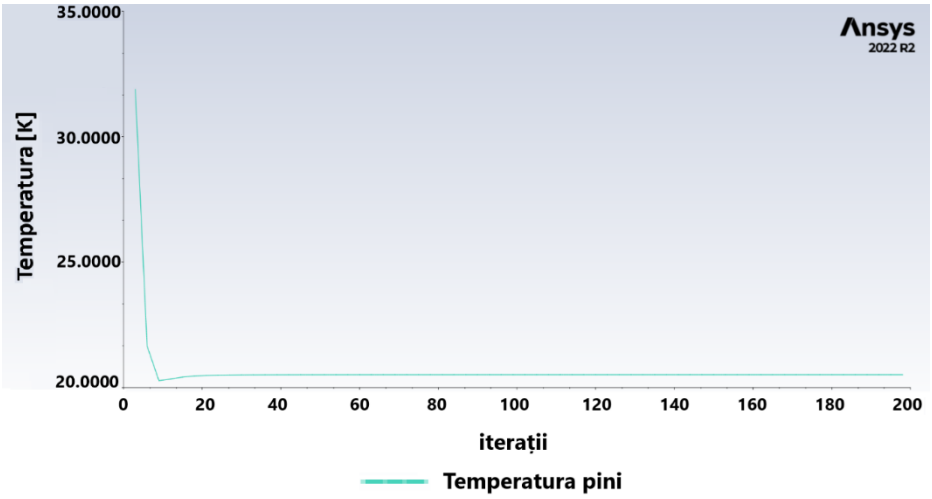


*Figure 7.4.1. Temperature variation of the finned surface of the condenser resulting from numerical simulation calculation with Ansys Fluent*

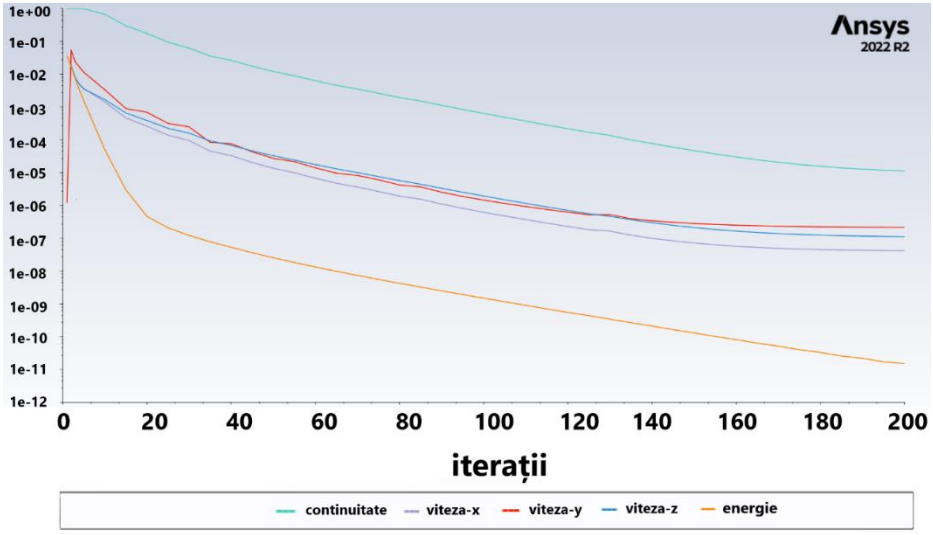


*Figure 7.4.2 Residue history for the continuity equation, momentum conservation and viscosity model resulting from the numerical simulation calculation with Ansys Fluent of heat transfer in the condenser*

## 7.5 POST-CALCULATION

The simulations resulted in the contour of the temperatures inside the liquefaction chamber (*fig. 7.5.1*), the velocity of the hydrogen gas and the contour of the temperatures of the finned or pin surfaces for the constructive versions of the condenser (*fig. 7.2.1.2*). The results obtained represent criteria for comparison (*fig. 7.5.1*) of the thermal performance of these condenser models.

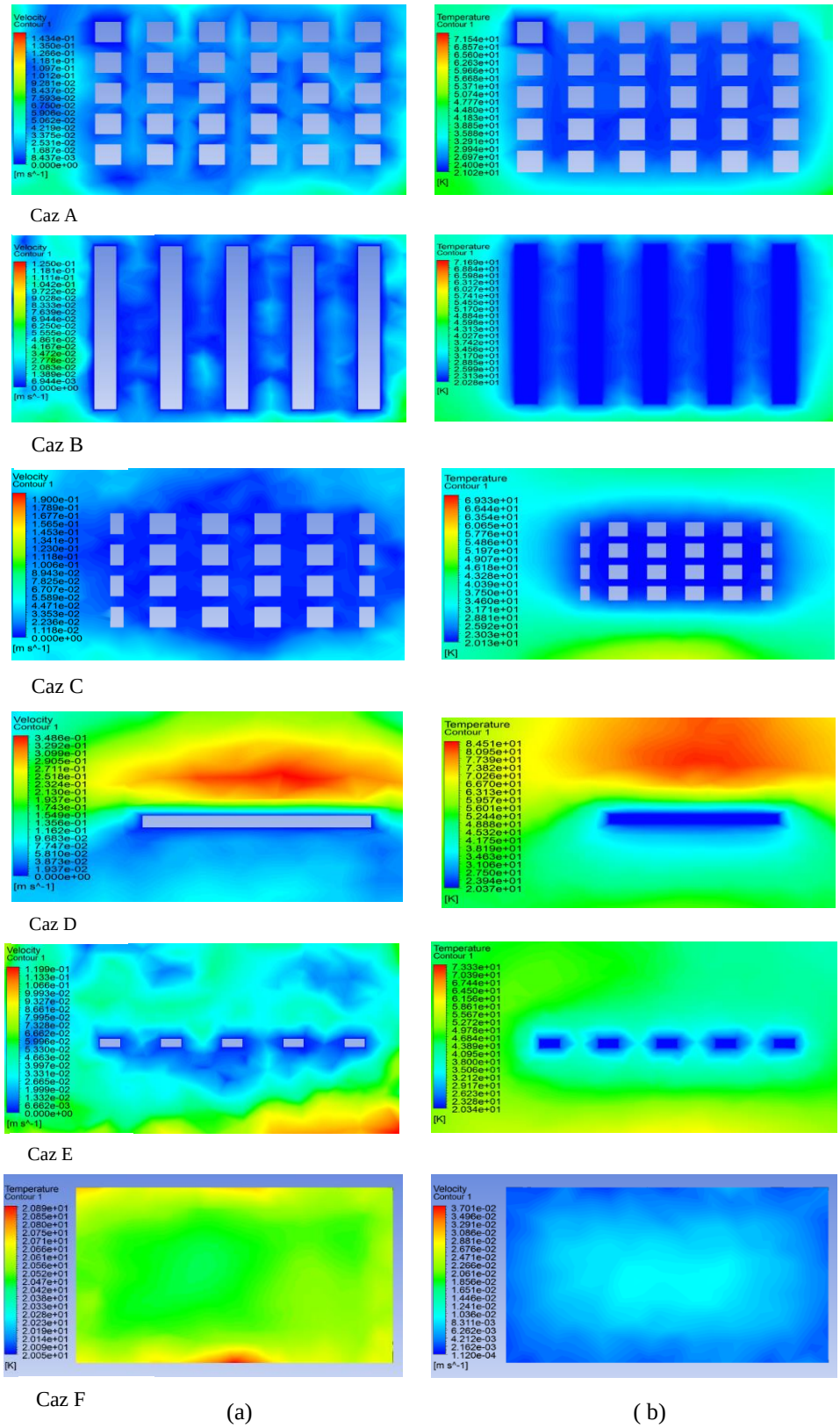


*Figure 7.5.1 a) Velocity and b) temperature distribution at a distance of 20 mm from the base of the condenser*

As we have shown in the chapter on condenser optimization (*Chapter 6.3 Performance criterion*), the most efficient heat transfer from the gas to the condenser surface is achieved by the gas with the highest local velocity (near the finned surface). This consideration is verified in the simulations by the fact that the lowest local temperature occurs in the areas where the gas has the highest velocity (*fig. 7.5.1 Case B*). The sample plane is at a distance of 20 mm from the base of the condenser on the XY axis. This distance represents the upper half of the height of the fins and pins

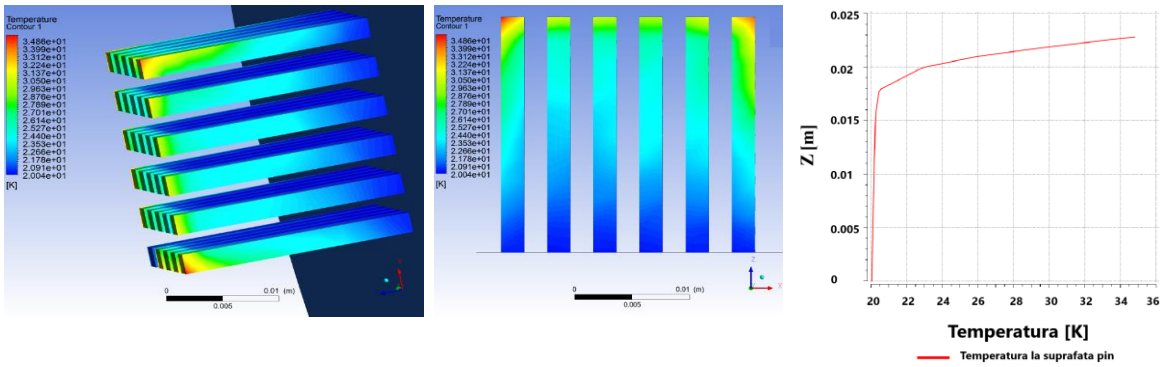


(a) ( b)

*Figure 7.5.2 Temperature variation at the surface of the pines*
*a) Temperature distribution on the height of the pins*
*b) Temperature variation graph for the central row of pins*

The simulations show that in case A the gas moves the fastest and in case F the gas has the slowest displacement ( *fig. 7.5.1* ). The areas colored in red are areas with the highest speed while the areas with dark blue have zero speed. To be a convection factor, the gas must move. The faster this movement (increases the speed of the gas), the better the heat transfer. This phenomenon is observed where the condenser temperature increases (in the middle of the finned surface) *(fig. 7.5.2)*, the explanation being the intensification of the heat exchange between hot gas and pins due to the increase in the speed of the gas flow. In this regard, the best gas cooling performance, compared to the fully finned or pin assembly, is the condenser in case A and the worst in case F. The results of the simulations show that the pin structure allows for better gas circulation and at the same time confirms the optimized condenser pattern. Based on the velocities, the Reynolds number and the mass flow rate were calculated for each simulation. The average heat transfer coefficients for each simulation are determined *(table 7.5.3)* and the results are compared (*fig. 7.2.1.2*) with the model theoretically calculated for each type of condenser. It can be seen that the results are close in values (*fig. 7.5.3* and *fig. 7.5.4*).

*Tabel 7.5.3 Results of heat transfer coefficients for square section condensers and comparison with theoretically calculated results*

| **Reynolds Number** | **Average heat transfer coefficient** | **Nusselt number** | | | | |
|---|---|---|---|---|---|---|
| | | **Numerical calculation results** | | | **Analytical calculation results** | **Deviation** |
| **Re** | **$h_m$** | Case | Fins/pins section | **$Nu_{num}$** | **$Nu_{an}$** | **ϵ** |
| **[-]** | **[W/(m² K)]** | | | **[-]** | **[-]** | **[%]** |
| 500 | 318.83 | A | square | 2.40 | 2.19 | -8.84 |
| | | B | | 1.97 | | 9.96 |
| | | C | | 2.33 | | -6.10 |
| | | D | rectangular | 17.49 | 16.09 | -8.02 |
| | | F | | 17.10 | | -5.92 |
| | | E | triangular | 16.50 | 15.87 | -3.80 |
| 800 | 329.87 | A | square | 2.64 | 2.55 | -3.26 |
| | | B | | 2.31 | | 9.55 |
| | | C | | 2.41 | | 5.64 |
| | | D | rectangular | 20.70 | 18.78 | -9.28 |
| | | F | | 20.10 | | -6.57 |
| | | E | triangular | 20.40 | 18.53 | -9.17 |
| 1000 | 340.46 | A | square | 2.73 | 2.84 | 3.97 |
| | | B | | 2.57 | | 9.60 |
| | | C | | 2.61 | | 8.19 |
| | | D | rectangular | 19.14 | 20.90 | 8.44 |
| | | F | | 19.27 | | 7.81 |
| | | E | triangular | 20.96 | 20.62 | -1.60 |

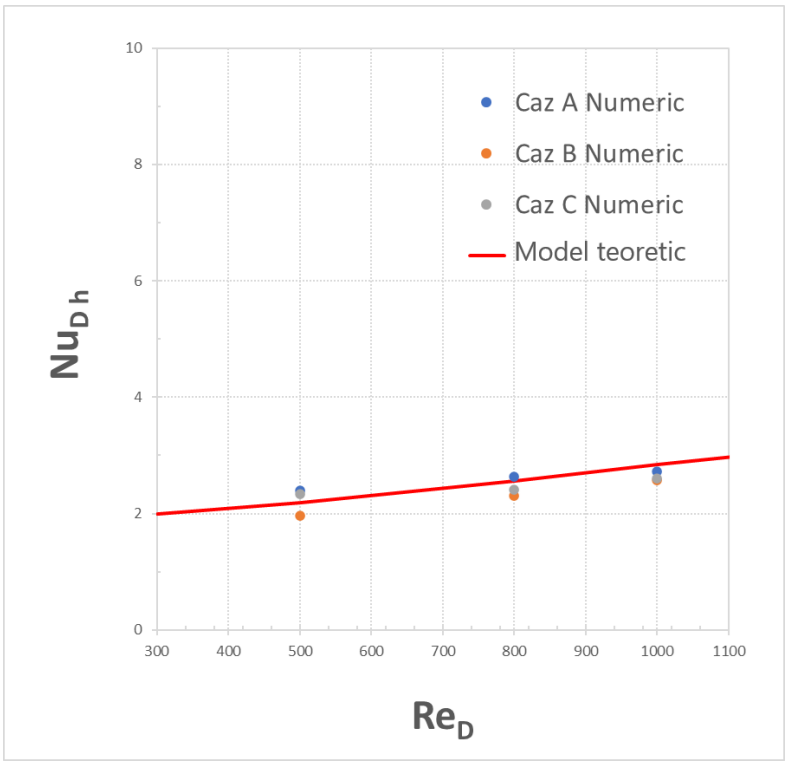


*Figure 7.5.3 Comparison of heat transfer coefficients for square section condensers*

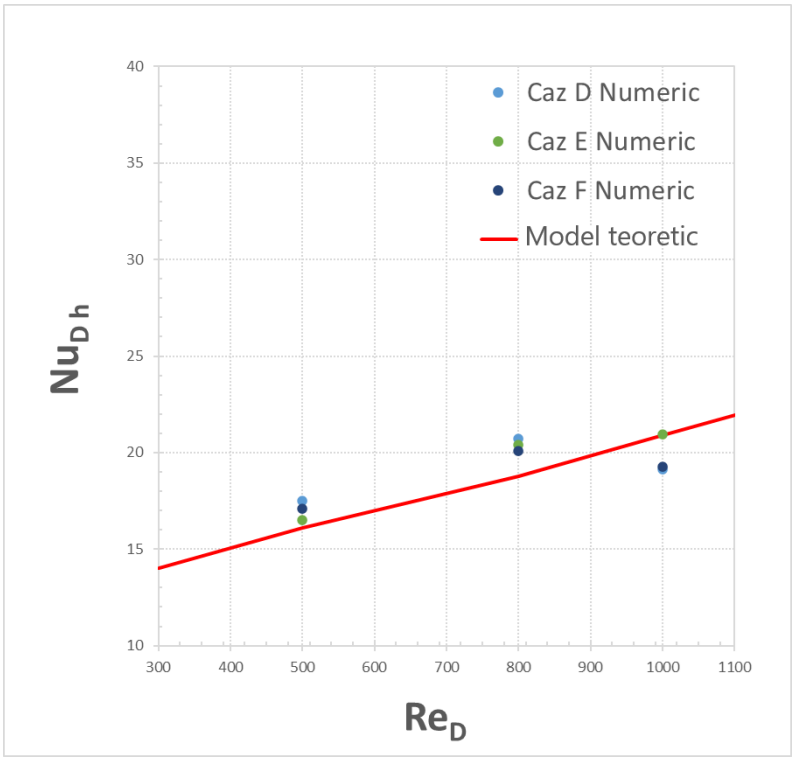


*Figure 7.5.4 Comparison of heat transfer coefficients for triangular (case E) and rectangular (case D and F) condensers*

# 8. CONDENSER FUNCTIONAL ANALYSIS AND PERFORMANCE EVALUATION

## 8.1 HYDROGEN CONDENSER EXPERIMENT PLANNING

The objective of the experimental research is to determine the comparative:

i. Heat transfer coefficient for two main condenser models: rectangular $R_1$ and conical $C_1$ and their versions: $R_{1.1}$, $R_{1.2}$ si $C_{1.2}$ si $C_{1.3}$ ( *fig. 8.1.1 , 8.1.*2)

ii. Heat transfer coefficient for the 6x4 pines condenser model ( *fig. 8.1.3* ) at different operating parameters: pressure, temperature and flow rate

Two types of tests have been carried out for the hydrogen condenser.

a) Model R1 b) Model R 1.2 c)

*Figure 8.1.1 Geometric configurations of rectangular condensers initially tested. Image and 3D model for: a) Type R1 b) Type R1.2 c) Type R1.3*

a) Model C1 b) Model C 1.2 c)

*Figure 8.1.2 Geometric configurations of conical condensers initially tested. Image and 3D model for: a) Type C1 b) Type C1.2 c) Type C1.3*

The second set of tests was performed for the optimized condenser C1.4 (fig. 8.1.3) by experimentally determining the heat transfer coefficient at condensation for hydrogen gas pressures and temperatures.

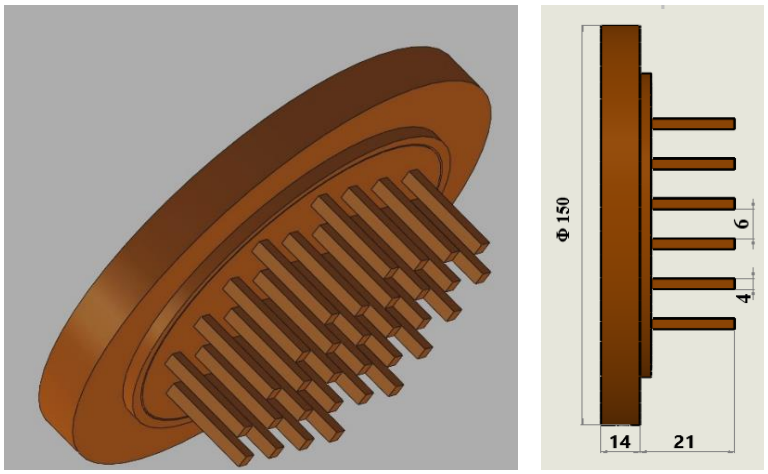


(a) ( b)

*Figure 8.1.3 Geometric configuration of the pin condenser model C1.4 tested on the experimental stand a) 3D model b) Dimensional scheme*

The purpose of these first set of tests was to experimentally confirm which geometric configuration applied for the new condenser model avoids condensation in film form and favors the obtaining of a condensate by dripping.

## 8.2 METHOD OF EVALUATING THE HEAT TRANSFER COEFFICIENT OF THE CONDENSER

The heat transfer coefficient of the condenser is determined experimentally by determining the thermal flux and the temperature variation of the condensate at the condenser surface.

### 8.3.5 Setting up the experimental installation for data determination

The basic process for evaluating the performance of the plant (fig. 8.3.5.3) is the cooling of the condenser ($CC_1$) and the liquefaction of hydrogen vapor in the $CT_2$ test chamber. The configuration of the experimental installation is designed to determine the heat transfer coefficient when condensing hydrogen gas over the condenser surface.

The method of calculating the condensing heat transfer coefficient contains the following parameters as variables that require measurement:

a) the temperature difference between the vapor and the condenser wall in the case of a constant liquid temperature value, and

b) vapor pressure for different values of the temperature difference between the vapor and the condenser wall, which is cooler.

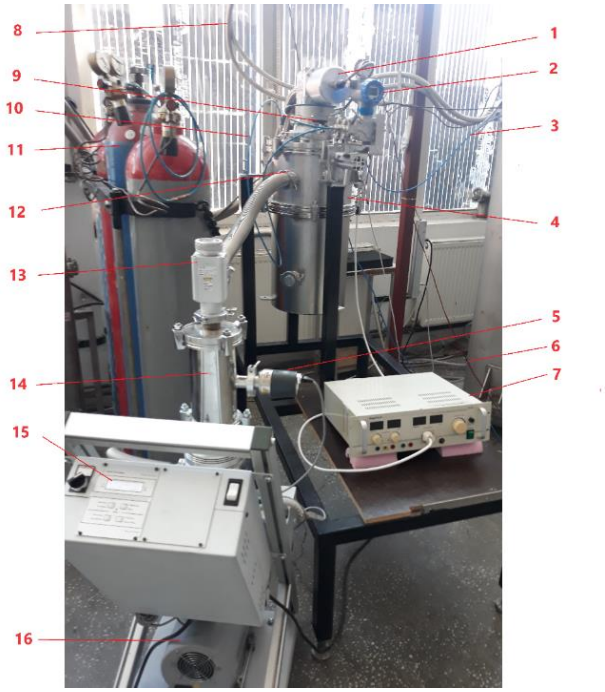


*Figure 8.3.2.1 Picture of the experimental test stand of the hydrogen liquefaction condenser*
*1. GM RDK 4K Cryocooler with two cooling stages 2. Liquid level indicator*
*3. Hydrogen gas supply route 4. Cryostat 5. Vacuum level gauge 6. Data cable to PLC panel 7. Electrical resistance power supply and regulator 8. Helium lines*
*9. Internal liquefaction vessel purge valve 10. Liquid level communication route*
*11. Hydrogen gas cylinder 12. Connector and cryostat vacuum passage*
*13. Screw route adjustment valve 14. High vacuum turbomolecular pump*
*15. Vacuum level indication 16. Intermediate vacuum pump*

The experiments are carried out in the following configuration of the installation. For the first step of the experiment according to point (a), the liquid accumulated at the base of the liquefaction chamber shall be heated by means of an electric resistance (7) (fig. 8.3.2). The vaporization process takes place until the thermodynamic equilibrium state is reached (about 60 min).

The experimental data for this steady state characterized by a certain value of the pressure of the liquid bath and the pressure in the liquefaction chamber are determined. So for this stabilized mode of operation, a maximum value of the temperature difference $\Delta T_o$ is obtained between the vapor ($T_v$) and the cold wall of the condenser( $T_{PL}$):

$$\Delta T_o = T_V - T_{PL} \qquad (8.3.5.1)$$

for which the condensing heat transfer coefficient $h_c$ is calculated. In this case, the power of the cryogenerator is equal to the condensing power.

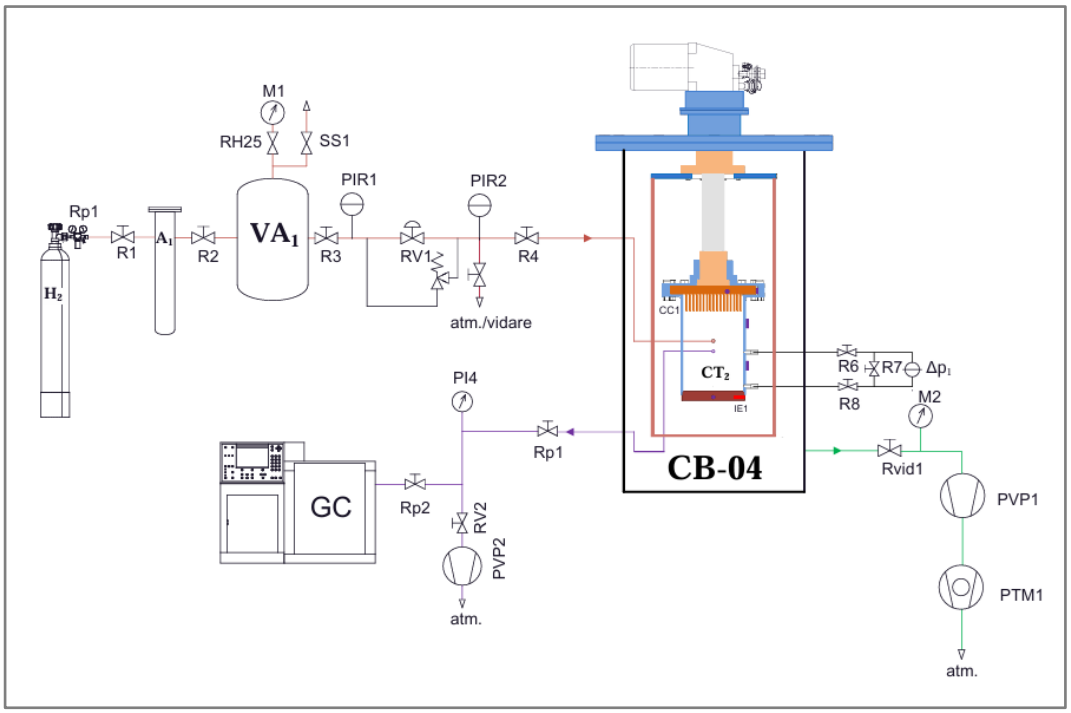


*Figure 8.3.5.3 The measurement and control scheme of the experimental test stand for rectangular hydrogen condenser with fins*
*$CT_2$- Test Chamber; VA - Feeding Vessel; A - Absorber; CC1 - Condenser head*
*CH1– Cryocooler; IE1 - Electric heater; CB04 - Cryostat; GC- Gas chromatograph*
*PVP – Preliminary Vacuum Pump; PTM1 – Turbomolecular Pump; Δp – Differential pressure; M – Manometer; RV- Valve; R - Manual Valve; PIR - Pressure measurements with indication and recording*

The next phase in this first stage *(point (a) above)* is the gradual and slow reduction of the heat input in the liquid hydrogen bath (with small temperature differences), by means of the electrical resistance. As a result of the decrease in the temperature in the vessel, the constant pressure in the condenser coolant is maintained by the reverse process of gradually and slowly increasing the heat input into the condenser by means of the electrical resistance. The effect achieved is to reduce the condensing power but maintaining a constant value of the temperature of hydrogen in liquid hydrogen. In this case, the power of the cryogenerator is equal to the condensing power to which is added the heat flux introduced into the condenser. This results in another value of the temperature difference between the vapor and the cold wall of the condenser (another steady state) for which the heat transfer coefficient is calculated according to the heat input introduced into the system.

In the second stage of the experiment *(point (b) above)*, for a certain value of the temperature difference between the vapor and the condenser wall, at a steady state, a gradual and slow increase of the heat input in the liquid hydrogen bath is achieved, with the help of the electrical resistance, which determines the change in the pressure value in the liquefaction vessel.

In the next phase of the second step, the cooling capacity of the cryocooler shall be adjusted by means of the electrical resistance in order to maintain a stable temperature difference between the condensed vapour and the cold wall of the condenser. The value of the vapor pressure, obtained at steady state, is characteristic of a certain temperature difference between the condensed vapor and the cold wall of the condenser for which the heat transfer coefficient values are calculated. For this steady state, the liquefaction power is equal to the heat flux introduced into the system by the two heaters plus the heat losses through the walls. Stable thermodynamic states are thus obtained for which the heat transfer coefficient values are calculated.

## 8.3.6 The method of determining the experimental data

After reaching the equilibrium state in the process, the following parameters are measured:

i. The vapour pressure $p_{vap}$ in the test chamber in [bar] which is used to determine the temperature of the $T_V$ vapour condensing on the surface of the condenser:

$$logp_{vap} = A + \frac{B}{T} + C \cdot logT + D \cdot \frac{p}{T^2} \qquad (8.3.6.1)$$

ii. Temperature of liquid hydrogen: $T_{LH}$

iii. Temperature difference $\Delta T_f$ between condenser wall temperature $T_{p.pl.cd}$ and liquid hydrogen temperature $T_{LH}$,, in [K]:

$$\Delta T_f = T_{p.pl.cd} - T_{LH} \qquad (8.3.6.2)$$

The method of determining the experimental data was applied for each geometric model of condenser, according to the configurations *(fig. 8.1.1, fig.8.1.2 and fig.8.1.3)*.

## 8.5.1 Experimental determination of the heat transfer coefficient of condensers with different heat exchange geometries

The heat transfer coefficient to condensation was determined according to the variation of the temperature of the condensation film and the thermal flux applied to the condenser

baseplate, determined from the experimental data as well as the area of the contact surface specific to each type of condenser as follows.

After the parameter measurements have been made, the measurement, monitoring and control data shall be transmitted remotely via data cable (6) (fig. 8.3.2.1), the following parameters shall be centralised and calculated:

*I) The temperature variation of the condensation film* with the expression *(4.2.2.14)*:

$$\Delta T_C = \Delta T_0 - \Delta T_f \qquad (8.4.6.3)$$

where:

$\Delta T_f$ = represents the temperature difference that is calculated with the values measured according to chap. 8.3.6 letter c)

$\Delta T_0$ = represents the difference in temperature, in [K]*:*

$$\Delta T_o = T_V - T_{LH} \qquad (8.4.6.4)$$

where:

$T_V$ = is the temperature of the condensing vapour on the surface of the condenser, in [K], calculated in accordance with *eq. 8.3.6.1*:

$$logp_{vap} = A + \frac{B}{T} + C \cdot logT + D \cdot \frac{p}{T^2} \qquad (8.4.6.5)$$

where:

$p_{vap}$ = is the vapour pressure inside the test chamber in [bar], measured in accordance with *chap. 8.3.6 letter c)*

$T_{LH}$ = the temperature of the liquid film $T_L$ ,in [K], measured according to *cap 8.3.6 letter c)*

*II) Heat transfer coefficient at vapor condensation:*

$$h_c = \frac{\dot{Q}_c}{\Delta t_c \cdot A_c} \qquad (8.4.6.6)$$

where:

$\dot{Q}_c$ = is the amount of heat transferred between the condenser surface and the condensing vapor, in [W], which is calculated as the enthalpy of vaporization of gases at the condenser surface: $h_{fg}$,

$$h_{fg} = \Delta v_v \left[\frac{C \cdot T^2 - B \cdot T - 2 \cdot D \cdot p}{\frac{T^2}{P} - D}\right] \qquad (8.4.6.7)$$

$\Delta T_C$ = reprezintă variația temperaturii peliculei de condens calculată cf. *ec. 8.4.6.3,* in [K]

$A_c$ = reprezintă aria suprafeței de transfer termic, în [$m^2$], care se calculează în funcție de geometria expusă fluxului de gaz a condensatorului care se testează.

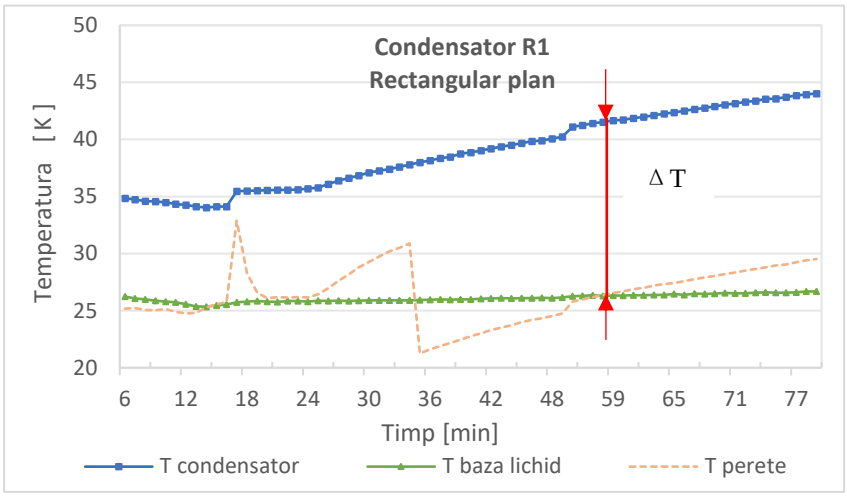


a)

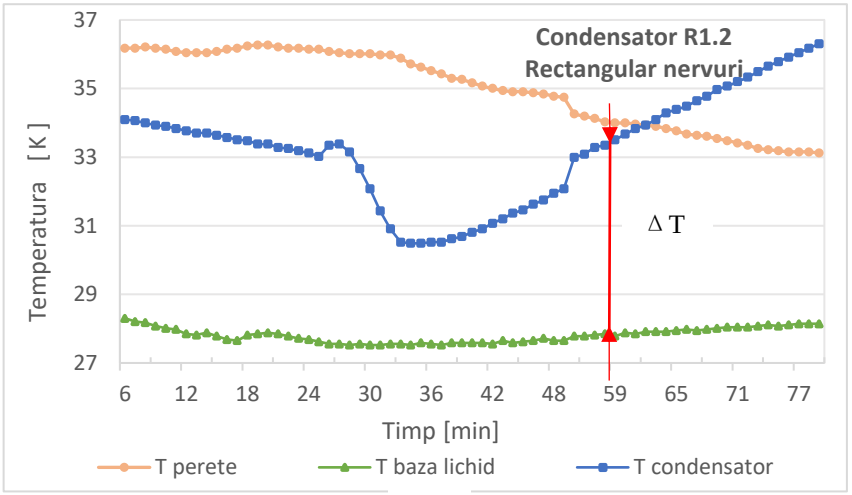


b)

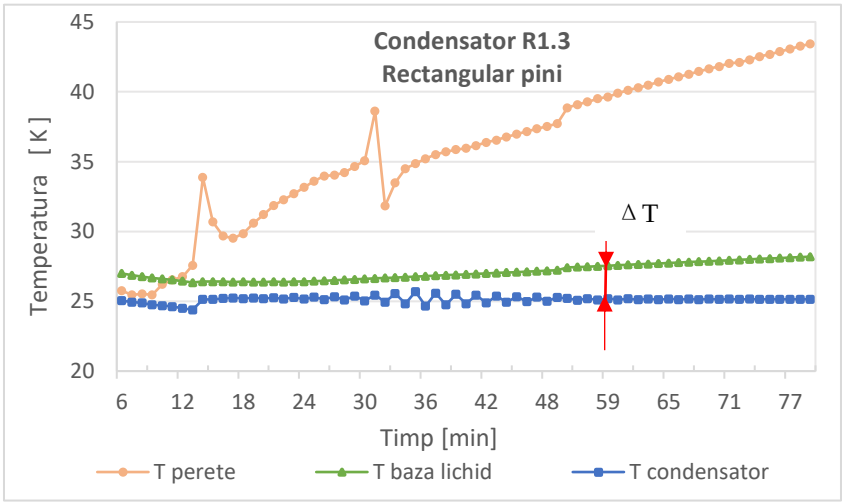


c)

*Figure 8.5.1.2 Temperature variation at the convection heat exchange surface: the temperature $T_{condenser}$ of the liquid condensate, $T_{base\ liquid}$ and the temperature of the wall $T_{vessel\ wall}$ , for rectangular condenser of the type: a) flat surface b) finned surface and c) pin surface*

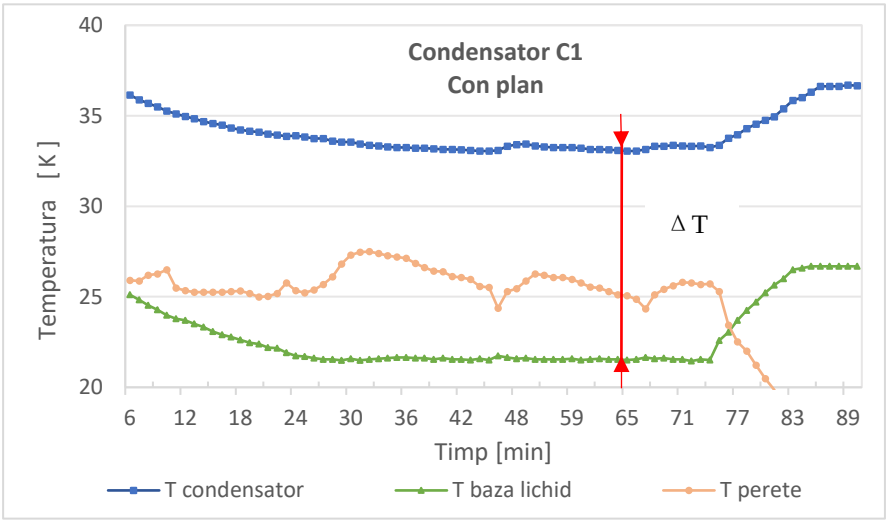


a)

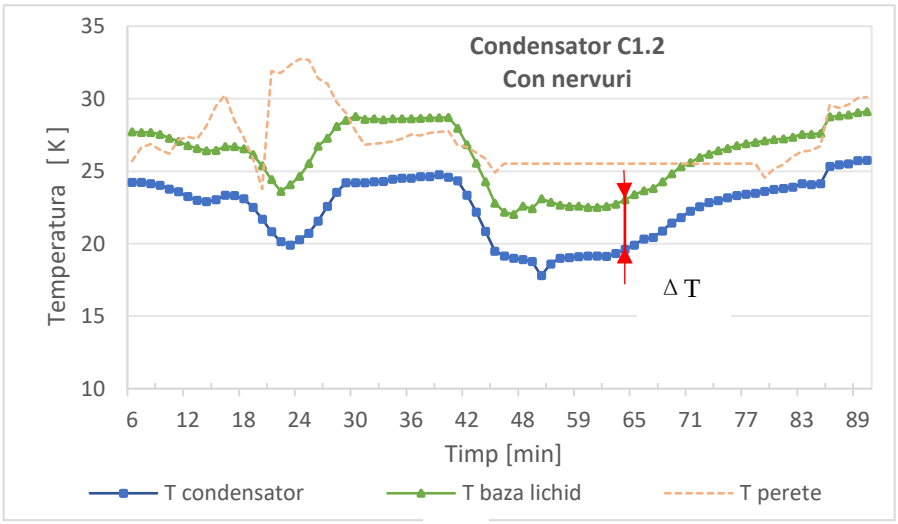


b)

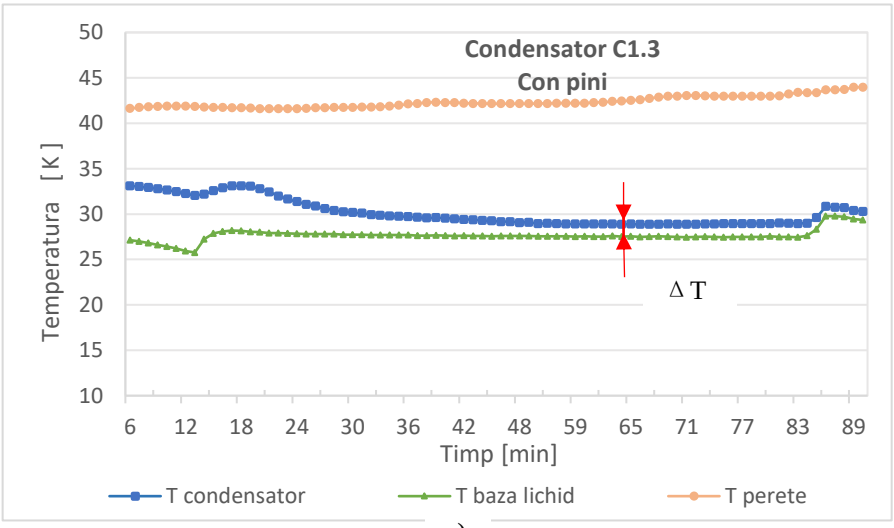


c)

*Figure 8.5.1.3 Temperature variation at the convection heat exchange surface: the temperature $T_{condenser}$ of the liquid condensate, $T_{base\ liquid}$ and the temperature of the wall $T_{vessel\ wall}$, for conical condenser of the type: a) flat surface b) finned surface and c) pin surface*

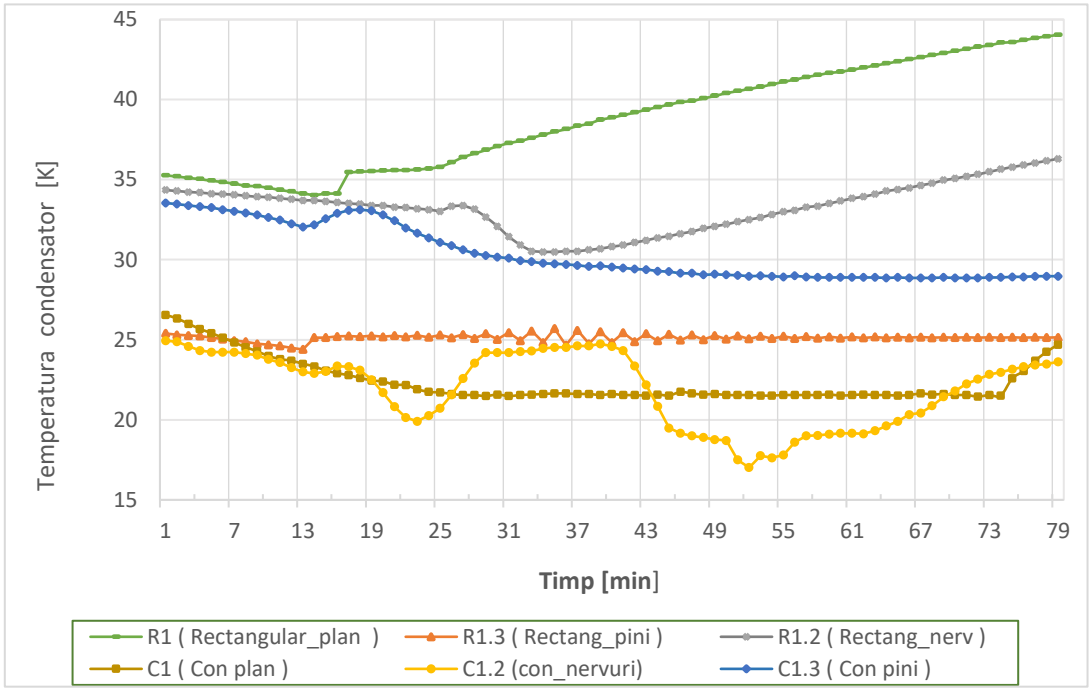


*Figure 8.5.1.4 Centralization of the temperature evolution at the convection heat exchange surface $T_{condenser}$ for rectangular and conical condensers in the versions: a) flat surface b) finned surface and c) pin surface*

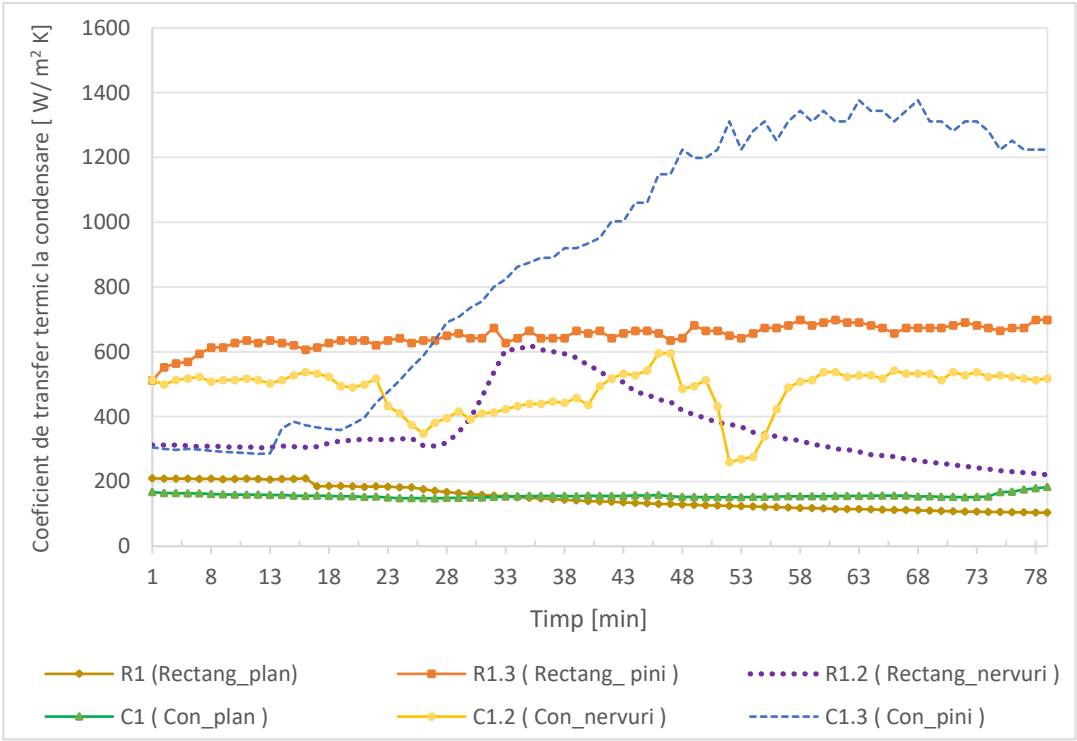


*Figure 8.5.1.5 Value of the heat transfer coefficient at condensation on the condenser wall obtained experimentally for the condenser models tested*

The experimental tests led to the following conclusions:

a) Condensers equipped with pins (conical and straight) have a stable operation and obtain the highest heat transfer coefficients at the condensate (over 600 W/m$^2$K)
b) Condensers equipped with fins obtain an acceptable coefficient of heat transfer to condensation (between 250 and 600 W/m$^2$K) but have relative oscillations in operation. The C1.2 finned cone condenser achieved the lowest liquid temperature value of 17.1K.
c) Condensers with a flat heat transfer surface get a minimal heat transfer (between 100 and 200 W/m$^2$K) leading to instability in operation. The condenser con plane C1 has obtained low values of liquid temperature ( 21.51K).

The achievement of higher condensation convection coefficients on the vertical walls of pinned condensers (inclined or straight) is due to the breakage of the condensate film that forms on the heat exchange surface with hydrogen gas and the formation of falling droplets. By freeing the surface from contact with the vapors, the condensation rate increases and implicitly the convection transfer coefficient. The inclined shape of the surface plays an important role in facilitating the flow and directing the flow of condensate.

### 8.6.2 Experimental determination of the heat transfer coefficient at condensing at different pressures and working temperatures for the pin condenser optimized

The second set of tests was performed for the theoretically optimized geometric configuration, namely the rectangular C1.4 condenser with 6 x 4 pines (*fig. 8.1.3*). Functional analysis aims to validate both the theoretically optimized model and the model calculated by numerical computer simulation. For this purpose, the heat transfer coefficient at condensation for different pressures was experimentally determined. From the graph in (fig. *8.6.2.1*) it appears that the best performance is achieved at the pressure of 4.5 bar. It is observed that at this pressure the heat transfer coefficient at condensation has double values compared to the rest of the tested pressures (1677 W/m$^2$K). For the working range of low pressures, close to atmospheric pressure, the pressure of 1.3 bar and 1.7 bar can be used. In this pressure range, a good heat transfer between 500-700 W/m$^2$K was obtained.

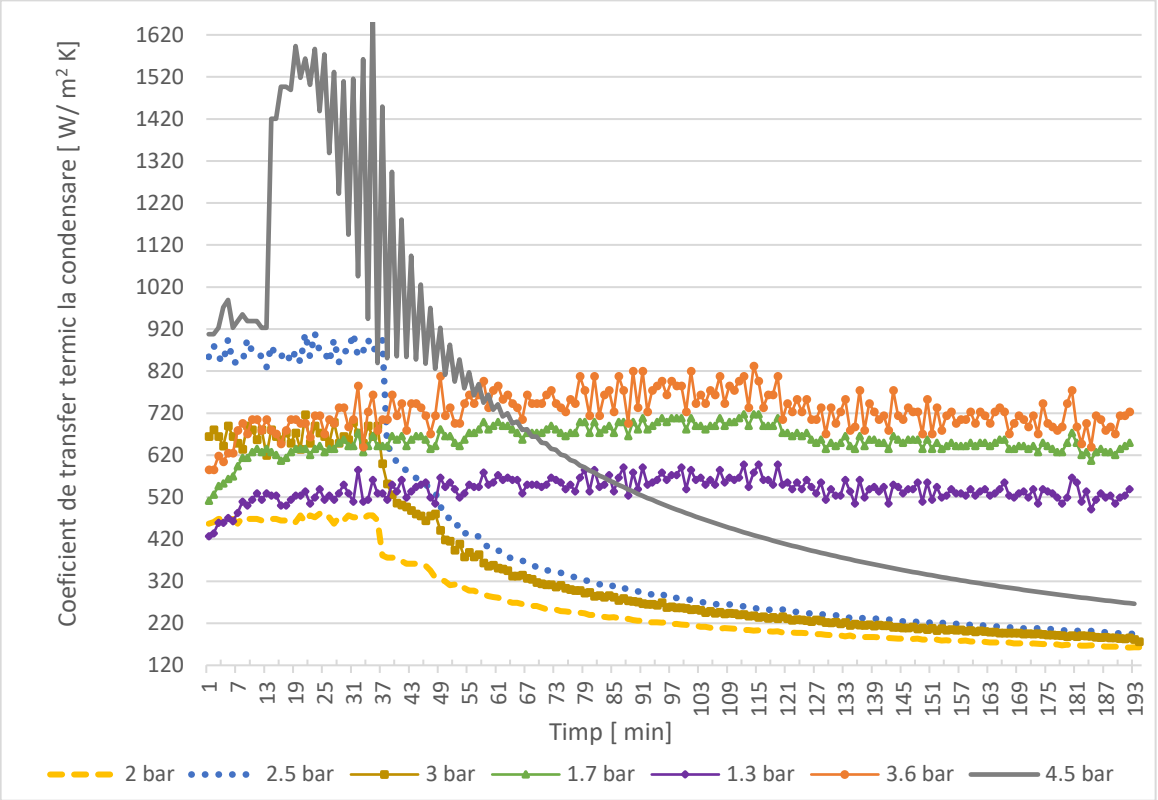


*Figure 8.6.2.1 Experimental condensing heat transfer coefficient value for different inlet gas pressure values, for 6x4 pin rectangular type C1.4 condenser model*

An useful information that can be extracted from this graph (*fig. 8.6.2.1)* is that in the 2÷3 bar pressure range the heat transfer is very low, below 300 W/m2K (the three curves at the bottom of the graph show a continuous downward trend). This is very important for the sizing of condensers in cryogenic distillation technology plants where the pressure used plays an important role in the performance and stability of the process.

*Table 8.6.2.1 Average experimental values of condensing heat transfer coefficient $h_{m\,exp}$ for C1.4 rectangular type 6x4 pin hydrogen condenser*

| **Vapor pressure** $p_v$ | **Vapor temperature** $T_v$ | **Flow** $\dot{m}$ | $\Delta T_c$ | $Q$ | $h_{m\,exp}$ |
|---|---|---|---|---|---|
| [bar] | [K] | [m/s] | [K] | [W] | [W/(m² K)] |
| 1.3 | 21.24 | 0.05 | 3.35 | 18 | **536.90** |
| 1.7 | 22.25 | 0.05 | 2.73 | 18 | **658.28** |
| 2 | 22.67 | 0.05 | 7.67 | 18 | **234.60** |
| 2.5 | 23.67 | 0.05 | 5.84 | 18 | **308.42** |
| 3 | 24.61 | 0.05 | 6.41 | 18 | **280.98** |
| 3.6 | 25.50 | 0.05 | 2.49 | 18 | **721.75** |
| 4.5 | 26.73 | 0.05 | 1.73 | 18 | **1042.59** |

From (*fig. 8.6.2.2*) it can be seen that the values of the heat transfer coefficients at condensation obtained experimentally were lower than those calculated with the theoretical Nusselt model. This is due to the simplifying assumptions (*Chapter 5.6.2 Theoretical calculation of the heat coefficient at the condenser surface*) of this model and which are no longer valid the lower the temperatures in the cryogenic range. That is why the Nusselt model for very low temperatures has deviations the lower the temperature, especially in the case of hydrogen, which presents the specificity of ortho-para transformation (*chapter 2.1.1. Isotopic forms of hydrogen*), which is an exothermic reaction with the release of energy, a phenomenon that is difficult to predict by Nusselt's theory. So, the conclusion is that the basic assumptions of Nusselt's theory can be applied to these types of distillation column condensers working in the cryogenic field, only with the corrections given by specific laboratory tests.

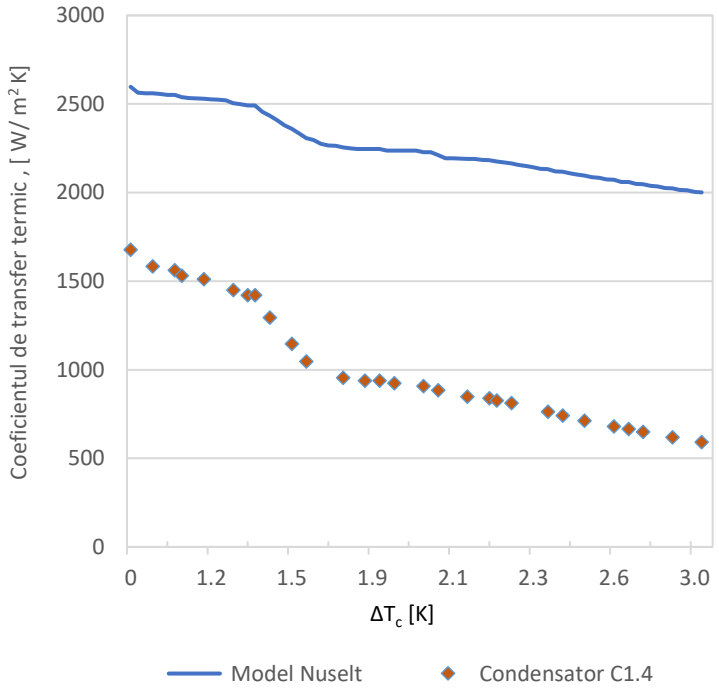


*Figure 8.6.2.2 Relating of experimental data to the Nusselt theoretical model for calculating the condensing heat transfer coefficient $h_{exp}$ of the C1.4 rectangular 6x4 pin hydrogen condenser*

The fact that this condenser in the optimized version C1.4 rectangular type with 6x4 pins has achieved good performance for several domains of operating parameters (*table 8.6.2.1*) confirms the correctness of the estimates and calculations made and validates the optimized condenser model.

# 9. CONCLUSIONS

## C1. GENERAL CONCLUSIONS

This work continues research into improving the heat transfer of heat exchangers in a distillation plant.

Following a bibliographic study of the literature on the current state of performance of cryogenic isotopic distillation technologies, carried out in chapter 2, we have identified methods and technologies for stabilizing technological processes that can be applied to the current $H_2$-$D_2$ cryogenic distillation installation for testing PEST components, assembled within the Cryogenics Laboratory of the ICSI Rm Vâlcea Research Institute.

In chapter 3 of the work, the energy and exergetic performance of the isotopic and cryogenic separation plant served by the refrigeration machine of the plant, namely the Stirling PPH cryo-generator, was evaluated, both for independent operation of the machine and integrated with the plant. The conclusions of the exergetic evaluation of the isotopic and cryogenic hydrogen separation installation led to the identification of a high irreversibility in the area of the tubular type condenser of the installation.

Thus, we continued the research in the following directions: stabilizing the liquid level in the condenser of the liquefaction installation by minimizing oscillations in operation and increasing the efficiency of the liquefaction process by increasing the liquid flow rate at the level of the cold surface of the condenser. In this regard, we have developed a new model of conical condenser as a new constructive solution that minimizes the possibility of hazard in the condensation process, leading to the stabilization of the liquefaction process.

The current scientific paper argues the proposed constructive choice by minimizing the condensation conditions in film form as well as by improving the heat transfer mode resulting from the implementation of this innovation. To confirm the functionality, we initially carried out parallel tests with the current model of tubular condenser and with the new type of condenser. A 2% increase in the overall exergetic efficiency of the distillation column was determined, in the case of using the conical condenser compared to the tubular condenser, under the same technical operating conditions. This first confirmation of the refrigeration efficiency of the new type of condenser led to the continuation during the thesis of the study of the technical implications of the use of the new type of condenser in cryogenic hydrogen separation installations. The initial condenser model, with a flat and inclined surface, was

developed by machining it with extended heat exchange surfaces (pins or fins) and channels that allow heat dissipation and droplet condensation.

In order to test the conductivity of this new type of condenser and its constructive options, in chapter 4 we presented the design and execution of an experimental stand separate from the cryogenic distillation column. The experimental test stand was designed based on the method of condensing hydrogen on the surface of the condenser and the theoretical calculation of the condensation rate according to the Nusselt theory of film condensation.

Next, in chapter 5, we made the thermal and sizing calculation of the experimental stand characterized by the cryogenic installation and the condenser attached to the 2nd stage of the refrigeration machine, the GM cryocooler. From these calculations result the main technical quantities for the design of this type of condenser as well as the test stand. It was found that the refrigeration machine falls within the limits of the designed thermal capacity of 17.71 W. It has been observed that for the calculated heat exchange level (heat transfer coefficient) the effective (real) height of the condenser is lower than originally designed. This can be explained in two ways: there is a higher heat flux but the lower part and the peripheral part of the condenser have a role for pre-cooling the heat flux or the assumptions of the theoretical calculation do not take into account all the real process data.

Therefore, taking into account the multitude of factors that influence the general heat transfer coefficient (geometric shape, heat transfer surface characteristics, material), for a more energy-efficient technical design of these condensers, in chapter 6 we presented the method of minimizing the production of MPE entropy for identifying and reducing the exergy destruction in the condenser heat exchanger. The calculation mode is applied for the hydrogen condenser with pins and thermal dissipation channels. The method consists of an exergetic comparative analysis by combining the conservation equations for mass and energy with the entropy balance for the condenser. The major sources of entropy production were taken into account: heat transfer through the exchanger walls and local pressure drop. The system of nonlinear equations was solved using the Newton-Raphson method with the establishment of certain constant construction parameters. Compared to the practice so far, the calculation method takes into account the pressure drop and the thermal resistance to fluid flow, giving originality to the thermal and exergetic analysis. In addition, the temperature of the thermal tank, the condenser, is considered constant. From the comparative analysis of the results of minimization of the entropy production rate by the variation of several factors (geometric and functional) resulted a constructively optimized geometric configuration of the pin condenser that has the lowest entropy generation rate.

For a confirmation of the optimization results, we performed a CFD numerical simulation in chapter 7, using the Ansys Fluent 2022 R2 program. Separate CAD models of the types of condensers tested were created for numerical simulations with different velocities of hydrogen, as a working gas, over the surface of the heat exchanger. Based on the velocities, the Reynolds number and the mass flow for each simulation were calculated. The average heat transfer coefficients for each simulation were determined and the results were compared with the theoretical and experimental models. It was found that the results are close in values. The results of the simulations show that the pin structure allows for better gas circulation and at the same time confirms the optimized condenser pattern.

In order to test the conductivity of this new type of condenser and its constructive options, including the optimized condenser model, we have carried out in chapter 8 multiple experimental tests to confirm and validate the results. It was found that higher convection coefficients were obtained when condensing on the vertical walls of the condensers provided with pins (inclined or straight), thus confirming the theory of the breaking of the condensate film that is formed on the heat exchange surface with hydrogen gas and the formation of droplets that fall and release the surface from contact with the vapors. This leads to an increase in the condensation rate and implicitly in the convection transfer coefficient. It is thus experimentally confirmed that the inclined shape of the surface has an important role in facilitating the flow and directing the flow of condensate.

Comparing the data of the practical experiments carried out in Chapter 8 with the theoretical design data calculated in Chapter 5 resulted in lower values of the heat transfer coefficient than those estimated by Nusselt's theory of film condensation on a vertical surface, in the very low temperature range. These differences are due to the increase in the thermal resistance of the condensate at very low temperatures, having as causes: the peculiarity of manifestation of the latent heat of hydrogen vaporization but also of the film layer that covers the surface of the condenser. Thus, in the case of condensation of hydrogen and the heavy isotope of deuterium hydrogen, there is an overheating of the hydrogen vapor, due to the thermal losses due to the ortho-para conversion presented in detail in Chapter 2. Therefore, the basic assumptions of Nusselt's theory represent an ideal case and for the condensers of cryogenic hydrogen distillation columns they should only be applied with corrections resulting from practical experiments.

From the experimental determinations for the optimized pin condenser, it resulted that the best heat transfer coefficient for condensate is obtained at a pressure of 4.5 bar. Also, for the working range of low pressures, close to atmospheric pressure, the pressures of 1.3 bar and 1.7

bar can be used. On the other hand, the pressure range 2÷3 bar has a low heat transfer. This information is important for the sizing of condensers in cryogenic distillation installations where the pressure used plays an important role in process performance and stability.

The results of the condenser optimization confirmed by the experimental tests, validate the fact that the geometry of the condenser has an important role in increasing the heat transfer through the shape of the contact surface, which avoids film condensation, respectively, through the weight reductions due to the optimization of the pin density.

The experimental analysis confirmed that the use of the new condenser model leads to minimizing irreversibility in operation and increasing the refrigeration performance of the cryogenic hydrogen distillation installations.

## C2. PERSONAL CONTRIBUTION

In view of the general conclusions presented above, personal contributions can be presented as follows:

C2.1) bibliographic study on the level of knowledge reached regarding the performance of this type of condensers;

C2.2) bibliographic study on the determination of the optimization method for the hydrogen condenser of conical configuration and extended geometry (pins, fins and thermal dissipation channels);

C2.3) technical calculations for the design of the cryogenic hydrogen isotope distillation system;

C2.4) execution of technological design documentation in the SolidWoks 19 program, which includes sketches, general and execution drawings;

C2.5) design and production of the P&ID documentation for the experimental stand provided with execution elements (valves, actuators) and control, measurement and monitoring system, with temperature, pressure, gas flow sensors, SCADA automation system, data collection and interpretation in the installation;

C2.6) execution of the exergetic calculation of the cryogenic distillation installation of hydrogen isotopes with a diameter of less than 12 mm equipped with both a tubular and the new type of pin condenser, comparison of calculation results and post-calculation plotting of graphs;

C2.7) modeling and exergetic analysis of the hydrogen condenser mounted on the experimental stand consisting of the liquefaction chamber inside the vacuum of a cryostat cooled with a Gifford McMahon cryocooler;

C2.8) simulation operations in the Ansys program of the condenser behavior in different operating situations, data interpretation, table making and plotting post-calculation graphs;

C2.9) monitoring the technical execution of the components of the experimental cryogenic stand for testing hydrogen condensers;

C2.10) physical assembly of the experimental hydrogen condenser test stand with increased attention on the installation of vacuum seals and cold zone seals;

C2.11) preliminary sealing tests, function tests, tests and commissioning of the experimental hydrogen condenser test stand;

C2.12) handling and monitoring 10e-6 mbar high vacuum system, equipped with preliminary vacuum pumps, turbomolecular vacuum pumps, valves and vacuum gauges;

C2.13) operating the experimental stand and monitoring the evolution of the testing processes;

C2.14) centralization and interpretation of experimental data, creation of post-calculation tables and graphs;

C2.15) realization of the method of minimizing the production of entropy for a hydrogen condenser mounted on a distillation installation with a diameter of less than 12 mm, comparison and centralization of results;

C2.16) Mathcad calculation program using the Newton-Raphson method for the calculation of the system of nonlinear equations resulting from the application of the entropy production minimization method for a hydrogen condenser used in isotopic and cryogenic distillation installations;

C2.17) realization of a pin copper condenser model with better refrigeration performance than the tubular steel condenser used in the cryogenic hydrogen distillation installation due to the avoidance of the occurrence of film condensation when boiling and allowing the flow in the form of droplets;

C2.18) realization of a pin condenser model for use in the cryogenic isotopic hydrogen distillation installation, optimized in terms of the material used (copper), geometric shape and density of the pines array.

## C3. ORIGINAL CONTRIBUTION

C3.1) Increase the exergetic efficiency of the isotopic and cryogenic hydrogen separation installation by 2% by using the new type of optimized condenser with a 24-pin configuration.

C3.2) Experimental determination of condensing heat transfer coefficient characteristic curves for copper condenser with a 24-pin square section configuration for hydrogen working gas inlet pressures of: 1.3 bar, 1.7 bar, 2 bar, 2.5 bar, 3 bar, 3.6 bar, 4.5 bar.

C3.3) Obtaining an optimal ratio between the height and the side of the square section of the pin: $\gamma = 5$ for pin condensers used in isotopic and cryogenic hydrogen separation installations, given that copper is used as material and the fluid is in laminar flow, with Prandl number: $Pr \leq 0.7$.

C3.4) Obtaining an optimal pin density: N=24 pins for square section pin condensers used in isotopic and cryogenic hydrogen separation plants, with a base plate distribution of: $N_L \times N_l = 6 \times 4$ pins, equal distances between pins in the range: $L_p = 4 \div 6$ mm and the side of the pin section in the range: $d = 2 \div 4$ mm, given that copper is used as a material and the fluid is in laminar flow, with Prandl number: $Pr \leq 0.7$.

## C4. FUTURE RESEARCH DIRECTIONS

Future research directions will mainly include the directions below.

C4.1) Development of the existing calculation program by making a generalized version of this optimization method by minimizing the production of entropy with extension to all types of materials and cryogenic fluids and taking into account the effects of the viscosity of the flowing fluid on the energy performance of the heat dissipation channels;

C4.2) Due to the fact that in the case of hydrogen, there is an accentuated phenomenon of diffusion, and not of permeation, I am considering making additional measurements and experimental determinations for the condenser optimized in the non-removable version, namely by welding it by dissimilar diffusion on the body of the distillation column;

C4.3) Conducting experimental tests with the application of a special technique of intensifying heat transfer when the operating temperature of the distillation column decreases. This effect consists of increasing the difference between the properties of the components of a mixture of hydrogen isotopes as the temperature decreases. The proposed purpose is to evaluate the distillation efficiency of such mixtures in the triple point temperature range up to boiling temperatures, at atmospheric pressure. This evaluation, however,

requires additional tests regarding the equilibrium parameters of the mixtures separated in this temperature range. It must also be possible to test the column elements, especially the condenser, at these temperatures. Therefore, in the situation of the current experimental stand, the current condenser cooling solution was chosen with a GM cryorefrigerator that allows these low temperatures to be reached, which leads to an increase in cooling power and thus to an improvement in liquefaction [52] by increasing the condensation rate.

C4.4) From the optimization calculations made (*chapter 6*) resulted a tendency to decrease the thermal resistance by decreasing the height of the pins. Thus, future calculations will consider experimenting with the condenser version with very low pins compared to the dimensions of the baseplate, in order to avoid clogging with liquid between the pins and fins. The declared purpose is to investigate their role in the breakage of the liquid film, by creating the conditions of flow by droplets, respectively the thermal efficiency of this type of condenser with low pins.

# PUBLISHED ARTICLES

**a) WOS indexed articles:**

1. **Catalin Brill**, Sebastian Brad, Claudia Bogdan, Aleksandr Grafov, Oleksandr Sirosh, Alin Lazar, Mihai Vijulie, Viorel Badescu, *Preliminary Design of a Cryogenic System with GM Cryocooler for Testing the Hydrogen Condensers of the Distillation Columns*, FUSION SCIENCE AND TECHNOLOGY, Volume 80, 2024, Issue 3-4, Pages 422-430, Special Issue SI: Selected papers from the 13th International Conference on Tritium Science and Technology, Published:MAY-18-2024, Indexed: 2023-12-29, Lucrarea este indexată în BDI(Scopus) DOI: 10.1080/15361055.2023.2283226 și ISI Thomson Reuters WOS:001125780000001, ISSN: 1536-1055, eISSN: 1943-7641, IDS Number: MY0J4, Conform JCI Category: NUCLEAR SCIENCE & TECHNOLOGY in SCIE edition, Category: Rank 27/40, Category Quartile: Q3, Factor de impact: 0.9 (2023).
   https://www.webofscience.com/wos/author/record/JEF-1160-2023

2. Claudia Bogdan, Sebastian Brad, Horia Necula, Oleksandr Sirosh, **Catalin Brill**, Mihai Vijulie, Alin Lazar, Aleksandr Grafov, *Design, Fabrication, and Test of a Prototype of Matrix Heat Exchanger for Cryogenic Distillation of Hydrogen Isotopes*, FUSION SCIENCE TECHNOLOGY, Volume 80, 2024, Issue 3-4, Pages 443-454, Special Issue SI: Selected papers and from the 13th International Conference on Tritium Science and Technology, Published: MAY 18 2024, Indexed: 2023-11-05, Lucrarea este indexată în BDI(Scopus) DOI:10.1080/15361055.2023.2259238 și ISI Thomson Reuters WOS:001088192900001, ISSN: 1536-1055, eISSN: 1943-7641, IDS Number: MY0J4, Conform JCI Category: NUCLEAR SCIENCE & TECHNOLOGY in SCIE edition, Category: Rank 27/40, Category Quartile:Q3, Factor de impact:0.9(2023).
   https://www.webofscience.com/wos/author/record/JEF-1160-2023

3. Sebastian Brad, Mihai Vijulie, Alin Lazar, Claudia Bogdan, Oleksandr Sirosh, **Catalin Brill**, Aleksandr Grafov, Anisoara Oubraham, Alina Niculescu, George Bulubasa, *New Achievements of $H_2$-HD-$D_2$ Isotopic Separation with the Cryogenic Distillation Experimental Stand from ICSI Cryogenic Laboratory*, FUSION SCIENCE TECHNOLOGY, Volume 80, 2024, Issue 3-4, Pages 455-464, Special Issue SI: Selected papers and from the 13th International Conference on Tritium Science and Technology, Published: MAY 18 2024, Indexed: 2023-10-28, Lucrarea este indexată în BDI(Scopus) DOI: 10.1080/15361055.2023.2236473 și ISI Thomson Reuters WOS:001082483800001, ISSN: 1536-1055, eISSN: 1943-7641, IDS Number: MY0J4, Conform JCI Category: NUCLEAR SCIENCE & TECHNOLOGY in SCIE edition, Category: Rank 27/40, Category Quartile:Q3, Factor de impact: 0.9(2023).
   https://www.webofscience.com/wos/author/record/JEF-1160-2023

4. Ingo Deppner, Claudia Bogdan, Sebastian Brad, **Catalin Brill**, Daniel Dorobantu, Aleksandr Grafov, Dong Han, Norbert Herrmann, Dongdong Hu, Alin Lazar, Wen Li, Mariana Petris, Mihai Petrovici, Andrii Rozhenstev, Oleksandr Sirosh, Yannick Söhngen, Kai Sun, Yongjie Sun, Mihai Vijulie, Botan Wang, Kaiyang Wang, Xinjian Wang, Yi Wang, Ming Yao, Jian Zhou, Yingjie Zhou, *Toward an environmental friendly operation of the CBM-TOF system*, EUROPEAN PHYSICAL JOURNAL PLUS, Volume 138, Issue 12, Article number 1080, Published: DEC 5 2023, Indexed: 2023-12-21, Lucrarea este indexată în BDI(Scopus) DOI: 10.1140/epjp/s13360-023-04712-9 și ISI Thomson Reuters WOS:001113234500001, ISSN: 2190-5444, IDS Number: Z6NW8, Conform JCI Category: PHYSICS, MULTIDISCIPLINAR *in SCIE edition*, Category: Rank 27/112, Category Quartile:Q1, Factor de impact: 2.8 (2023), https://www.webofscience.com/wos/author/record/JEF-1160-2023.

5. Curuia Marian, Anghel Mihai, **Brill Catalin**, Sirosh Oleksandr, Varlam Mihai, *Modelling of the Thermal Radiation Shields for Cryogenic Systems*, REFRIGERATION SCIENCE AND TECHNOLOGY, Volume Part F147717, Pages 428 – 434, Conference Paper of 15th International Institute of Refrigeration Conference on Cryogenics, CRYOGENICS 2019, Prague 8 -11 April 2019, Published: 2019, Indexed: 2019-07-10, Lucrarea este indexată în BDI (Scopus) DOI: 10.18462/iir.cryo.2019.0071 și ISI Thomson Reuters WOS:000472960900058, ISBN: 978-2-36215-025-8, ISSN: 0151-1637, IDS Number: BN0IX, Research Areas: Thermodynamics; Physics, Web of Science Categories: Thermodynamics; Physics, Applied.
https://www.webofscience.com/wos/author/record/JEF-1160-2023.

6. **Brill Catalin**, Curuia Marian, Varlam Mihai, Jianu Catalin, Marinoiu Adriana, Badescu Viorel, *Cryogenic performance of a conduction cooled cryostat for hydrogen isotopes separation experiments at low temperature*, REFRIGERATION SCIENCE AND TECHNOLOGY, Pages 203 – 209, Conference Paper of the 16th IIR International Institute of Refrigeration Conference, Cryogenics 2021 online, October 5-7, 2021, Publication date: 2021, Indexed: 2021-01-01, Lucrarea este indexată DOI 10.18462/iir.cryo.2021.0009 și ISI Thomson Reuters WOS: 001304907400027, ISBN: 978-2-36215-047-0, ISSN: 0151-1637, IDS Number: BX5YC, Research Areas: Thermodynamics; Physics, Web of Science Categories: Thermodynamics; Physics, Applied, DOI: http://dx.doi.org/10.18462/iir.cryo.2021.0009.
https://www.webofscience.com/wos/author/record/JEF-1160-2023.

**b) WOS non-indexed articles:**

7. Claudia Bogdan**, Catalin Brill**, Oleksandr Sirosh, Mihai Vijulie, Alin Lazar, *Preliminary development of a conceptual model of matrix heat exchanger*, SMART ENERGY AND SUSTAINABLE ENVIRONMENT, ISSN: 2668-957X, 2021, Volume 24, Issue 1, Pages 29-40, Publication date: *march-apr 2021*, DOI: https://doi.org/10.46390/j.smensuen.24121.435.

# SELECTIVE BIBLIOGRAPHY

[1] Programul Nucleu INC-DTCI-ICSI, ctr. Nr. 9N/2019, elaborat cu sprijinul Ministerului Cercetarii, Inovarii si Digitalizarii, proiect nr. PN 19 11 01 04, *Solutie inovatoare de proces CECE pentru promovarea unei noi tehnologii de decontaminare a deseurilor lichide slab concentrate in tritiu si pentru recuperarea deuteriului*

[3] Floarea Pop, *Distilarea izotopică a hidrogenului. Experimentari*, Techno Media, Sibiu, 2012

[7] Lazar, A., Brad, S., Vijulie, M., Oubraham, A., *Cryogenic distillation experimental stands for hydrogen isotopes separation*, Fusion Engineering and Design Volume 146, Part B, September 2019, Pages 1998-2001, https://doi.org/10.1016/j.fusengdes.2019.03.085

[8] Lazar, A., Brad, S., Vijulie, M., Oubraham, A., Vasut, F., Sirosh, A. (2019). *Preliminary tests on a hydrogen isotope separation cryogenic facility, at the laboratory scale, within the "Cryogenic laboratory" from ICSI Rm. Valcea*. Progress of Cryogenics and Isotopes Separation, 22(2), 5-12, https://www.energ-en.ro/pages/article/68

[9] I. Alekseev, O. Fedorchenko, P. Kravtsov, A. Vasilyev and M. Vznuzdaev (2008) *Experimental Results of Hydrogen Distillation at the Low Power Cryogenic Column for the Production of Deuterium Depleted Hydrogen*, Fusion Science and Technology, 54:2, 407- 410, https://doi.org/10.13182/FST08-A1841

[13] Andrey Ovcharov, Richard Szczepanski, Jacek Kosek, Nuno Pedrosa, Xiaofei Lu, Lorenzo Basili, Rosa Lo Frano & Donato Aquaro (2020) *Rigorous Dynamic Simulation of Cryogenic Distillation of Hydrogen Isotopologues in the Fuel Cycle of a Thermonuclear Reactor Based on UV Flash, Fusion Sc. and Techn.*, 76:3, 179-190, doi: 10.1080/15361055.2019.1689891

[14] Mengyu Liu et al, *A Separated two stage helium liquefier using a 4 K GM cryocooler*, IOP Conf. Series: Materials Science and Engineering 502(2019) 012079, IOP Publishing, doi:10.1088/1757-899X/502/1/012079, https://doi.org/10.1088/1757-899X/502/1/012079

[16] X. X. Chu, M. M. Zhang, D. X. Zhang, et al., *Cryogenic system with GM cryocooler for krypton, xenon separation from hydrogen-helium purge gas,* AIP Conference Proceedings 1573, 1638 (2014); https://doi.org/10.1063/1.4860903

[22] M. Peculea, *Instalatii criogenice*, Ed. Conphys, 1997

[27] I.G. Deac, *Elemente de criogenie*, Ed. Napoca Star Cluj- Napoca, 2010.

[40] Brill Catalin, Curuia Marian, Mihai, Jianu Catalin Adriana, Badescu Viorel, *Cryogenic performance of a conduction cooled cryostat for hydrogen isotopes separation experiments at low temperature*, Proceedings of the 16th IIR International Conference Online,October 5-7, 2021, Cryogenics 2021 online, International Institute of Refrigeration, Publication date: 2021/10/05, DOI: http://dx.doi.org/10.18462/iir.cryo.2021.0009

[42] Thomas.F, Cryogenic Engineering, Marcel Dekker, New York, 2005

[47] Marinescu M., Baran N., Radcenco V., Badescu V., *Termodinamica Tehnica*, vol 3, Ed. Matrixrom, Bucuresti, 1998

[50] Cengel,Y.A, *Heat Transfer, A Practical Aproach*, Second Edition

[78] Bejan A., *Entropy generation minimization: the method of thermodynamic optimization of finite-size systems and finite-time processes*, New York: CRC Press; 1996.

[107] A. BORNEA et al., *Investigation Related to Hydrogen Isotopes Separation by Cryogenic Distillation*, Fusion Sci. Technol., 54, 2, 426 (2008); https://doi.org/10.13182/FST08-A1846

[108] Brad Sebastian, *Model experimental de condensator pentru o coloană de distilare criogenică pentru concentrații ridicate de tritiu*, Etapa_de raportare proiect, Nucleu INC-DTCI-ICSI, 2022.

[118] Brad Sebastian, *Raportare proiect Nucleu, Etapa 10*, INC-DTCI-ICSI, 15.03.2022

[119] Brad Sebastian, *Raportare proiect Nucleu, Etapa 7*, INC-DTCI-ICSI, 15.04.2021

Aguilar D.J.M, Hidalgo J. A .A, Martínez M.E.P, *Analysis of the operating parameters in a Stirling cryocooler*, ISEC 2021, E3S Web Conf., Volume 313, 10002 (2021) 2021

[121] Brad Sebastian, *Raportare proiect Nucleu, Etapa 6*, INC-DTCI-ICSI, 10.12.2020

[128] Catalin Brill, Sebastian Brad, Claudia Bogdan, Aleksandr Grafov, Oleksandr Sirosh, Alin Lazar, Mihai Vijulie, Viorel Badescu, *Preliminary Design of a Cryogenic System with GM Cryocooler for Testing the Hydrogen Condensers of the Distillation Columns*, Fusion Science and Technology, Volume 80, 2024 - Issue 3-4: Selected papers from the 13th Int. Conf. on Tritium Sc. and Tech., https://doi.org/10.1080/15361055.2023.2283226

[130] Culham, R. J. and Muzychka, Y. S., *Optimization of Plate Fin Heat Sinks Using Entropy Generation Minimization*, IEEE Transactions on Components and Packaging Technologies, Vol. 24, No. 2, pp. 159-165, 2001.